The Dynamics and Statistics of Public Opinion

विद्या वाचस्पति की
उपाधि की अपेक्षाओं की आंशिक पूर्ति में प्रस्तुत शोध प्रबंध

A thesis
submitted in partial fulfillment of the requirements of the degree
of Doctor of Philosophy

द्वारा / By
रितम पाल / Ritam Pal

पंजीकरण सं. / Registration No.: 20193704

शोध प्रबंध पर्यवेक्षक / Thesis Supervisor
प्रो. एम. एस. संथानम / Prof. M. S. Santhanam

भारतीय विज्ञान शिक्षा एवं अनुसंधान संस्थान पुणे
INDIAN INSTITUTE OF SCIENCE EDUCATION AND RESEARCH PUNE

2025

Certificate

Certified that the work incorporated in the thesis entitled **"The Dynamics and Statistics of Public Opinion"** submitted by **Ritam Pal** was carried out by the candidate under my supervision. The work presented here or any part of it has not been included in any other thesis submitted previously for the award of any degree or diploma from any other university or institution.

Date: June 27, 2025

Prof. M.S. Santhanam

(Supervisor)

Declaration

Name of Student: Ritam Pal

Reg. No.: 20193704

Thesis Supervisor: Prof. M. S. Santhanam

Department: Physics

Date of joining program: August 1, 2019

Date of Pre-Synopsis Seminar: November 27, 2024

Title of Thesis: The Dynamics and Statistics of Public Opinion

I declare that this written submission represents my idea in my own words and where others' ideas have been included; I have adequately cited and referenced the original sources. I declare that I have acknowledged collaborative work and discussions wherever such work has been included. I also declare that I have adhered to all principles of academic honesty and integrity and have not misrepresented or fabricated or falsified any idea/data/fact/source in my submission. I understand that violation of the above will be cause for disciplinary action by the Institute and can also evoke penal action from the sources which have thus not been properly cited or from whom proper permission has not been taken when needed.

The work reported in this thesis is the original work done by me under the guidance of Professor M. S. Santhanam.

Ritam Pal

Date: June 27, 2025

Ritam Pal

(20193704)

Acknowledgments

This is probably the end of my student life in the formal sense, though I believe I will always be a student in some way. As I look back, I feel the need to thank the people, places, and experiences that have helped shape who I am.

First, I want to thank my supervisor, Prof. M. S. Santhanam. Over the past six years, his support and guidance have been constant. I have learned a lot from him – not just about research, but also about how to approach problems, think clearly, and stay steady. I am deeply grateful, and I hope to continue learning from him in the future.

IISER Pune has played a big role in my life. It gave me the space, freedom, and support I needed to grow – both academically and personally. I am thankful for everything the institute has provided.

To the people who made my time here special – *Aakash, Aanjaneya, Barnali, Bharathi, Dipanshu, Harshini, Karthikeyan, Mayank, Nisarg, Rajiv, Shaunak, and Sreeram* – thank you for being there, for the conversations, the help, the shared moments. I'm sure I've missed a few names, and to them, too, thank you.

And finally, to my family, thank you for always being there. I would not be here without you.

– *Ritam*

to Prof. M. S. Santhanam

Abstract

How do individual opinions, shaped through everyday interactions, give rise to large-scale patterns in public discourse and democratic outcomes? This thesis explores that question through two domains where opinions are both formed and revealed: online social networks and electoral systems.

The first part addresses polarization in digital environments, driven by homophilic interactions and algorithmic reinforcement. To mitigate this, a simple intervention – the random nudge – is introduced, enabling occasional exposure beyond one's echo chamber. Simulations across various opinion dynamics models show that even a small probability of such encounters can significantly reduce polarization, breaking echo chambers while preserving diversity and autonomy.

The second part examines the statistical structure of electoral competition. Using a newly assembled dataset spanning 34 countries and multiple spatial resolutions, we uncover a striking universal pattern: when margins of victory are normalized by local turnout and rescaled by their national average, the distribution collapses onto a single curve across democracies. To explain this, the Random Voting Model (RVM) is proposed – a minimal, parameter-free stochastic model that reproduces the universal curve and accurately predicts scaled distributions of margins, winner, and runner-up votes.

These models go beyond description: the random nudge suggests a viable strategy to reduce polarization online, while deviations from RVM predictions signal potential electoral anomalies, as shown in case studies from Ethiopia and Belarus. Together, these findings reveal simple, robust statistical principles underlying complex collective decisions – and offer new tools to better understand and strengthen democracy.

Synopsis

Collective human behavior, particularly as manifested in opinion formation within social networks and the outcomes of democratic elections, presents substantial challenges for quantitative understanding, prediction, and constructive intervention. This thesis applies tools from statistical physics, network science, and dynamical systems to uncover emergent macroscopic patterns in these domains. It argues that randomness, far from being merely noise, can act as a unifying explanatory principle and a source of practical interventions in complex social systems.

Chapter 1 – Statistical Physics of Collective Decision-Making

This chapter lays the conceptual and methodological foundation by framing human society as a multi-scale complex system composed of interacting individuals whose collective behaviors give rise to emergent phenomena. This perspective justifies applying statistical physics to model social systems. The chapter reviews key literature on opinion dynamics – from classical models like DeGroot, Voter, and Sznajd to more recent extensions incorporating homophily, bounded confidence, and algorithmic feedback – as well as studies on universal statistical regularities in democratic elections. These strands collectively motivate the thesis's focus on randomness as a potentially generative and organizing force.

Chapter 2 – Random Nudge: A Strategic Intervention for Digital Polarization

This chapter addresses the growing problem of online polarization by introducing the *random nudge* – an intervention where agents occasionally interact with random others outside their homophilic circles. Simulations show that small degrees of randomness reduce polarization, though too strong an intervention risks eliminating diversity by collapsing the system into consensus. This leads to an optimization problem: how to balance depolarization with opinion heterogene-

ity. The robustness of the random nudge is demonstrated across multiple models, highlighting its broad potential for real-world implementation. The work described in this chapter is published in Ref. [1].

Chapter 3 – Electoral Data: Collection and Preparation Framework

Here, the thesis details the construction of a large-scale, cross-national electoral dataset spanning 34 countries and multiple electoral levels, from polling booths to national constituencies. Data sources include national election portals, academic repositories, and historical records, necessitating customized pipelines for extraction and cleaning. A distinctive feature is the multi-scale resolution, particularly in countries like India, where data ranges from $\sim 10^3$ to $\sim 10^6$ voters. This curated dataset underpins all subsequent empirical analyses of electoral regularities.

Chapter 4 – Universality in Electoral Competition

Chapter 4 presents a central empirical finding: the scaled margin of victory – normalized by turnout and rescaled by the national mean – follows a universal distribution across democracies. This pattern appears robust across 32 countries, different voting systems, and spatial resolutions. The finding suggests the presence of deep, context-independent statistical regularities underlying electoral competition, pointing to universality in democratic processes. The central finding described in this chapter is published in Ref. [2].

Chapter 5 – Random Voting Model: Analytical Framework

This chapter introduces the *Random Voting Model (RVM)*, a parameter-free stochastic model that explains the observed universality in scaled margins. Candidates receive random preference scores, which are normalized to generate expected vote shares. Using tools from order statistics, the model analytically predicts the margin distribution in three-candidate elections. Once the empirical turnout distribution is provided, the model accurately replicates the observed country-

level margin distributions, highlighting the explanatory power of randomness.

Chapter 6 – Beyond Margins: Winner and Runner-Up Votes

Building on the RVM, this chapter models the scaled vote shares of winners and runner-ups using Indian election data across electoral levels. By incorporating the *effective number of candidates*, the model captures competitiveness more accurately than raw candidate counts. The model's predictions match empirical distributions from polling booths to parliamentary constituencies, and the scaled distributions exhibit a remarkable scale-invariance unique to India, revealing new structural insights about large-scale electoral behavior. Ref. [3] details the findings, which is demonstrated in this chapter.

Chapter 7 – From Theory to Practice: Applications and Interventions

This chapter explores real-world applications of the thesis's findings. The random nudge mechanism could be integrated into platform algorithms to counteract echo chambers with minimal invasiveness. In electoral contexts, the RVM offers tools for anomaly detection: deviations from predicted distributions may flag potential manipulation. Case studies from Ethiopia and Belarus illustrate how these methods can support democratic integrity, showing that physics-based models are not just descriptive but also diagnostic.

Chapter 8 – Summary and Outlook

The final chapter synthesizes the thesis's findings, emphasizing randomness not merely as disorder but as a source of structure, predictability, and intervention. By revealing universal features in both opinion dynamics and electoral behavior, the thesis demonstrates the utility of principled, minimal models. Future directions include enriching opinion models with cognitive realism and dynamic networks, extending the RVM to include strategic or partisan behavior, and developing statistical indicators for detecting anomalies in complex social systems. The work advocates for

an interdisciplinary synthesis between physics and social science to build predictive, transparent, and actionable models of collective human behavior.

References

1. Ritam Pal, Aanjaneya Kumar, M. S. Santhanam. *Depolarization of opinions on social networks through random nudges,* Physical Review E 108, 034307 (2023).

2. Ritam Pal, Aanjaneya Kumar, M. S. Santhanam. *Universal statistics of competition in democratic elections,* Phys. Rev. Lett. 134, 017401 (2025).

3. Ritam Pal, Aanjaneya Kumar, M. S. Santhanam. *Voter turnout govern key electoral statistics,* ArXiv preprint arXiv:2501.01896 (2025).

List of Publications

The contents of the thesis are based on the following papers.

1. **Ritam Pal**, Aanjaneya Kumar, M. S. Santhanam. *Depolarization of opinions on social networks through random nudges,* Physical Review E 108, 034307 (2023)

2. **Ritam Pal**, Aanjaneya Kumar, M. S. Santhanam. *Universal statistics of competition in democratic elections,* Phys. Rev. Lett. 134, 017401 (2025)

3. **Ritam Pal**, Aanjaneya Kumar, M. S. Santhanam. *Voter turnout govern key electoral statistics,* ArXiv preprint arXiv:2501.01896 (2025)

Contents

CHAPTER 1

Statistical Physics of Collective Decision-Making

Society is among nature's most intricate complex systems – a vast ensemble of interacting individuals whose collective behaviors emerge across multiple scales, from ephemeral digital trends to enduring democratic institutions. The emergent properties arising from these interactions often manifest as non-trivial macroscopic patterns that cannot be easily inferred from individual behaviors [1]. This thesis employs tools from statistical physics, network science, and dynamical systems to investigate two fundamental aspects of collective public opinion: polarization in social networks and universal patterns in democratic elections. Through this examination, we demonstrate that randomness, properly understood and harnessed, serves as both an explanatory principle and an intervening force for understanding and improving such social systems.

1.1 Complex Systems Framework for Social Dynamics

Human society operates across extraordinarily diverse scales, both spatial and temporal. Spatially, interactions span from local communities to global networks, encompassing physical proximity interactions and increasingly, technology-mediated connections that transcend geographic constraints [2]. Temporally, processes range from millisecond-scale information transmission to decade-spanning political movements and generational cultural shifts. This multi-scale nature creates layered feedback mechanisms that make social systems resistant to reductionist analysis.

Consider how a single tweet can trigger cascading reactions across millions of users within minutes, while simultaneously contributing to slowly evolving cultural narratives that unfold over years. These cross-scale interactions create feedback loops where macro-level structures shape individual behaviors, which in turn reshape those very structures – a dynamic reminiscent of how atoms collectively determine the properties of materials, which then constrain atomic movement.

Within this complex landscape, opinion formation and electoral processes represent critical mechanisms through which individuals collectively navigate their shared environment. These processes share common features with physical systems that have long been studied using sta-

tistical mechanics – they involve numerous interacting components, exhibit emergent behaviors, and often display robust statistical regularities despite their apparent complexity [3, 4]. However, they also present unique challenges: human agents possess agency, adaptability, and strategic behavior absent in physical particles.

The statistical physics approach to social dynamics leverages powerful analytical tools developed for understanding physical systems while acknowledging these distinctive features of social interactions. This approach focuses not on predicting individual behavior but on identifying statistical patterns that emerge at the population level, along with the mechanisms that generate them. The value of such an approach lies in its ability to abstract away unnecessary details while preserving essential dynamics that govern system behavior.

1.1.1 Opinion Dynamics and Polarization Models

The study of opinion formation has long fascinated researchers across disciplines, from sociology and political science to statistical physics. From a physics perspective, opinions are viewed not as fixed attributes of individuals, but as dynamic variables that evolve through social interactions, akin to spins in an interacting many-body system.

One of the earliest formal frameworks for understanding how opinions evolve in groups is the DeGroot model [5]. In this model, individuals iteratively update their beliefs by taking weighted averages of their neighbors' opinions. Under suitable connectivity and weight conditions, this process can lead to convergence to a shared opinion – making it a useful null model for how information may flow and aggregate in a connected population. Its appeal lies in its mathematical tractability and clear interpretation of consensus as an emergent group belief. The DeGroot model also serves as a foundational reference point for later models that incorporate more complex social dynamics.

Building upon this, various models grounded in the framework of interacting particles have been proposed. The voter model [6, 7] is one of the simplest such models, where each individual (or "agent") randomly adopts the opinion of a randomly chosen neighbor. Despite its simplicity, the voter model captures the stochastic nature of opinion change and predicts consensus under certain conditions, although the time to reach it can be long and depends heavily on system size and dimensionality.

Another influential model is the Sznajd model [8, 9], which introduces a more structured social mechanism. In this model, a pair of neighboring agents sharing the same opinion can convince their neighbors to adopt it. This local group influence mechanism reflects the notion of social reinforcement: people are more likely to adopt an opinion when they observe agreement among their peers. In closed systems, the model leads either to complete consensus or to persistent disagreement, reflecting the possibility of both dictatorship and stalemate.

At their core, these models capture a fundamental insight: opinions evolve through social influence. Much like how particles exchange momentum upon collision, individuals adjust their beliefs based on those around them. The underlying assumption in these early models is that interactions gradually reduce opinion differences, thereby pushing the system toward consensus.

However, real-world observations often contradict this outcome. Empirical studies have shown that, especially on controversial topics, opinion distributions tend to become bimodal or polarized rather than convergent [10–12]. This mismatch has led to the development of more nuanced models that incorporate features of human psychology and social behavior.

One such model is the Axelrod model for cultural dissemination [13], which represents individuals as vectors of cultural features. Interaction is more likely between individuals with similar traits (homophily), and interactions can lead to greater similarity. Interestingly, while the model allows for local convergence of opinions, it also frequently results in global polarization – regions of cultural similarity that resist further assimilation. This is a direct consequence of homophily inhibiting interaction between dissimilar groups.

Another class of models that captures the emergence of persistent disagreement is the family of Galam models [1, 3, 4, 14]. These models simulate group discussions and majority rule decision-making, often in small, randomly formed groups. Notably, they can account for the influence of stubborn minorities or inflexible agents who never change their opinion. These agents play a critical role in maintaining polarization and even swaying majority opinions under certain conditions [15–17]. Galam's work demonstrates that the presence of even a small fraction of such agents can lead to surprising macroscopic consequences.

Similarly, bounded confidence models [18, 19] extend the idea of social influence by assuming that individuals only interact with others whose opinions lie within a certain confidence interval. These models are capable of generating a rich variety of opinion distributions – ranging from con-

sensus to bimodal or multimodal clusters – depending on the initial distribution and confidence bounds. Such models reflect the psychological tendency of people to avoid engaging with views they find too extreme or unfamiliar.

As the importance of online interaction grew, more recent models began incorporating algorithmic feedback and digital homophily, which are essential in understanding opinion dynamics in social media settings. A significant development in this direction is the model by Baumann et al. [20], which introduces social influence, homophily, and a simple algorithmic recommender mechanism. Their model reproduces empirically observed features of online polarization, such as the emergence of echo chambers, opinion clusters, and persistent active extremists.

This new generation of models reflects a growing awareness that digital technologies are not neutral platforms but active mediators of opinion dynamics. Empirical evidence of echo chamber effects has been documented across multiple platforms like Facebook and Twitter [21–24]. These studies show that people tend to be exposed predominantly to views that align with their own, a phenomenon often reinforced by engagement-maximizing recommendation algorithms.

Building on these insights, a handful of models have begun explicitly modeling the platform-level mechanisms behind polarization. For instance, Baumann et al. [25] explore how ideological polarization can arise even when users initially have moderate opinions, due to interaction rules and feedback effects. Similarly, models in [26, 27] study how features such as link recommendations, selective unfollowing, and peer reinforcement accelerate the divergence of opinions and lead to fragmented public spheres.

Traditional models from statistical physics primarily predict convergence toward consensus. However, they fail to capture the persistent and often deepening polarization observed in the real world. The incorporation of psychological realism (e.g., homophily and bounded confidence), network effects, and algorithmic feedback mechanisms has allowed newer models to qualitatively reproduce phenomena such as echo chambers, ideological segregation, and the proliferation of extreme views. Together, these models serve as a vital toolbox for both interpreting observed social patterns and exploring potential interventions to mitigate harmful polarization.

1.1.2 Mitigating Polarization in Digital Networks

While diversity of opinion is essential for a healthy public sphere, extreme polarization can lead to structural fragmentation in social networks [28]. As individuals increasingly cluster into like-minded groups, network segregation emerges, restricting the pathways through which information can spread. This hampers exposure to diverse viewpoints at the individual level and limits the potential for shared understanding at the societal level – undermining the common factual basis required for informed collective decision-making.

A closely related phenomenon is that of echo chambers, where individuals are primarily exposed to information that reinforces their existing beliefs. Empirical studies show that such environments can sustain misinformation for longer periods than more open networks [29, 30]. Echo chambers function as self-contained information loops, where content circulates within a closed group with limited external input. As a result, individuals in such environments become increasingly resistant to alternative perspectives, making opinion shifts rare and depolarization more difficult.

This feedback-driven isolation is not merely a passive outcome of individual preference; it is actively shaped by the design of online platforms. Recommendation algorithms, optimized to maximize engagement, tend to connect users with similar views and promote content that aligns with their prior preferences. Over time, this reinforces belief homogeneity and deepens polarization. While the tendency to engage with like-minded others (homophily) is a well-known social bias, the algorithmic amplification of this tendency leads to structurally entrenched echo chambers.

These challenges necessitate careful consideration of intervention mechanisms. From a systems perspective, one can think of these interventions as analogous to controlled perturbations in physics – small, targeted changes introduced to study or steer the evolution of a complex system. The goal in this case is to reduce harmful polarization without compromising autonomy, privacy, or engagement. However, designing such interventions involves a delicate balance. For instance, increasing exposure to opposing views may reduce polarization for some users but provoke backlash or disengagement in others.

Moreover, it is not clear what constitutes a “healthy” distribution of opinions. While consensus may not be realistic or even desirable, excessive clustering around ideological extremes poses

risks to deliberative democracy. Interventions must therefore be guided not only by empirical findings but also by normative considerations – ensuring that diversity, openness, and informed disagreement are preserved.

The persistence of polarization in digital spaces – especially on controversial topics – raises the question of whether debate and interaction inevitably lead to further division. Yet, most models suggest that polarization emerges not from interaction per se, but from the selective nature of interaction – particularly when it is confined to ideologically similar peers. This insight opens up the possibility for counteracting mechanisms. For example, algorithmic strategies could be redesigned to promote diverse but non-antagonistic exposure, enabling opinion adjustment without confrontation.

Overall, addressing polarization and echo chambers requires a shift from treating online networks as neutral infrastructures to understanding them as active mediators of social dynamics. Intervening in such systems must be grounded in both rigorous modeling and empirical validation, with a recognition that the solution space is constrained by competing goals: reducing polarization, protecting autonomy, preserving engagement, and safeguarding democratic values.

1.2 Electoral Systems and Statistical Patterns

Electoral processes represent a formalized mechanism through which individual preferences aggregate to produce collective decisions. They are episodic events that condense the ongoing, often diffuse, processes of opinion formation into measurable outcomes. These outcomes – election results – are shaped by a multitude of interacting individual decisions made simultaneously across a population, and have the potential to substantially influence the structure and direction of governance.

Elections, the cornerstone of democratic societies, are often regarded as unpredictable due to the complex interactions that shape them at various scales – ranging from individual voter preferences to institutional rules and social influences. Democratic elections constitute some of the most extensively documented instances of large-scale collective human behavior, with records spanning decades, encompassing diverse electoral systems, and involving hundreds of millions of voters across varying geographies and time periods.

One of the central tenets of democratic systems is that governance must rest on a represen-

tation of the collective will of the citizens. The institution of elections is key to the operational success of this principle. Elections to public office remain among the clearest expressions of collective decision-making by human populations. Their outcomes are determined by multiple interacting agents – voters, candidates, parties – distributed across a range of spatial and temporal scales. These features make elections a fertile testing ground for tools from statistical physics, whose key lesson is that a multitude of complex interactions between microscopic units of a system can manifest into robust, *universal* behavior at a macroscopic level [31–43]. Classical examples of such emergent macroscopic features include ideal gases or magnetic materials composed of many interacting particles [44], as well as large-scale phenomena like earthquakes [45, 46] and financial market crashes [47]. In the context of elections, identifying such universal patterns can help distill the complexities of electoral dynamics into simplified, interpretable models, and may provide benchmarks for evaluating the integrity and competitiveness of electoral systems.

1.2.1 Universal Statistical Patterns in Elections

Given these features, the possibility of discovering universal statistical patterns in elections has attracted sustained interest from physicists, political scientists, and data scientists alike [48–54]. These efforts often focus on two core quantities: the distribution $q(\sigma)$ of vote shares σ obtained by candidates, and the distribution $g(\tau)$ of voter turnout τ across electoral units. The former captures the spread of popularity among competing candidates, while the latter reflects the scale of participation.

Studies have found that under certain conditions – such as elections conducted within the same country or using similar electoral protocols – both $q(\sigma)$ and $g(\tau)$ can show recurrent statistical features across different election years and regions [48–50]. For instance, Fornari and Castellano [49] analyzed vote-share distributions and showed consistent scaling across different Italian municipal elections. Similarly, in the case of Brazilian elections, Borghesi and Bouchaud [50] reported universal features in turnout distributions, noting similarities with models of self-organized criticality.

However, subsequent analyses have identified notable departures from these claimed universalities. Deviations arise especially in cross-country comparisons, where differences in electoral institutions, district sizes, the role of political parties, and sociopolitical contexts introduce vari-

ability [53, 55–58]. For example, Kalampokis et al. [55, 56] highlighted the absence of consistent scaling laws in many European elections, pointing to the non-trivial influence of contextual variables such as multi-party dynamics, compulsory voting laws, and heterogeneous district sizes. In some cases, the assumption of universality was undermined by methodological issues such as inconsistent normalization, aggregation biases, or limitations in data availability.

Furthermore, while spatial correlations in voting behavior – where neighboring regions exhibit similar turnout or candidate preference – have been observed [59–62], these too tend to be context-dependent. For example, the strength and scale of such correlations differ markedly between urban and rural areas or between centralized and decentralized political systems. The presence of geographic and cultural clustering, media bubbles, and partisan strongholds all contribute to the diversity of outcomes.

Despite extensive efforts and the growing availability of high-resolution election data, the field has yet to identify a robust, reproducible universal behavior that holds across multiple countries, election types, and spatial scales. This lack of a well-validated, generalizable statistical pattern in election outcomes – particularly one that connects microscopic behavior (individual voter choice) to macroscopic observables (outcome distributions) – represents a key open challenge in the statistical study of elections.

1.2.2 Electoral Competitiveness Metrics

Among the many statistics of interest, the *margin of victory* – defined as the difference in vote share between the top two candidates in a constituency – encapsulates critical information about the competitiveness of elections. Prior studies have examined margins from political and computational perspectives, often in the context of electoral reform, redistricting, and prediction [63–68]. However, most of these analyses treat margins as independent indicators, rarely exploring their joint distribution with turnout.

Our empirical analysis, drawing on large-scale election data from 34 countries across six continents and multiple decades [69–72], reveals a strong correlation between margins of victory and voter turnout. This insight further helps us to discover a scaled measure of electoral competition which follow a universal distribution.

1.3 Thesis Structure and Contributions

The thesis proceeds through several interlinked investigations to uncover the dynamics and statistics of public opinion.

Chapter 2 introduces and optimizes the "random nudge" intervention strategy against digital polarization. Building on our understanding of opinion dynamics, we demonstrate how carefully calibrated random interventions can counteract the reinforcement mechanisms that drive polarization without compromising system integrity.

Chapter 3 details extensive data collection and curation efforts, laying the empirical foundation for electoral analysis. This chapter bridges theory with real-world observation, establishing the robust dataset necessary for testing universal patterns.

Chapter 4 explores and empirically validates the universality in scaled margin-to-turnout ratios across multiple electoral systems. We demonstrate how properly normalized electoral statistics reveal striking patterns across diverse democratic contexts.

Chapter 5 develops the Random Voting Model (RVM), analytically deriving and validating predictions against extensive electoral data. This model demonstrates how stochastic processes, properly understood, can capture essential features of complex social decision-making.

Chapter 6 further explores the Random Voting Model to predict several other key electoral statistics, with a focus on the Indian context. This extends our theoretical framework to additional empirical tests, strengthening the potential of the model.

Chapter 7 demonstrates some practical applications, from intervention design to detecting electoral malpractices. Here, we translate theoretical insights into pragmatic tools for improving social systems.

Chapter 8 provides a comprehensive discussion synthesizing our findings across both opinion dynamics and electoral patterns, offering broader implications and future research directions.

Having established the foundational context, we now embark on our first critical inquiry – designing an effective intervention to mitigate online polarization through strategic randomness.

CHAPTER 2

Random Nudge: A Strategic Intervention for Digital Polarization

In the previous chapter, we established the motivation for understanding complex societal phenomena through the lens of statistical physics. We now shift our focus towards a specific challenge of the digital age: the polarization of opinions in online social networks. In this chapter, we will introduce and analyze a novel intervention strategy – the "random nudge" – that can effectively reduce polarization without causing undesirable side effects.

2.1 Opinion Dynamics in Digital Social Networks

Having examined the broader landscape of opinion formation in Chapter 1, we now focus on developing tangible solutions to the polarization challenge. As previously established, the empirically observed bimodal opinion distributions and the formation of echo chambers represent significant challenges in modern digital environments. These patterns resist the consensus predictions of traditional opinion dynamics models and create self-reinforcing information silos that impede healthy discourse.

Building on the foundation of existing models, we will adapt a recently introduced framework that successfully captures key empirical features of online opinion dynamics, including polarization, echo chambers, and the tendency for more active users to hold stronger opinions. This model provides an ideal testbed for exploring intervention strategies aimed at reducing harmful polarization.

The central question we address is whether a minimal intervention can effectively disrupt the reinforcement cycles that drive polarization without compromising individual agency or platform engagement. Specifically, we will demonstrate that a carefully calibrated "random nudge" can achieve substantial depolarization while avoiding the pitfalls of radicalization.

While Chapter 1 provided a comprehensive review of opinion dynamics models, we'll focus here on the specific framework that will enable us to test our intervention strategies. Of particular

relevance is the model introduced by Baumann et al. [20], which successfully captures key empirical features observed in online social networks: polarized opinion distributions, echo chamber formation, and the tendency for more active users to hold more extreme opinions. This model demonstrates how homophilic interactions – the preference to connect with those holding similar opinions – naturally lead to polarized states even from initially diverse opinion distributions.

Our intervention approach is motivated by the underlying mechanism of polarization: the reinforcement of opinions through homophilic interactions. We hypothesize that by strategically disrupting this reinforcement cycle, we can achieve depolarization. Specifically, we introduce a "random nudge" intervention that exposes agents to more diverse opinions. Through simulation and analysis, we will demonstrate that this approach can effectively break echo chambers when calibrated appropriately.

However, our findings also reveal an important caution: excessive intervention can lead to radicalization [73, 74] – a state where all agents adopt the same stance on an issue. This creates a delicate optimization problem: finding the precise intervention strength that reduces polarization without triggering radicalization. We will formulate and solve this optimization problem to compute the optimal nudge parameters for achieving a healthier opinion distribution.

2.2 Theoretical Framework: A Model of Opinion Dynamics

Having identified our approach, we now provide a detailed mathematical formulation of the opinion dynamics model that will serve as our experimental testbed. We adapt the framework introduced by Baumann et al. [20], which allows us to rigorously analyze how interventions affect the evolution of opinions in digital social networks.

2.2.1 Opinion Dynamics Framework and Formulation

The model has N interacting agents, and it is assumed there are only two possible sides to an issue. This is typical of many, but not all, issues – for example, to allow abortion or not. Opinion on a given issue is denoted by x_i, which can take any real value in the range $(-\infty, \infty)$. The sign of the x_i corresponds to the stance of the agent in the corresponding issue, and $|x_i|$ denotes the conviction of the agent in their respective stance. This implies that the larger the value of $|x_i|$, the more extreme the agent's opinion is.

The model used to capture the evolution of opinion is activity driven [75–78], *i.e.*, at each time step, only active agents can influence other agents. Based on empirical data [75, 77], the distribution of agent's activity is described as,

$$F(a) = \frac{1-\gamma}{1-\varepsilon^{1-\gamma}} a^{-\gamma}, \tag{2.1}$$

where a is the activity, ε is the minimum activity (chosen in this work to be 10^{-2}), and γ controls how steep the function $F(a)$ which is chosen to be 2.1.

In simpler terms, this activity distribution means that most agents have low activity levels (they rarely post or interact), while a few agents are highly active (frequent posters) – similar to what we observe in real social media platforms, where a small percentage of users generate the majority of content.

Agents' opinions evolve based on their interactions with other agents, and this information is encoded in the time-dependent adjacency matrix $A_{i,j}(t)$. Further, opinion evolution also depends on the strength of social interaction $K > 0$ and the controversialness of the issue $\alpha > 0$. The opinion dynamics is given by the following N coupled differential equations [20]

$$\dot{x}_i = -x_i + K \left(\sum_{j=1}^{N} A_{ij}(t) \tanh\left(\alpha x_j\right) \right). \tag{2.2}$$

To understand this equation intuitively, an agent's opinion (x_i) changes based on two opposing forces – a natural tendency to moderate their view over time (the $-x_i$ term), and the influence from other agents they interact with (the sum term). The parameter K determines how much weight social influence has compared to the natural moderation tendency. While people with extreme opinions have a stronger influence than moderately opinionated ones, the $\tanh$ function ensures the social influence of each person is limited between -1 and 1

In this, $A_{i,j}(t)$ is the temporal adjacency matrix of interaction at time t. If at time t agent j influences agent i, than $A_{i,j}(t) = 1$, and $A_{i,j}(t) = 0$ otherwise. If agent i is active at time t, they will interact with m other agents, weighted by the probability $P_{i,j}$.

Further, the probabilistic reciprocity factor $r \in [0, 1]$ determines the chance that an interaction is mutually influential, *i.e.*, $A_{ij}(t) = A_{ji}(t) = 1$. The interaction probability is defined to be a

function of the magnitude between two agents' opinions.

$$P_{ij} = \frac{|x_i - x_j|^{-\beta}}{\sum_k |x_i - x_k|^{-\beta}}, \tag{2.3}$$

where β is the homophily factor which quantifies the tendency for agents with similar opinions to interact with each other: $\beta = 0$ refers to the absence of interaction preference, and $\beta > 0$ implies that the agents with similar opinions are more likely to interact with one another. Evidently, Eq. (2.3) is modeled as a power-law decay of connection probabilities with only a small chance for agents with opposite opinions to interact. Since most of the interactions tend to occur between agents with similar opinions, this can lead to the formation of echo chambers.

This homophily equation captures the tendency we observe in real life: people prefer to interact with those who share similar opinions. The higher the β value, the stronger this tendency – representing how we might naturally gravitate toward content and people who reinforce our existing views, creating "filter bubbles" or echo chambers.

2.2.2 Three Fundamental Opinion States

Now that we have established the mathematical foundation of our model, we can examine the emergent collective behaviors that arise from these individual interactions. Depending on the strength of social interaction (K) and the homophily factor (β), the model exhibits three distinct steady states that closely resemble opinion distributions observed in real-world scenarios.

The interaction dynamics in the model is enforced by the activity-driven temporal network that is fully encoded by the parameters $(\varepsilon, \gamma, m, \beta, r)$, together with the parameters that characterises the issue, (K, α). Asymptotically, this model features three distinct states in the distribution of opinions. If the Social interaction K is sufficiently small, then the opinion of every agent decays to zero, and this state is known as the neutral consensus state. This is demonstrated in panel (a) of Fig. 2.1. However, if social interaction K is large but the homophily factor β is small, then due to statistical fluctuations, all the opinions either become positive or negative. This state, where each agent has the same stance (the sign of x_i for all i is the same) with possibly different convictions, is called radicalization. It is important to note that radicalization is an absorbing state of this model. This is because when all agents have opinions with the same sign, the dynamics does not allow for a sign-change of any agent's opinion. The most interesting case emerges when social

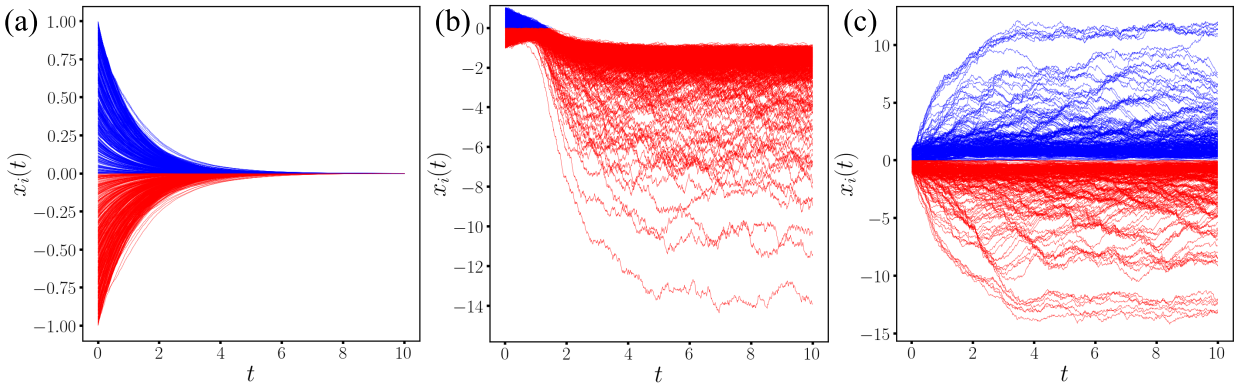

Figure 2.1: Opinion trajectories, illustrating the three fundamental states of opinion dynamics. Panel (a): The consensus state, characterized by all agents converging to neutral opinions (near zero) in the absence of strong social interaction. Panel (b): The radicalization state, where all agents adopt the same stance (all negative opinions, in this case) with varying degrees of conviction. Panel (c): The polarized state, where the population is split evenly between positive and negative opinions, with a very few neutral opinionated agents.

interaction K and homophily factor β are large enough. In this case, a meta-stable polarized state emerges, which is characterized by a bimodal opinion distribution. The opinion trajectories, in panels (b) and (c) of Fig. 2.1, depict such radicalized and polarized states, respectively.

2.2.3 Polarization Measurement Metrics

Before we delve into the details of the intervention strategy and results, we discuss the three quantities employed to measure the degree of polarization based on the opinion distribution $P(x)$. They are defined as: (a) Polarization is measured through $\bar{\Delta}$, defined as the distance between the average of positive opinions and the average of negative opinions. (b) When opinion distribution exhibits a bimodal character, the distance between the two peaks, denoted by Δ_{peak}, can also be used as a measure of polarization [79]. (c) A gross measure of polarization could also be the standard deviation σ of the entire opinion distribution [26]. Fig. 2.2 illustrates the schematics of all three measures of polarization. It must be noted that if polarization decreases due to the intervention proposed in Eq. (2.4), ideally, all these three quantifiers must decrease.

These measures have practical applications in analyzing real-world opinion data. For example, $\bar{\Delta}$ can be calculated from survey data where respondents rate their agreement with statements on a numerical scale. In social media analysis, Δ_{peak} might be observed in the distribution of sentiment scores on controversial topics, where comment sentiment often clusters around two

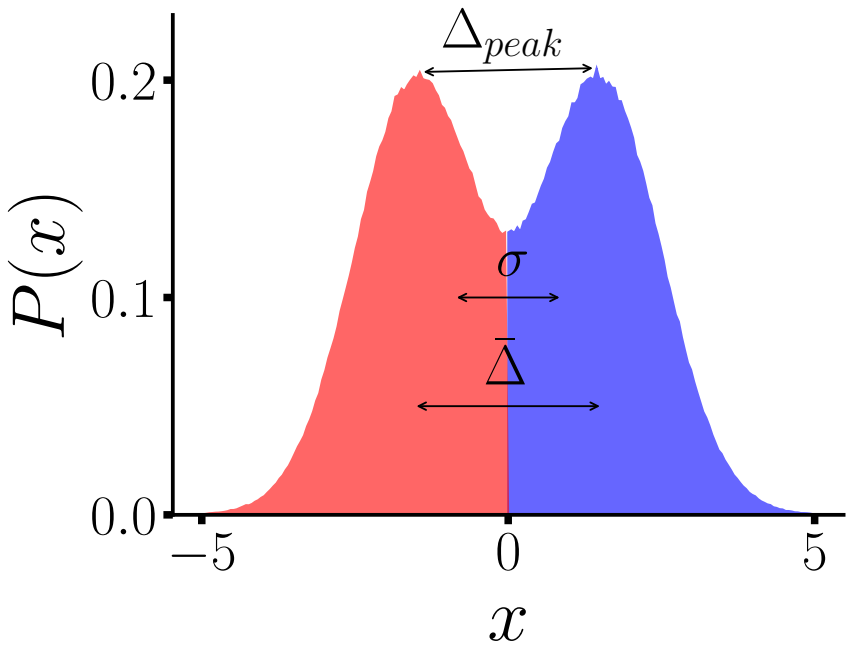

Figure 2.2: Schematic illustration of three complementary measures of polarization used in this study. $\bar{\Delta}$ (left) represents the distance between mean positive and negative opinions, capturing the average separation between opposing groups. Δ_{peak} (center) measures the distance between the two peaks in a bimodal opinion distribution, highlighting the gap between the most common opposing viewpoints. σ (right) denotes the standard deviation of the entire opinion distribution, quantifying the overall spread of opinions across the population. All three metrics decrease when polarization is successfully reduced.

opposing positions. The standard deviation σ is particularly useful when analyzing large-scale data from platforms like Twitter or Reddit, where the full spectrum of opinions can be mapped and quantified.

Importantly, these metrics capture complementary aspects of polarization. $\bar{\Delta}$ focuses on the "distance" between opposing groups, Δ_{peak} highlights the most prominent opinion clusters, while σ measures the overall spread regardless of modality. By tracking all three simultaneously, we can distinguish between different types of opinion shifts – for instance, distinguishing between genuine depolarization versus a shift where opinions remain far apart but become less concentrated around specific values.

2.3 Random Nudge Intervention Strategy

Having established the model dynamics and identified how polarization emerges and can be measured, we now turn our attention to a key question: How can we effectively counter the formation of echo chambers and reduce polarization in online social networks?

2.3.1 Echo Chamber Formation Mechanisms

Echo chambers are increasingly becoming more apparent in online social media platforms. These self-reinforcing information environments arise from two primary mechanisms:

- First, there is our natural tendency toward homophily – we prefer to interact with people who hold similar opinions to our own. In our model, this is captured by the homophily factor β, where larger values represent more closed and isolated echo chambers.
- Second, this natural tendency is often amplified by recommendation engines on social media platforms. These algorithmically driven systems recommend similar connections or content to keep users engaged, inadvertently strengthening opinion bubbles.

The challenge lies in developing interventions that can effectively disrupt these echo chambers while simultaneously maintaining user engagement on the platforms and respecting user privacy and preferences. Such interventions should ideally not require knowledge of users' specific opinions and should create sustainable diversity rather than just temporary exposure to different viewpoints. This is a delicate balance to achieve in practice.

2.3.2 The Random Nudge Mechanism

To address these challenges, we propose a simple yet powerful intervention strategy – the "random nudge." The core principle is introducing a controlled amount of randomness into user interactions:

With probability p (where $p < 1$), active agents will interact uniformly with any other agents in the network, regardless of opinion similarity. With the complementary probability $(1 - p)$, interactions proceed according to the normal homophily-based probability given in Eq. (2.3).

This approach offers several advantages over more direct interventions. It preserves privacy since it requires no knowledge of agent opinions or beliefs. The intervention strength can be

precisely controlled by adjusting the parameter p, allowing for fine-tuning based on the specific context. Additionally, it maintains the platform's engagement-driven structure while introducing just enough diversity to prevent echo chamber formation. Perhaps most importantly, it creates natural opportunities for cross-opinion exposure without forcing specific content on users, which could lead to disengagement or reactance.

2.3.3 Mathematical Implementation

We implement this random nudge by modifying the interaction probability as follows:

$$\widetilde{P}_{ij} = p \times \frac{1}{N-1} + (1-p) \times P_{ij}. \tag{2.4}$$

The first term represents the uniform random interaction (each agent has equal probability $\frac{1}{N-1}$ of interacting with any other agent), while the second term preserves the homophily-driven interactions proportional to the original P_{ij}. The parameter p controls the strength of the intervention – higher values introduce more randomness, while values closer to zero preserve more of the natural homophily-driven structure.

This modified interaction probability is used for all subsequent simulations presented in this chapter. As we will demonstrate, even small values of p can lead to dramatic reductions in polarization and the breakdown of echo chambers.

2.4 Intervention Results and Analysis

With the intervention strategy introduced in Sec. 2.3, we find that with sufficiently small random nudge probability p, significant depolarization can be obtained, which is evident as the opinion distributions approach towards a unimodal distribution along with the decay of all three measures of polarization. To see the effects of nudge, we perform numerical simulations of the basic model in Eq. (2.2) using the interaction probability given in Eq. (2.3) and the intervention model in Eq. (2.4). The simulations are performed with $N = 5000$ agents for 1000 time steps with $dt = 0.01$. At initial time x_i is uniformly chosen from a small interval, *i.e.*, $x_i \in [-1, 1]$ for $i = 1, 2 \ldots N$. The model parameters are chosen to be $\alpha = 3$, $\beta = 3$, $K = 3$, $m = 10$, $\gamma = 2.1$, $\varepsilon = 0.01$ and $r = 0.5$ for all the simulations unless mentioned otherwise. The parameters chosen for the simulations lead to a polarized state in the original model without intervention. Our

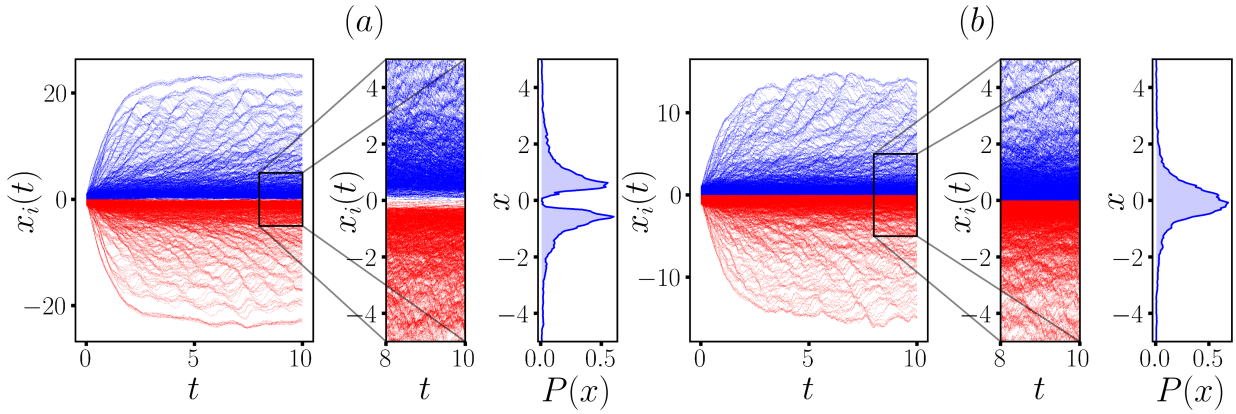

Figure 2.3: Visualization of opinion trajectories and resulting distributions with and without the random nudge intervention. (a) Without nudge ($p = 0$): Opinion trajectories show clear divergence, avoiding the moderate region around $x = 0$ (shown in the magnification). The resulting distribution (right panel) is distinctly bimodal, indicating strong polarization with few moderate opinions. (b) With a small nudge ($p = 0.01$): Opinion trajectories show significant crowding around $x = 0$ (magnification), leading to a nearly unimodal symmetric distribution (right panel). This demonstrates how even a minimal random intervention can substantially reduce polarization by promoting moderate viewpoints.

analysis reveals several key insights into how small perturbations can lead to significant changes in collective behavior patterns.

2.4.1 Depolarization Effects

In Fig. 2.3, we show the contrast between the trajectories of individual opinions and the opinion distribution with and without the application of a nudge. In the absence of nudge ($p = 0$), the simulation results in Fig. 2.3(a) show fewer trajectories with opinions $x_i \approx 0$. This leads to a bimodal distribution of opinions characteristic of a polarized state. In contrast, in Fig. 2.3(b), a small nudge with a probability of $p = 0.01$ is applied, and we find significantly more trajectories with moderate opinions. This, effectively, is seen to lead to an absence of polarization, which is evident from the unimodal opinion distribution. The magnifications of the region around $x_i = 0$ and its distribution (shown in Fig. 2.3) reveal a clear distinction between these two scenarios.

2.4.2 Network Effect: Breaking of Distinct Clusters

To examine the effect of network nudge, we analyze the underlying time-averaged structures of the temporal interactions network. Without nudge, the interaction network has two distinct clusters; most of the connections are among positive opinionated agents or negative opinionated

agents. There exist very few connections between these two groups other than for the agents with extreme opinions. This is expected since the agents with extreme opinions are also those who tend to be more active on social networks fora; hence on average, they form more connections. This enables them to be relatively more connected to the agents with opposing opinions. These results are visually depicted in Fig. 2.4 as two snapshots of evolving network diagrams. If $p = 0$, no nudge is applied. In this case, as Fig. 2.4(b) shows, a polarized network, made up of two distinct blue and red-colored clusters, is formed. Blue color corresponds to nodes with $x > 0$, and red color to $x < 0$. The opinion distribution shown in Fig. 2.4(a) confirms the existence of polarization.

However, when a nudge is applied, even for the case when the nudge probability is as small as $p = 0.01$, we find the network to be well mixed (large blue and red clusters have disappeared) (Fig. 2.4(e)), and this leads to a significantly depolarized state indicated by the approximate unimodality of the opinion distribution as shown in Fig. 2.4(d).

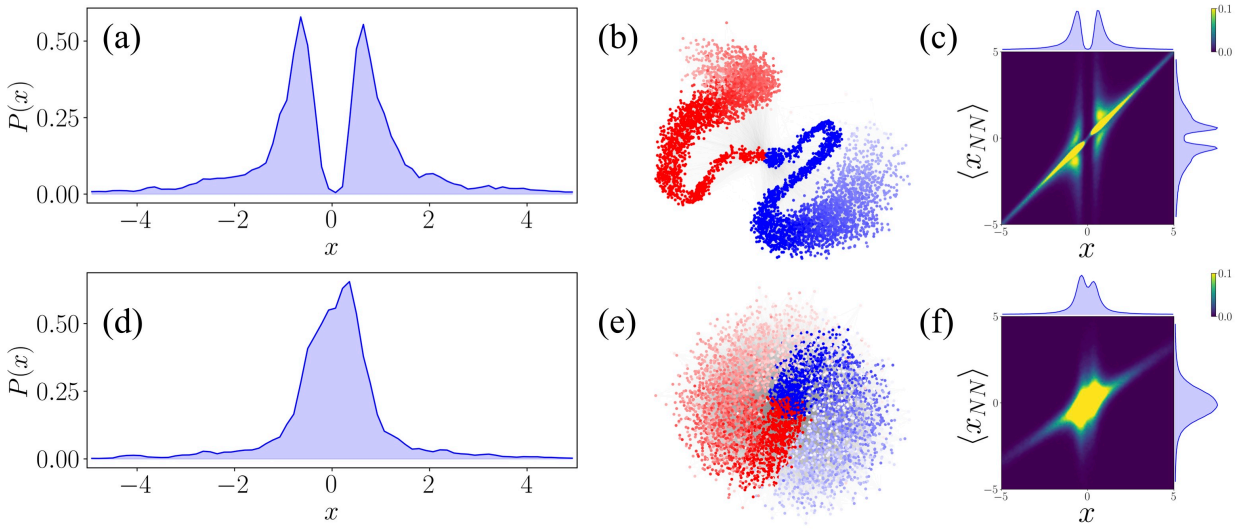

Figure 2.4: Comprehensive analysis showing how random nudges affect opinion distribution, network structure, and echo chamber formation. Top row (a-c): No nudge ($p = 0$) condition showing (a) polarized opinion distribution, (b) segregated network with two distinct clusters (blue nodes for positive opinions, red for negative, with color saturation indicating conviction strength), and (c) two distinct lobes in the heatmap of agent opinions versus their neighbors' mean opinions, confirming strong echo chamber effects. Bottom row (d-f): With nudge ($p = 0.01$) showing (d) depolarized, single-peak opinion distribution, (e) well-mixed network without clear clustering, and (f) single-lobed heatmap confirming the successful weakening of echo chambers. This demonstrates how a small intervention in connection patterns can fundamentally alter the macro-level opinion landscape.

The term echo chamber describes a situation where the beliefs or opinions of people are reinforced by interactions among a closed group of people who hold similar opinions. In recent years, this has been widely discussed in the context of online communities [21–24]. However, some studies appear to suggest that the effects of echo chambers are overestimated [80]. To infer the presence of echo chamber-type effects, we calculate the average opinion of the nearest neighbors (NN) of each agent [20, 24]. This is denoted by

$$\langle x_{NN} \rangle = k_i^{-1} \sum_j a_{ij} x_j, \quad \text{and} \quad k_i = \sum_j a_{ij}, \tag{2.5}$$

where a_{ij} is the temporally aggregated (over the last 100 time-steps) adjacency matrix. When a nudge is not applied ($p = 0$), a colored heatmap of x and $\langle x_{NN} \rangle$, in Fig. 2.4(c) reveals two disjoint hot spots corresponding to the two distinct echo chambers. And we find a strong bimodality in the marginal distributions. Now, when we apply a nudge with probability $p = 0.01$, we can observe only one hot spot indicating the existence of only one closed group (Fig. 2.4(f)). All the agents are inside this closed group, and the echo chamber effect is largely diluted or non-existent. We did not find perfect unimodality in the marginal distribution of x, which can be attributed to the fact that different realizations can lead to either of these three distributions: (a) slight bimodal distribution with significant reduction in all three polarization parameters, (b) unimodal distribution with a slight skew towards positive opinions and (c) similar distribution with a skew towards negative opinions. As the heat maps and the marginal distributions are created from data averaged over 200 realizations, all the above factors contribute to the slight bimodality in the marginal distribution of x. Nevertheless, the marginal distribution corresponds to a signification reduction in polarization and echo chambers.

2.4.3 Quantitative Depolarization Analysis

To obtain a global picture of how depolarization sets in as a function of nudge probability p, we plot the three measures of polarization as a function of p. All three measures, $\bar{\Delta}, \Delta_{peak}$ and σ, have been computed from the simulation results. The results shown represent an average over the last 100 time steps of the simulations and averaged over 200 realizations. In Fig. 2.5, we observe that all three measures of polarization decrease as the strength of the nudge p increases. In particular, $\bar{\Delta}$ and σ are found to decrease as a stretched exponential function $\exp(-p^\gamma)$, and

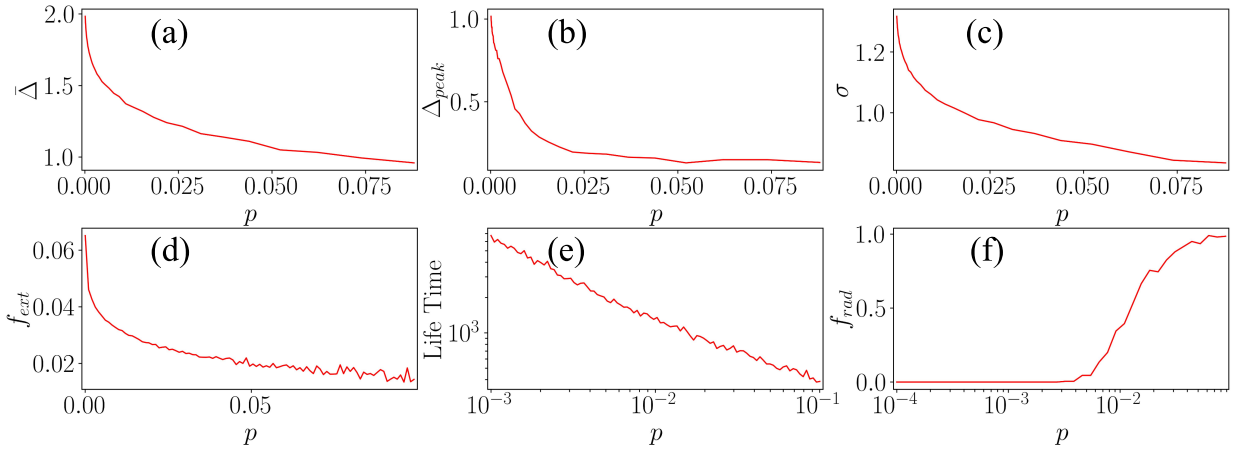

Figure 2.5: Quantitative analysis of polarization measures as functions of nudge strength p. (a-c) Three measures of polarization: (a) $\bar{\Delta}$ (distance between mean opinions), (b) Δ_{peak} (distance between peaks), and (c) σ (standard deviation of opinions) all decrease with increasing nudge strength, following an approximate stretched exponential decay. (d) The fraction of agents with extreme opinions (f_{ext}) similarly decreases, showing the nudge reduces extremism alongside polarization. (e) The lifetime of polarized states decreases as a power law with increasing nudge strength, indicating faster transitions to the radicalization state. (f) The fraction of simulations resulting in radicalization increases sharply beyond $p \approx 10^{-2}$, revealing the critical threshold where the intervention begins producing undesirable outcomes. All results represent averages over 200 simulations, excluding radicalized cases for panels (a-d).

the stretching factor γ is determined through regression to be approximately 0.3. A recent work studying the depolarization of echo chambers [79] considered adding an effective noise term dependent on a random sample of opinions to Eq. (2.2). While this approach succeeds in making the opinion distribution unimodal, it increases the width of the distribution significantly, which as a consequence, corresponds to an increase in extreme opinions. To quantify the effect of the nudge on the extreme opinions, we define f_{ext} as the fraction of agents with conviction $|x| > x_{th}$, where x_{th} is a positive threshold. And indeed our framework of nudging the mechanism of forming social connections in online interactions works well in decreasing width of the opinion distribution (Fig. 2.5 (c)) as well as extreme opinions (Fig. 2.5 (d)) and also suggests direct algorithmic interventions for recommender systems. In the original model, the authors found the polarized state to be meta-stable and showed that with an increased value of β, the lifetime of the state has a faster than exponential growth. Our intervention adds more randomness to the system and increases statistical fluctuations. Hence, for large p, we observe a drastic decrease in the average lifetime of the polarized and depolarized states. An approximate straight line in the log-log plot indicates

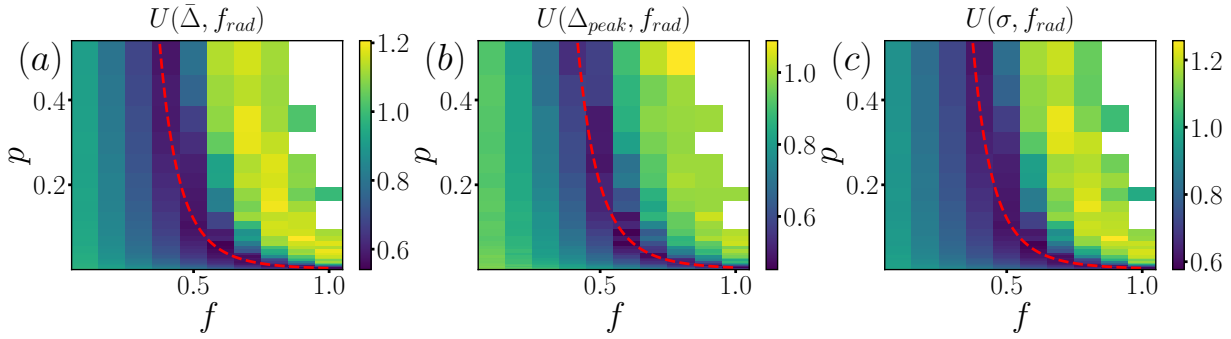

Figure 2.6: Optimization analysis for balancing depolarization against radicalization risk. The heatmaps show utility values (combining polarization reduction and radicalization avoidance) as functions of nudge strength p and population fraction f being nudged. Panels (a), (b), and (c) correspond to utilities based on $\bar{\Delta}$, Δ_{peak}, and σ measures respectively. The red dashed curves, following $p \cdot f^A = B$ (where A and B are constants), indicate the optimal parameter combinations that maximize depolarization while minimizing radicalization risk. This analysis provides practical guidance for implementing nudge strategies in real-world systems by showing that nudging a smaller fraction of the population more strongly can be as effective as nudging everyone weakly.

the lifetime of polarized or depolarized states decreases as a power law as nudge strength (p) is increased (see Fig. 2.5 (e)). Fig. 2.5 (f) also captures the same effect as we see that radicalization is either non-existent or a rarity for $p < 10^{-2}$, but it increases quickly and becomes the norm for $p > 10^{-2}$.

2.5 Balancing Depolarization Against Radicalization Risk

In many situations, radicalization is as much undesirable as polarization. Hence, to solve the issue of radicalization at a high value of nudge probability, rather than nudging all the people in the population, at each time step of the simulation, we randomly select f fraction of the population and nudge them. We define a simple linear utility function $U(\bar{\Delta}, f_{rad}) = \tilde{\bar{\Delta}} + f_{rad}$ Where $\tilde{\bar{\Delta}}$ is $\bar{\Delta}$, linearly scaled to be between 0 and 1, and f_{rad} is the fraction of radicalized simulations. The structure of the utility function is the same for the other two measures of polarization.

2.5.1 Optimal Parameter Identification

This utility function represents a fundamental trade-off: we want to minimize both polarization (measured by $\bar{\Delta}$) and the risk of radicalization (f_{rad}). In practical terms, this means finding intervention parameters that create enough opinion diversity to prevent echo chambers, but not so

much randomness that the system tips into a radicalized state.

Fig. 2.6 depicts the heat map of the utility functions corresponding to the three utility functions. The optimal population fraction and nudge probability is numerically found to follow the curve $p \cdot f^A = B$, where A and B are constants.

This power-law relationship reveals an important insight: there's a mathematical trade-off between how many people we nudge (f) and how strongly we nudge them (p). For example, it suggests that nudging 10% of the population with a stronger intervention might be as effective as nudging everyone with a weaker intervention. This finding has significant practical implications for platform design, as it means targeted interventions could potentially be as effective as system-wide changes while requiring less disruption to the overall user experience.

2.6 Cross-Model Validation

To ensure the robustness of our intervention framework, we applied network nudge to another recent model [81] of opinion dynamics, which, together with homophily, exhibits the effect of echo chambers. This validation demonstrates that the random nudge strategy is not limited to a single model but represents a more general principle for disrupting echo chambers across different mathematical frameworks. The dynamics of the model is governed by the following N coupled differential equations:

$$\dot{x}_i(t) = |x_i| \sin\left(x_i^0 - x_i\right) + K \left(\sum_{j=1}^{N} A_{ij}(t) \sin\left(x_i - x_j\right) \right). \tag{2.6}$$

In contrast to the original model [81], the variable x_i is chosen to be the opinions of the people on a single topic, and the temporal adjacency matrix is formed according to homophily probability (2.3). x_i^0 is the initial opinion of agent i, and all the other variables and parameters have the same meaning as in the previous model (2.2). In Fig. 2.7, we show that when the social interaction and the homophily factor are high enough ($K = 4$, $\beta = 4$), many echo chambers are formed, which is clear from the trajectories of the opinion as well as from the multiple communities seen in the aggregated network (Fig. 2.7 (a, b)). But when we introduce a slight nudge ($p = 0.002$), the effect of echo chambers is reduced drastically. The opinion trajectories seem to converge to a moderate value, and the interaction network is well-connected without any obvious segregated communities (Fig. 2.7 (c, d)).

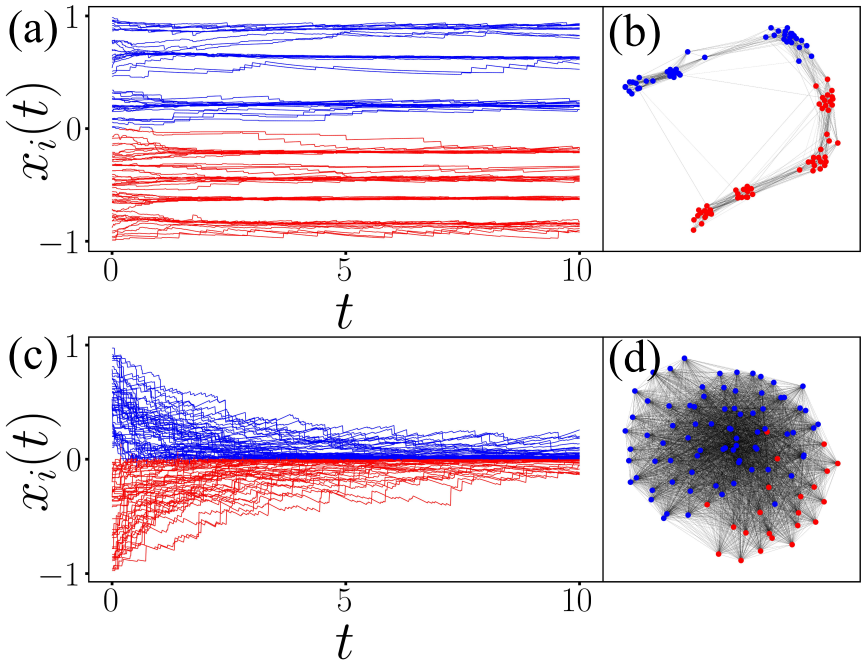

Figure 2.7: Demonstration of the random nudge effectiveness in an alternative opinion dynamics model (Equation (2.6)). (a) Without nudge: Opinion trajectories display multiple stable clusters, showing the formation of several distinct echo chambers. (b) The corresponding interaction network shows clear community structure with limited cross-group connections. (c) With a small nudge ($p = 0.002$): Opinion trajectories converge toward moderate values, showing successful depolarization. (d) The resulting interaction network becomes well-connected without distinct communities. This cross-model validation confirms that the random nudge strategy represents a robust intervention principle applicable across different mathematical frameworks of opinion dynamics.

2.7 Discussion

The widespread use of the internet, and consequently, social media platforms, have drastically altered the way humans consume and interact with information. Polarization and the formation of echo chambers have been shown to negatively impact constructive discussions and debates – two fundamental pillars of a healthy democracy. Building on the recent advances in the modeling of opinion dynamics in social networks, in this work, we study the possibility of depolarizing a population using a stochastic nudge. The implications of our findings extend beyond digital platforms to broader questions about how collective opinions shape societal outcomes and decision-making processes.

Our results suggest that a small number of randomized interactions, which are otherwise dominated by homophily-driven mechanisms, can lead to a significant reduction in polarization.

This reduction was quantitatively captured by three different measures of polarization. While we show that minimal nudges can burst echo chambers and lead to socially desirable distributions of opinions, increasing the strength of this nudge can result in radicalization. Given this sensitivity on the nudge strength, we show that a possible resolution is obtained if, instead of nudging each agent, only a fraction f of the agents are nudged. We highlight that this interplay of the nudge strength p and the fraction f of nudged individuals leads to an interesting optimization problem. This optimization can help inform the fraction of individuals to be nudged for a fixed nudge strength for optimal depolarization.

We believe that the strongest case for the application of such randomized nudges can be made for recommendation systems. While ubiquitous, recommender algorithms are optimized for increasing engagement [82], which we now know can come at the cost of creating echo chambers [83], increase in the representation of extreme ideologies [84], and even the tampering of users' preferences [85]. In such settings, the randomized nudges can be potentially operationalized as the poisoning of a viewer's watch history with a limited amount of random content, uncorrelated with the viewer's preferences [86]. While there are several ethical and legal considerations that must be accounted for before implementing any such interventions, it certainly opens up several interesting avenues for future research to build on. Non-invasive interventions may be important to reduce the detrimental effects of polarization. However, an important first step is to build reliable tools to quantify polarization from data [87], which in itself constitutes an intriguing direction for future research.

The random nudge offers a promising, algorithmically implementable strategy for addressing polarization at the individual level. However, this raises important questions about how individual-level interventions might affect collective decision-making processes. The statistical principles underlying opinion formation and the emergence of consensus or polarization may manifest across different scales of human organization. Understanding these connections becomes particularly relevant when considering how societies make collective choices and how the quality of public discourse influences the outcomes of democratic processes. These insights motivate further investigation into the statistical patterns that govern competitive dynamics in various forms of collective decision-making.

In the next chapter, we will shift our focus from opinion dynamics to electoral systems, exam-

ining empirical data from elections across different countries. While not directly employing the opinion models developed here, the underlying theme of how individual choices aggregate into collective outcomes remains central. By analyzing the statistical patterns in election margin distributions, we will uncover universal properties that emerge across diverse electoral systems. These patterns provide a different but complementary perspective on how collective decision-making processes operate at scale, offering insights into the robustness and predictability of democratic institutions regardless of their specific implementation details.

CHAPTER 3

Electoral Data: Collection and Preparation Framework

In the previous chapter, we explored how random nudges can effectively reduce polarization in online social networks. We now shift our focus to a different but related arena of collective decision-making: democratic elections. Just as individual opinions can aggregate into social patterns, individual votes aggregate into electoral outcomes. Elections represent the ultimate test of democratic opinion dynamics at scale, where millions of citizens express their preferences through a structured process. However, before we can uncover any meaningful patterns or universals in electoral behavior, we must first establish a solid empirical foundation through careful data collection, preparation, and analysis.

3.1 From Opinion Formation to Electoral Analysis

Individual opinions ultimately aggregate into collective choices through elections. While the previous chapter dealt with the dynamics of opinion formation and the potential interventions to mitigate polarization, this chapter focuses on the empirical foundation of electoral analysis. Elections represent the most structured and widespread manifestation of collective decision-making, offering a rich dataset for studying how individual preferences translate into societal outcomes.

The quality of data is paramount for any meaningful electoral analysis. Without robust, comprehensive, and well-curated data, theoretical insights remain untethered from reality. This chapter details our extensive data collection and preparation efforts, establishing the empirical backbone that will enable the discovery of universal patterns in subsequent chapters.

3.2 Data Collection Methodology

To conduct a comprehensive analysis of electoral patterns across different democratic systems, we compiled election data from 34 countries spanning six continents. Our data collection began with an ambitious survey of 180 countries and territories worldwide, from which we ultimately

selected 34 countries that met our stringent quality criteria for statistical analysis.

Our primary data sources included the Constituency-Level Election Archive (CLEA) website for constituency-level data of lower chamber legislative elections across the globe [70]. For specialized datasets, we collected polling booth level data for India and Canada directly from their respective Election Commission websites [69, 71], employing semi-automated techniques using Python libraries to handle the diverse data formats. County-level data for the United States was obtained from the MIT Election Data and Science Lab [72].

The data collection process faced considerable technical challenges due to the heterogeneous formats in which electoral data is published worldwide. While constituency-level data from CLEA was consistently formatted in tabular structures, polling booth-level data presented significant extraction challenges, ranging from structured tabular formats to machine-generated and scanned PDFs. We developed robust data cleaning procedures using combinations of Python libraries to handle these varied formats systematically.

For countries like India, we successfully collected data across multiple electoral scales that span three orders of magnitude in voter numbers. At the finest granularity, polling booth level data encompasses approximately 10^2 voters per unit, assembly constituency level data covers approximately 10^5 voters, and parliamentary constituency level extends to approximately 10^6 voters. This multi-scale approach enables investigation of scale-dependent electoral phenomena that have rarely been studied systematically across such a broad range of democratic contexts.

3.3 Dataset Architecture

The raw election data was collected across various countries through different sources. The typical structure of the scraped data varied from tabular, machine-generated PDFs to scanned PDFs. Figs 3.1, 3.2, and 3.3 show representative examples of the constituency-level, parliamentary constituency-level, and polling booth-level election data from CLEA, Election Commission of India, and Election Commission of India, respectively. While the CLEA data is in a tabular format, the data from the Election Commission of India is in PDF format, which poses a challenge for automated data extraction. The original election data contained several essential variables that form the foundation of our electoral analysis. Voter turnout represents the actual number of voters who cast ballots in each electoral unit, serving as a crucial scale parameter for our statis-

tical models. Candidate vote tallies provide the detailed breakdown of votes received by each competing candidate, from which we derive the winner and runner-up vote counts. The winning margin, defined as the difference between votes secured by the winner and runner-up, captures the competitiveness of each electoral contest.

ctr_n	ctr	yr	mn	sub	cst_n	cst	ma	pty_n	pty	can	pev1	vot1	vv1	ivv1	to1	cv1	cvs1	pv1	pvs1
Afghanistan	4	2005	9	-990	Badakhshan	1	9	Independent	6121	Abdul Muqadar	400918	243740	232095	11645	0.607954743862835	2676	0.0115297615200672	-990	-990
Afghanistan	4	2005	9	-990	Badakhshan	1	9	Independent	8748	Zulmai Mujada	400918	243740	232095	11645	0.607954743862835	14145	0.0609448717120145	-990	-990
Afghanistan	4	2005	9	-990	Badakhshan	1	9	Independent	8734	Zaynab Attayee	400918	243740	232095	11645	0.607954743862835	504	0.00217152459122342	-990	-990
Afghanistan	4	2005	9	-990	Badakhshan	1	9	Independent	7938	Mohammad Ra	400918	243740	232095	11645	0.607954743862835	751	0.00323574398414442	-990	-990
Afghanistan	4	2005	9	-990	Badakhshan	1	9	Independent	8203	Qari Abdul Fatt	400918	243740	232095	11645	0.607954743862835	1342	0.00578211508218617	-990	-990
Afghanistan	4	2005	9	-990	Badakhshan	1	9	Independent	6043	Abdul Ghias Kh	400918	243740	232095	11645	0.607954743862835	541	0.00233094207113466	-990	-990
Afghanistan	4	2005	9	-990	Badakhshan	1	9	Independent	8215	Qari Ziauddeen	400918	243740	232095	11645	0.607954743862835	2674	0.0115211443589909	-990	-990
Afghanistan	4	2005	9	-990	Badakhshan	1	9	Independent	6503	Asal Mohamma	400918	243740	232095	11645	0.607954743862835	672	0.00289536612163123	-990	-990
Afghanistan	4	2005	9	-990	Badakhshan	1	9	Independent	8173	Pir Mohammac	400918	243740	232095	11645	0.607954743862835	359	0.00154678041319287	-990	-990
Afghanistan	4	2005	9	-990	Badakhshan	1	9	Independent	8240	Qazi Tajuddeen	400918	243740	232095	11645	0.607954743862835	1256	0.00541157715590599	-990	-990
Afghanistan	4	2005	9	-990	Badakhshan	1	9	Independent	8410	Sayyad Abdul T	400918	243740	232095	11645	0.607954743862835	1660	0.00715224369331524	-990	-990
Afghanistan	4	2005	9	-990	Badakhshan	1	9	Independent	7610	Marziya Ahmac	400918	243740	232095	11645	0.607954743862835	1282	0.00552360024989767	-990	-990
Afghanistan	4	2005	9	-990	Badakhshan	1	9	Independent	7524	Kubra Dehqan	400918	243740	232095	11645	0.607954743862835	1825	0.00786315948210862	-990	-990
Afghanistan	4	2005	9	-990	Badakhshan	1	9	Independent	6732	Doctor Sayyad	400918	243740	232095	11645	0.607954743862835	2599	0.0111980008186303	-990	-990
Afghanistan	4	2005	9	-990	Badakhshan	1	9	Independent	8737	Ziauddeen Was	400918	243740	232095	11645	0.607954743862835	2551	0.0109911889527995	-990	-990
Afghanistan	4	2005	9	-990	Badakhshan	1	9	Independent	8130	Noor Ahmad At	400918	243740	232095	11645	0.607954743862835	1217	0.00524354251491846	-990	-990
Afghanistan	4	2005	9	-990	Badakhshan	1	9	Independent	7715	Mir Zaidullah B	400918	243740	232095	11645	0.607954743862835	1837	0.00791486244856632	-990	-990
Afghanistan	4	2005	9	-990	Badakhshan	1	9	Independent	6953	Ghulam Rabani	400918	243740	232095	11645	0.607954743862835	3713	0.0159977595381202	-990	-990
Afghanistan	4	2005	9	-990	Badakhshan	1	9	Independent	7486	Kashaf	400918	243740	232095	11645	0.607954743862835	3848	0.0165794179107693	-990	-990
Afghanistan	4	2005	9	-990	Badakhshan	1	9	Independent	6477	Anis Gul Akhga	400918	243740	232095	11645	0.607954743862835	1411	0.00607940713931795	-990	-990
Afghanistan	4	2005	9	-990	Badakhshan	1	9	Independent	6111	Abdul Malik Ba	400918	243740	232095	11645	0.607954743862835	4350	0.0187423253409164	-990	-990
Afghanistan	4	2005	9	-990	Badakhshan	1	9	Independent	7893	Mohammad M	400918	243740	232095	11645	0.607954743862835	1454	0.00626467610245804	-990	-990
Afghanistan	4	2005	9	-990	Badakhshan	1	9	Independent	7567	Malik Beg	400918	243740	232095	11645	0.607954743862835	626	0.00269717141687671	-990	-990
Afghanistan	4	2005	9	-990	Badakhshan	1	9	Independent	7508	Khidher Khan B	400918	243740	232095	11645	0.607954743862835	873	0.00376139080979771	-990	-990
Afghanistan	4	2005	9	-990	Badakhshan	1	9	Independent	6116	Abdul Manan H	400918	243740	232095	11645	0.607954743862835	989	0.00426118615222215	-990	-990
Afghanistan	4	2005	9	-990	Badakhshan	1	9	Independent	8409	Sayyad Abdul C	400918	243740	232095	11645	0.607954743862835	8950	0.0385617958163683	-990	-990
Afghanistan	4	2005	9	-990	Badakhshan	1	9	Independent	8449	Sayyad Moham	400918	243740	232095	11645	0.607954743862835	2365	0.0101897929727051	-990	-990
Afghanistan	4	2005	9	-990	Badakhshan	1	9	Independent	6578	Daulat Moham	400918	243740	232095	11645	0.607954743862835	4809	0.0207199638079235	-990	-990
Afghanistan	4	2005	9	-990	Badakhshan	1	9	Independent	7920	Mohammad Na	400918	243740	232095	11645	0.607954743862835	2622	0.0112970981710076	-990	-990
Afghanistan	4	2005	9	-990	Badakhshan	1	9	Independent	6135	Abdul Qahar Sa	400918	243740	232095	11645	0.607954743862835	739	0.00318404101768672	-990	-990
Afghanistan	4	2005	9	-990	Badakhshan	1	9	Independent	6901	Fazluddeen Taq	400918	243740	232095	11645	0.607954743862835	3972	0.0171136818974989	-990	-990
Afghanistan	4	2005	9	-990	Badakhshan	1	9	Independent	6823	Engineer Moha	400918	243740	232095	11645	0.607954743862835	1119	0.00482130162218057	-990	-990
Afghanistan	4	2005	9	-990	Badakhshan	1	9	Independent	8105	Nawrooz	400918	243740	232095	11645	0.607954743862835	737	0.00317542385661044	-990	-990
Afghanistan	4	2005	9	-990	Badakhshan	1	9	Independent	6024	Abdul Basir Ishı	400918	243740	232095	11645	0.607954743862835	637	0.00274456580279627	-990	-990
Afghanistan	4	2005	9	-990	Badakhshan	1	9	Independent	6147	Abdul Qudoos	400918	243740	232095	11645	0.607954743862835	550	0.00236971929597794	-990	-990
Afghanistan	4	2005	9	-990	Badakhshan	1	9	Independent	8047	Muzafarudin	400918	243740	232095	11645	0.607954743862835	144	0.000620435597492406	-990	-990
Afghanistan	4	2005	9	-990	Badakhshan	1	9	Independent	7466	Jamshaid Khaw	400918	243740	232095	11645	0.607954743862835	3190	0.0137443719166721	-990	-990
Afghanistan	4	2005	9	-990	Badakhshan	1	9	Independent	7994	Mohammad Za	400918	243740	232095	11645	0.607954743862835	1533	0.00660505396497124	-990	-990
Afghanistan	4	2005	9	-990	Badakhshan	1	9	Independent	8529	Shair Ali	400918	243740	232095	11645	0.607954743862835	809	0.00348564165535664	-990	-990
Afghanistan	4	2005	9	-990	Badakhshan	1	9	Independent	6158	Abdul Raouf Ba	400918	243740	232095	11645	0.607954743862835	891	0.00383894525948426	-990	-990
Afghanistan	4	2005	9	-990	Badakhshan	1	9	Independent	7403	Hajimohamma	400918	243740	232095	11645	0.607954743862835	5480	0.0236110213490166	-990	-990
Afghanistan	4	2005	9	-990	Badakhshan	1	9	Independent	6741	Doctor Sibghat	400918	243740	232095	11645	0.607954743862835	816	0.00351580171912363	-990	-990
Afghanistan	4	2005	9	-990	Badakhshan	1	9	Independent	8546	Sharafuddeen A	400918	243740	232095	11645	0.607954743862835	410	0.0017665180206381	-990	-990
Afghanistan	4	2005	9	-990	Badakhshan	1	9	Independent	6403	Al-haj Safar Mo	400918	243740	232095	11645	0.607954743862835	4813	0.020737198130076	-990	-990
Afghanistan	4	2005	9	-990	Badakhshan	1	9	Independent	8411	Sayyad Abdul W	400918	243740	232095	11645	0.607954743862835	1540	0.00663521402873823	-990	-990
Afghanistan	4	2005	9	-990	Badakhshan	1	9	Independent	7650	Mawlawi Ghula	400918	243740	232095	11645	0.607954743862835	486	0.00209397014153687	-990	-990
Afghanistan	4	2005	9	-990	Badakhshan	1	9	Independent	6099	Abdul Maajid C	400918	243740	232095	11645	0.607954743862835	1318	0.00567870914927077	-990	-990
Afghanistan	4	2005	9	-990	Badakhshan	1	9	Independent	8000	Mohammad Ze	400918	243740	232095	11645	0.607954743862835	1477	0.0063637734548353	-990	-990
Afghanistan	4	2005	9	-990	Badakhshan	1	9	Independent	7258	Haji Mohamma	400918	243740	232095	11645	0.607954743862835	3044	0.0131153191581034	-990	-990
Afghanistan	4	2005	9	-990	Badakhshan	1	9	Independent	8012	Monawar Shah	400918	243740	232095	11645	0.607954743862835	386	0.0016631120877227	-990	-990

Figure 3.1: A representative example of the constituency-level election data from CLEA [70]. The dataset contains various fields, including name of the party, candidate's name, and several other identifiers. However, for our analysis purpose we only considered the columns *cv1*, and *cv2* (not visible in the above example), which corresponds to the votes received by the candidates in first and second rounds, respectively. The voter turnout for a electoral unit is calculated as the sum of all the votes received by all the candidates (combining both rounds). The negative values in several columns correspond to missing parameter values or other errors.

Election Commission of India, Elections,2019 (17 LOK SABHA)

33 - CONSTITUENCY WISE DETAILED RESULTS

Andhra Pradesh

Constituency: 1 . Aruku **(Total Electors** 1451418)

SL NO	CANDIDATE NAME	SEX	AGE	CATEGORY	PARTY	Symbol	Votes Secured			% of votes secured	
							GENERAL	POSTAL	TOTAL	Over total elctors in constituency	Over total votes polled in constituency
1	Shruti Devi Vyricherla	Female	46	st	INC	Hand	17656	74	17730	1.22	1.64
2	Kishore Chandra Deo	Male	72	st	TDP	Bicycle	336163	1938	338101	23.29	31.36
3	Goddeti. Madhavi	Female	26	st	YSRCP	Ceiling Fan	557561	4629	562190	38.73	52.14
4	Swamula. Subrahmanyam	Male	50	st	JAJGP	Mike	4705	5	4710	0.32	0.44
5	Dr. Kosuri Kasi Viswanadha Veera Venkata Satyanarayana Reddy	Male	54	st	BJP	Lotus	17578	289	17867	1.23	1.66
6	Gangulaiah Vampuru.	Male	49	st	JnP	Glass Tumbler	42245	549	42794	2.95	3.97
7	Biddika Ramayya.	Male	57	st	IND	Battery Torch	7863	4	7867	0.54	0.73
8	Kangala Baludora	Male	61	st	IND	Cup & Saucer	13810	16	13826	0.95	1.28
9	Anumula Vamsikrishna	Male	41	st	IND	Helicopter	10211	29	10240	0.71	0.95
10	Narava Satyavathi	Female	37	st	IND	Bangles	11231	5	11236	0.77	1.04
11	Nota				NOTA		47955	22	47977	3.31	4.45
					TOTAL		**1066978**	**7560**	**1074538**	**74.03**	**99.66**

Figure 3.2: A representative example of the constituency-level election data from the Election Commission of India [69].

FORM 20
FINAL RESULT SHEET
[SEE RULE 56C(2)©]
Assembly Constituency No. & Name : 1-Ratabari (SC)
Total No. of Electors in Assembly Constituency/ Segment : 119793

LSE-2004

Polling Stations		No. of valid votes cast in favour of.....								Total of Valid Votes	No.of Rejected votes	Total	No.of Tendered votes
No.	Name	AGP	BJP	INC	IND	IND	IND	IND	IND				
1		2	3	4	5	6	7	8	9	10	11	12	13
1	TOLAKONA ME SCHOOL	3	314	110	1	0	0	0	0	428	0	428	0
2	RANGPUR VENTURE L.P. SCHOOL	93	175	639	4	5	4	0	1	921	0	921	0
3	144 NO. DEBODWAR L.P. SCHOOL	32	146	334	11	4	2	0	12	541	0	541	0
4	442 NO. CHERARPAR L.P. SCHOOL	29	28	343	0	0	0	0	0	400	0	400	0
5	SWAMI VIVEKANANDA H.E. SCHOOL	8	260	226	3	2	1	11	2	513	0	513	0
6	315 DARGARBOND L.P. SCHOOL	25	306	244	4	1	2	5	3	590	0	590	0
7	312 NO. DANIRBOND L.P. SCHOOL	37	41	337	1	0	2	0	1	419	0	419	0
8	148 NO. CHOTOKONA L.P. SCHOOL	95	217	254	5	4	5	1	3	584	0	584	0
9	489 NO. RAMKRISHNA L.P. SCHOOL	80	254	197	5	5	2	0	2	545	0	545	0
10	BHAIRABNAGAR M.V. SCHOOL	9	277	127	2	4	1	2	3	425	0	425	0
11	345 NO. BHAIRAB NAGAR L.P. SCHOOL	2	216	87	5	3	6	4	7	330	0	330	0
11(A)	BHAIRAB NAGAR M.V. SCHOOL	5	189	58	2	1	0	0	1	256	0	256	0
12	988 NO. RISHI ARAVINDA L.P.SCHOOL	2	316	198	2	0	1	1	2	522	0	522	0
13	662 NO. SAILANAGAR L.P. SCHOOL	9	217	332	5	8	2	1	0	574	0	574	0
14	572 NO. JOGENDRANATH L.P. SCHOOL	39	223	394	6	1	2	1	4	670	0	670	0
15	313 NO. GAMARIA L.P. SCHOOL	66	190	262	7	2	8	10	14	559	0	559	0
16	490 NO. SANTOSHPUR L.P. SCHOOL	8	252	166	7	4	4	3	11	455	0	455	0
17	SUBHASH M.E. SCHOOL	1	122	129	0	0	1	1	0	254	0	254	0
18	263 NO. NABINGRAM L.P. SCHOOL	13	310	169	3	3	1	5	5	509	0	509	0
19	495 NO. GANDHINAGAR L.P. SCHOOL	11	368	119	6	0	2	5	7	518	0	518	0
20	387 NO. KHALAGRAM L.P. SCHOOL	135	96	343	7	4	6	2	3	596	0	596	0
21	532 NO. SANTIPUR L.P. SCHOOL	9	223	229	7	2	0	3	9	482	0	482	0
22	NETAJINAGAR HIGH SCHOOL (EASTERN SIDE)	11	149	135	5	1	2	2	1	306	0	306	0
23	GARERBOND M.V. SCHOOL	45	190	201	2	1	0	1	4	444	0	444	0
24	502 NO. MANGALPUR L.P. SCHOOL	8	227	99	0	3	2	1	0	340	0	340	0
25	188 NO. PALTALA L.P. SCHOOL	4	203	174	1	0	2	0	1	385	0	385	0

Page 1 of 5

Figure 3.3: A representative example of the form 20, which contains the polling booth-level election data from the Election Commission of India [69].

3.4 Data Processing Protocol

The raw data required extensive cleaning and standardization procedures to ensure analytical integrity. Our systematic data cleaning approach addressed multiple technical challenges inherent in cross-national electoral data compilation. Missing values were handled through careful exclusion of affected data points rather than imputation, preserving the authenticity of electoral outcomes. Format inconsistencies were systematically standardized, with particular attention to turnout and margin calculations to ensure cross-country comparability.

Statistical robustness requirements drove our implementation of stringent filtering criteria that ultimately shaped our final dataset. We established a minimum threshold of 400 consolidated data points per country to ensure adequate statistical power for universality demonstration while maintaining the capability for electoral fraud detection. This threshold proved effective for identifying potential electoral misconduct in Ethiopia and Belarus while preserving robust statistical foundations for analysis. Cases with zero turnout were systematically excluded from analysis, as were

electoral units with fewer than two competing candidates, ensuring that our margin calculations reflected genuine electoral competition.

Our filtering criteria necessitated significant dataset reduction from the initial survey of 180 countries to the final analytical set of 34 countries. This reduction prioritized data quality over mere quantity, ensuring that each included country contributed statistically meaningful information to our cross-national analysis. To maintain consistency in our turnout calculations, we defined turnout as the sum of valid votes received by all candidates in each electoral unit, avoiding discrepancies that might arise from different approaches to calculating voter participation rates.

The temporal consolidation of multiple elections from each country created unified statistical ensembles that capture long-term electoral patterns while maintaining sufficient sample sizes for robust statistical inference. For Indian elections specifically, our dataset spans from 1962 to 2019 for parliamentary constituencies, 1999 to 2019 for assembly constituencies in general elections, 2004 to 2019 for polling booth level data, and 1961 to 2023 for state assembly elections, providing comprehensive temporal coverage across multiple electoral scales and types.

3.5 Cross-National Electoral Patterns

Our cleaned and standardized dataset reveals remarkable diversity in electoral patterns across countries and scales, providing insights into the fundamental characteristics of democratic competition worldwide. The consolidated electoral data demonstrates substantial variation in mean turnout values, ranging from Denmark's constituency-level average of approximately 2,700 voters to India's parliamentary constituency average exceeding 569,000 voters. Similarly, mean margins of victory exhibit considerable cross-national variation, reflecting different degrees of electoral competitiveness across democratic systems.

The temporal depth of our dataset provides exceptional analytical power, with some countries contributing over 150 years of electoral history. The United States congressional district data spans from 1788 to 2020 across 167 elections, while the United Kingdom's constituency data covers 1832 to 2019 through 46 electoral cycles. This extensive temporal coverage enables investigation of long-term electoral trends and system evolution across different democratic contexts.

Table 3.1 presents comprehensive summary statistics for our dataset, illustrating the extraordinary diversity of electoral scales and patterns across different democratic systems. The table

demonstrates the multi-scale nature of our analysis, with electoral unit sizes varying by more than three orders of magnitude within single countries and by over four orders of magnitude across the complete dataset.

Country	Time span	Number of elections	Scale	Mean turnout	Mean margin	Number of electoral units (consolidated)
Australia	1901-2016	37	Constituency	7.37×10^4	1.31×10^4	1740
Bangladesh	1973-2008	4	Constituency	1.57×10^5	3.15×10^4	1188
Belarus	2004-2019	5	Constituency	4.83×10^4	2.61×10^4	441
Canada	1867-2019	43	Constituency	2.76×10^4	5.50×10^3	10662
Canada	2004-2021	7	Polling Booth	5.56×10^2	1.35×10^2	489919
Chile	1945-2017	7	Constituency	1.07×10^5	1.05×10^4	420
Denmark	1849-2019	30	Constituency	2.70×10^3	4.64×10^2	2178
Ethiopia	2010-2010	1	Constituency	4.95×10^4	4.18×10^4	492
France	1973-2017	3	Constituency	7.88×10^4	1.10×10^4	1712
Germany	1871-2017	19	Constituency	1.37×10^5	2.26×10^4	5108
Ghana	1992-2016	6	Constituency	3.75×10^4	9.88×10^3	1410
Hungary	1990-2018	6	Constituency	5.32×10^4	8.57×10^3	936
India	1951-2019	18	Constituency	5.69×10^5	8.33×10^4	8389
India	2004-2019	4	Polling Booth	5.82×10^2	1.89×10^2	752786
Japan	1947-2017	26	Constituency	2.88×10^5	2.35×10^4	4603
Kenya	1961-2013	2	Constituency	3.72×10^4	1.19×10^4	417
Korea	1948-2012	13	Constituency	6.17×10^4	1.01×10^4	2258
Lithuania	1992-2020	8	Constituency	3.24×10^4	3.98×10^3	570
Malawi	1994-2019	4	Constituency	2.31×10^4	6.29×10^3	755
Malaysia	1959-2018	13	Constituency	3.41×10^4	8.90×10^3	2199
Myanmar	2010-2015	2	Constituency	6.76×10^4	2.32×10^4	634
New Zealand	1943-2020	9	Constituency	3.04×10^4	6.94×10^3	637
Nigeria	2003-2019	2	Constituency	7.75×10^4	2.20×10^4	710
Pakistan	1988-2013	3	Constituency	1.28×10^5	2.45×10^4	683
Papua New Guinea	1972-2017	8	Constituency	5.07×10^4	5.66×10^3	841
Philippines	1946-2013	17	Constituency	1.83×10^5	2.63×10^4	2525
Solomon Islands	1967-2019	14	Constituency	3.67×10^3	4.37×10^2	543
Taiwan	1986-2020	11	Constituency	2.33×10^5	1.98×10^4	482
Tanzania	2005-2020	2	Constituency	5.37×10^4	2.01×10^4	492
Thailand	1969-2011	12	Constituency	1.86×10^5	1.46×10^4	2263
Trinidad and Tobago	1925-2020	13	Constituency	1.53×10^4	5.12×10^3	411
Uganda	2006-2021	4	Constituency	4.45×10^4	1.08×10^4	1430
UK	1832-2019	46	Constituency	3.43×10^4	6.30×10^3	23105
Ukraine	1998-2019	5	Constituency	8.89×10^4	1.67×10^4	1072
United States	1788-2020	167	Congressional District	1.14×10^5	2.96×10^4	33946
United States	2000-2020	6	County	1.78×10^5	2.00×10^4	18905
Zimbabwe	2005-2018	4	Constituency	1.77×10^4	6.55×10^3	743

Table 3.1: Typical values of Margin and turnouts at different scales for different countries. The available data for the mentioned time spans were consolidated for each country and used to calculate the mean turnout and mean margin. The consolidated number of electoral units (in the last column) is calculated by adding the number of valid electoral units for all the elections that happened in the mentioned time span. The data for an electoral unit is considered to be valid if (a) a list of votes received by all the candidates is available, (b) at least two candidates are contesting, and (c) the turnout is non-zero. For example, in polling booth level data for India, lists of votes for all the polling booths are not always available. We could obtain valid data for 752786 polling booths from the four elections held during the time span of $2004 - 2019$ for which the above-mentioned conditions were met. Only national-level elections are considered in this dataset.

The summary statistics reveal several fundamental patterns in our comprehensive dataset. Electoral unit scales demonstrate extraordinary variation both within and across countries, exemplified by the contrast between Canadian polling booths averaging 556 voters and Indian parliamentary constituencies averaging 569,000 voters. The consolidated number of electoral units provides insight into the statistical power available for each country, ranging from Ethiopia's limited 492 units to India's extensive polling booth dataset encompassing 752,786 units. The temporal coverage demonstrates the robustness of our longitudinal analysis, with consolidated data representing decades or centuries of democratic evolution. Countries like Australia contribute 37 elections from 1901 to 2016, while Canada's constituency-level data spans a remarkable 43 elections from 1867 to 2019. This extensive temporal depth enables investigation of how electoral patterns evolve over time within stable democratic systems, providing insights into the persistence or change of competitive structures across different historical periods.

3.6 Discussion

This comprehensive dataset represents the empirical foundation upon which our discovery of electoral universality rests. The systematic collection, cleaning, and validation of data from 34 countries across six continents provides unprecedented analytical power for investigating fundamental patterns in democratic competition. Our dataset encompasses millions of electoral units when consolidated across all countries and scales, representing one of the most extensive cross-national electoral databases assembled for statistical physics analysis.

The quality-first approach in our data collection is essential to uncover robust statistical patterns. Rather than pursuing maximum geographical coverage, we prioritized statistical robustness by maintaining stringent quality thresholds for each included country. This methodology enabled us to demonstrate genuine universality in electoral statistics while providing sufficient statistical power to detect deviations indicative of electoral irregularities.

The multi-scale architecture of our dataset, particularly exemplified by the Indian election data spanning three orders of magnitude in electoral unit size, enables investigation of scale-invariant phenomena that would be impossible with single-scale analysis. The successful collection of polling booth level data for India and Canada, representing hundreds of thousands of electoral units, provides the granular resolution necessary for detecting universal statistical sig-

natures across different scales of democratic aggregation.

With this empirically grounded foundation established, we possess the analytical infrastructure necessary to pursue our central research question: do universal statistical patterns emerge in democratic competition that transcend the specific institutional, cultural, and temporal contexts of individual electoral systems? The subsequent chapters will demonstrate how this carefully curated dataset enables the discovery of remarkable universality in electoral margins when properly scaled, revealing fundamental principles governing competitive democratic processes across vastly different contexts.

CHAPTER 4

Universality in Electoral Competition

Building on the empirical foundation established in Chapter 3, we now embark on a focused search for universal patterns in electoral competition. Although elections vary dramatically across democracies in their rules, contexts, and scales, our aim is to uncover whether there are fundamental statistical signatures that transcend these differences. In this chapter, we undertake a systematic search for universal patterns in electoral data. We first focus on two key variables, the margin of victory and voter turnout. While the former captures the essence of democratic competition across different electoral systems, the latter sets the scale of the election. With extensive election data [69–72] from 34 countries (from 6 continents) spanning multiple decades and electorate scales, we analyze distributions of these variables, gradually uncovering a remarkable universal distribution. Finally, we develop a minimal statistical model that explains this universal pattern, offering insights into the fundamental nature of democratic competition.

4.1 The Electoral Process: A Template

A template of a basic electoral process is as follows. At each electoral unit, candidates compete against each other to win the votes of the electorate, who can cast their vote in favor of only one of the candidates. The candidate securing the largest number of polled votes is declared the winner. This template, as illustrated in the schematic of Fig. 4.1, represents the core process in many electoral systems. It is the standard first-past-the-post system followed in many countries, e.g., India, the UK, and the USA. In an instant-run-off system (such as in Australia) or two-round run-offs (such as in France), the final run-off round boils down to this template. Typically, national or regional elections following this template consist of many electoral units made up of polling booths, precincts, constituencies, or counties. These units set a size scale in terms of the number of electorates – a polling booth represents the smallest scale, while a constituency (subsuming many polling booths) represents the largest scale. For our analysis, an "election" could be either a national, regional, or even a city-level electoral process encompassing N electoral units, and

Figure 4.1: Basic template of an election. The map highlights a single electoral unit within a larger region. In this unit, multiple candidates (colored icons) compete for votes cast by the electorate (black icons). A representative voter casts a ballot for one candidate. The distribution of votes is summarized by key quantities on the right. The *turnout* T (top bar) denotes the number of participating voters and sets the scale of the contest. Among these, the candidate securing the *most votes* (V_w, blue) is declared the winner, while the one with the *second-highest votes* (V_r, red) is the runner-up. The *margin of victory* $M = V_w - V_r$ (gray) quantifies the degree of competition – smaller margins reflect tight races, while larger margins indicate strong consensus. This template abstracts the first-past-the-post electoral mechanism used in countries like India, the UK, and the USA, and serves as the basis for analyzing competitiveness and engagement across electoral units.

each unit could be a polling booth, county, or constituency.

In any such election, an informative indicator of the degree of competition and the extent of consensus is the margin of victory. A vanishing margin of victory signifies tight competition and a divided electorate, whereas large margins of victory indicate a decisive mandate and overwhelming consensus in favor of one candidate. Let $c_i, i = 1, 2, \ldots N$, denote the number of candidates contesting an election in the i-th electoral unit. The winning and runner-up candidates receive, respectively, $V_{i,w}$ and $V_{i,r}$ votes such that $V_{i,w} > V_{i,r}$. The margin is given by $M_i = V_{i,w} - V_{i,r}$. If $n_i > 0$ is the size of the electorate, *i.e.*, number of registered voters in the i-th unit, then $0 \leq M_i \leq n_i$. However, in practice, only a fraction of the electorate participates in voting. In such cases, the number of voters who show up to cast their vote is termed as the turnout T_i, such that $0 \leq T_i \leq n_i$, and consequently, the margin is further restricted by $0 \leq M_i \leq T_i$.

4.1.1 Turnout-Margin Relationship

To fix our ideas, we might focus on the elections in one country, e.g., the general elections in India. Then, the object of interest would be M_i and T_i ($i = 1, 2, \ldots N$). To be statistically robust, the data is consolidated from many elections spread over several decades (For India, 18

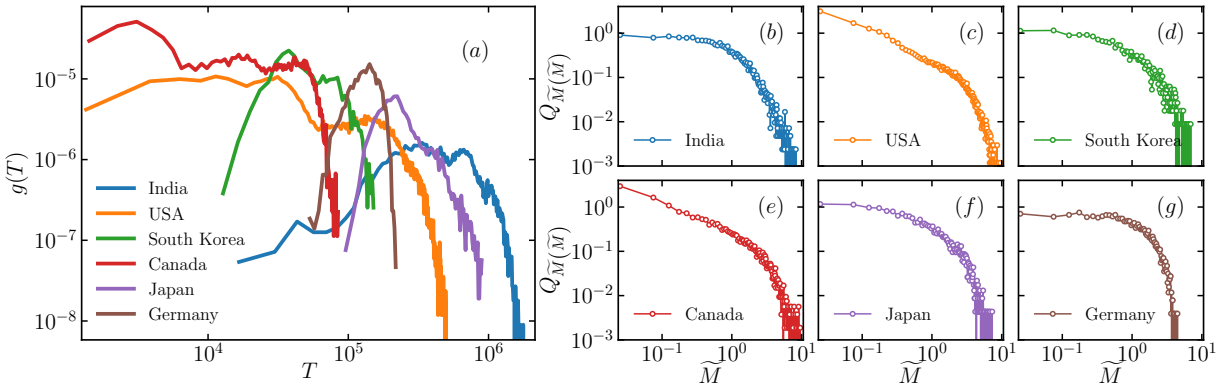

Figure 4.2: (a) Turnout distribution $g(T)$ obtained from election data for different countries. Note the differences in shapes and ranges for $g(T)$. (b-g) Scaled margin distribution $Q_{\widetilde{M}}\left(\widetilde{M}\right)$ obtained from election data (open circles with solid lines) for India, USA, South Korea, Canada, Japan, and Germany. Despite their distinct electoral systems and political cultures, these distributions show broad similarities but also notable differences in their decay patterns.

elections from 1951 to 2019). This leads to the associated empirical distributions $Q_M(M)$ and $g(T)$, respectively, for margin and turnout. Figure 4.2(a) displays the distribution of raw turnout $g(T)$ at the constituency level for national elections in six countries, namely, India, USA, South Korea, Canada, Japan, and Germany. Striking dissimilarities in $g(T)$ are visible in the shape and support of distribution for countries. For Germany, $g(T)$ has a unimodal character, while that for Canada and the USA display multiple peaks. Further, we scale the margin distribution with the sample mean $\langle M \rangle$, hoping to find a universal pattern. However, as displayed in Fig. 4.2(b-g), the distributions of scaled margin $\widetilde{M} = M/\langle M \rangle$ (computed from the consolidated margin data for each country) demonstrate certain noticeable differences. In particular, $Q_{\widetilde{M}}\left(\widetilde{M}\right)$ for German elections in Fig. 4.2(g) has a sharp cutoff, but for India and Japan in Fig. 4.2(b, f) the distribution has a slower decay.

Next, we investigate how the electoral scale affects the distributions of our key variables, an essential consideration for any claim of universality. In large countries, depending on the size of the electoral unit, the typical turnout can differ by several orders of magnitude. For example, in India, the polling booths have a typical electoral size $\sim 10^3$, while at the parliamentary constituency level it is about 10^6. Further, the shapes of $g(T)$ are also vastly different at different scales. Figure 4.3(a) captures the striking differences in range and shape of $g(T)$ for India, the US, and Canada at two different scales. The dashed lines represent smaller scales (polling booths

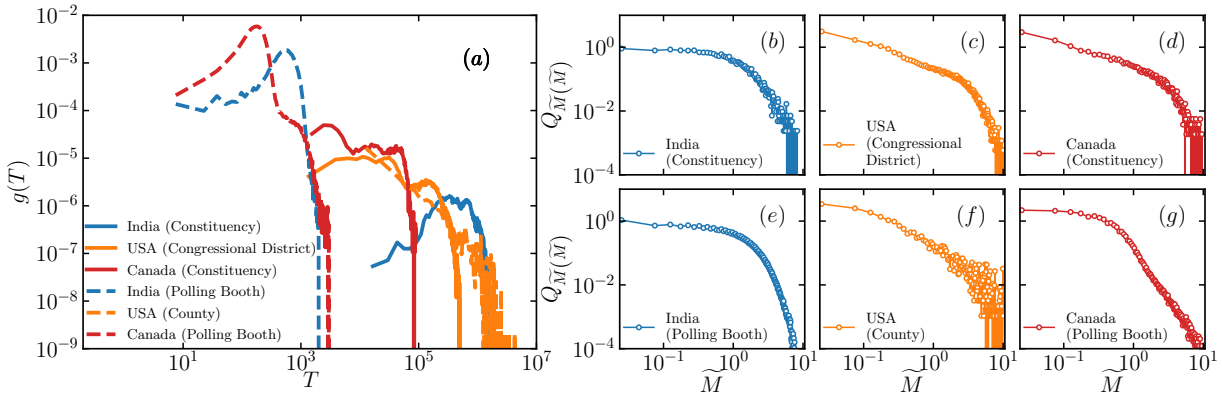

Figure 4.3: The turnout distribution $g(T)$ and scaled margin distribution $Q_{\widetilde{M}}\left(\widetilde{M}\right)$ for India (blue), the USA (orange), and Canada (red), at two widely different scales, *i.e.*, size of electoral units. (a) $g(T)$ at two different scales for each country. The dashed line is for smaller scales (polling booth for India and Canada, County for the USA), while the solid line represents a larger scale (constituency for India and Canada, congressional district for the USA). (b-g) $Q_{\widetilde{M}}\left(\widetilde{M}\right)$ from election data (open circles). Despite the differences in scale and shape of $g(T)$, the empirical $Q_{\widetilde{M}}\left(\widetilde{M}\right)$ shows certain consistent patterns, though scale effects are still evident.

for India and Canada, counties for the USA), while solid lines represent larger scales (constituencies for India and Canada, congressional districts for the USA). The corresponding scaled margin distributions $Q_{\widetilde{M}}\left(\widetilde{M}\right)$ are shown in Figure 4.3(b-g). Figure 4.3(b, c, d) shows the empirical distribution of scaled margins (in national elections) at the constituency-level scale, and Figure 4.3(e, f, g) shows the same at the scale of polling booths (county for USA). For each country, the distributions at different scales show certain similarities but also notable differences. For instance, in the USA, the county-level distribution (Figure 4.3(f)) displays a heavier tail compared to the congressional district level (Figure 4.3(c)), reflecting the influence of the underlying turnout distribution. Similar scale-dependent effects are visible in the data from India and Canada.

This variability in the scaled margin distribution suggests that $Q_{\widetilde{M}}\left(\widetilde{M}\right)$ still carries the imprint of the underlying turnout distribution and is affected by the scale of electoral units.

4.1.2 Scale-Invariant Measure Requirement

The variations in distributions observed across countries and scales clearly demonstrate that neither raw turnout nor simple scaled margin can reveal universal patterns in electoral competition. The influence of electoral scale and country-specific factors persists in these measures. This sug-

gests we need a more fundamental approach – one that effectively normalizes out the scale effects while capturing the essential competitive dynamics common to all democratic elections. Such a measure would need to account for both the margin and the contextual scale of each electoral contest.

4.2 Specific Margin: A Scale-Invariant Metric

Given the observed dependencies between margins and turnouts, and the constraint that $M \leq T$, we consider a new measure: the specific margin $\mu = M/T$. This ratio represents the margin normalized by the turnout at each electoral unit, producing a measure of electoral competitiveness that is independent of the size of the electorate. The specific margin μ ranges from 0 to 1, where values close to 0 indicate extremely competitive elections (nearly tied results), and values approaching 1 represent complete consensus (where nearly all voters chose the same candidate). By normalizing the margin by the local turnout, we effectively remove the scale dependency that affected our earlier analysis.

4.2.1 Universal Scaled Distribution

The true breakthrough comes when we examine the scaled specific margin $\widetilde{\mu} = \mu/\langle\mu\rangle$, where $\langle\mu\rangle$ is the average specific margin for each country. Figure 4.4 shows the distribution $Q_{\widetilde{\mu}}(\widetilde{\mu})$ of this scaled specific margin computed from electoral data across 32 countries.

Remarkably, Figure 4.4 reveals that the scaled specific margin distributions $Q_{\widetilde{\mu}}(\widetilde{\mu})$, follows a universal trend across all 32 countries, despite vast differences in their electoral systems, cultural contexts, and historical backgrounds. Each colored point in the figure represents a specific country's data, and while there are small fluctuations around the aggregated distribution (attributable to finite-size effects), the overall pattern is strikingly consistent.

This represents a remarkable finding: despite the immense complexity and diversity of electoral systems worldwide, the scaled specific margin follows a universal distribution, suggesting that the fundamental process of electoral competition—when appropriately normalized—follows the same statistical pattern regardless of where or how the election takes place.

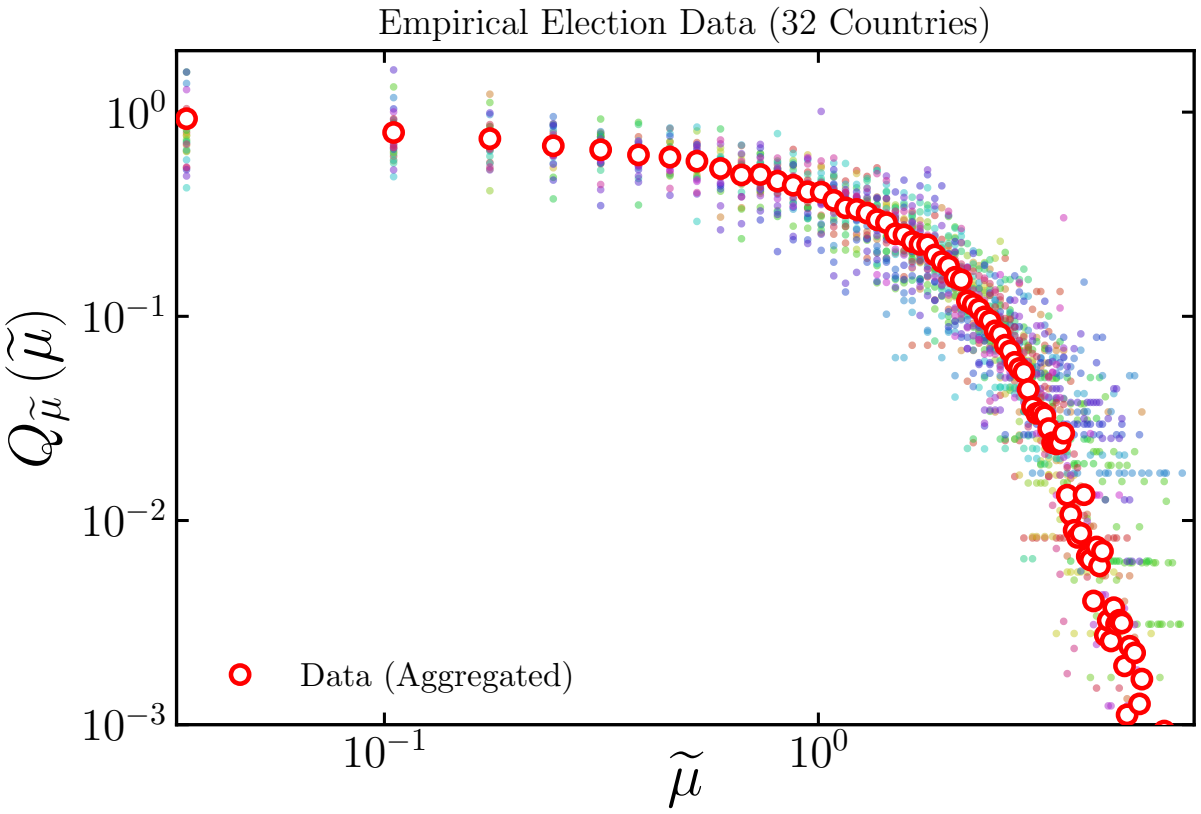

Figure 4.4: The empirical distribution of $\widetilde{\mu} = \mu/\langle\mu\rangle$ from election data of 32 countrie. Each color indicates a specific country for which the empirical election data is consolidated over several elections. The average of these empirical distributions is shown as red open circles.

4.3 Theoretical Model Requirements

While the empirical universality we have discovered is compelling, it raises a fundamental question: Why does this universal pattern emerge across such diverse electoral systems? What underlying mechanism could generate such consistent statistical behavior despite the vast differences in political contexts, voter behaviors, and electoral rules?

4.3.1 Random Voting Model Introduction

The consistency of the pattern suggests that there might be a simple but powerful statistical principle at work – something fundamental to the process of competitive selection itself, rather than specific to electoral politics. The universality we have discovered hints that once turnout is "normalized out" through the specific margin, what remains is a fundamental statistical process common to all competitive elections, suggesting that a minimal model focused on the core statistical

features of electoral competition might be sufficient to explain the observed universality.

With this insight, we propose a simple stochastic model, called the Random Voting Model (RVM). In this model, each voter in a constituency selects one of the candidates according to *some* probability p_j for $j = 1, 2, 3$. While in the next chapter we address the precise choice of these probabilities as well as the detailed analysis of the model, for now, we focus on their statistical consequences. We solve the model in the limit of large turnout ($T \gg 1$), meaning when the number of voters is sufficiently large. In this limit, the votes received by the j-th candidate can be approximated as $v_j \approx p_j T$ (the probability of voting for that candidate multiplied by the turnout), and the margin of victory as $M \approx \left(p_{(3)} - p_{(2)}\right) T$, where $p_{(k)}$ denotes the k-th order statistic [88] of the probabilities assigned to the candidates – in simpler terms, $p_{(3)}$ is the probability of the winner and $p_{(2)}$ is the probability of the runner-up. Evidently, in this limit, the specific margin $\mu \approx p_{(3)} - p_{(2)}$ becomes the difference between these probabilities and its distribution has no explicit dependence on turnout T. With this insight, we obtain the distribution of specific margins as:

$$Q_\mu(\mu) = \frac{(1-\mu)(5+7\mu)}{(1+\mu)^2(1+2\mu)^2}. \tag{4.1}$$

Thus, the distribution $Q_{\widetilde{\mu}}\left(\widetilde{\mu}\right)$ of the scaled specific margin $\widetilde{\mu} = \mu/\langle\mu\rangle$ is:

$$Q_{\widetilde{\mu}}\left(\widetilde{\mu}\right) = \langle\mu\rangle Q_\mu\left(\widetilde{\mu}\langle\mu\rangle\right), \tag{4.2}$$

with $\langle\mu\rangle = \frac{1}{2} + \ln\left(\frac{9\sqrt[4]{3}}{16}\right)$ and the distribution is independent of the underlying turnout distribution $g(T)$. In figure 4.5(a) we demonstrate that $Q_{\widetilde{\mu}}\left(\widetilde{\mu}\right)$, computed from RVM simulations with vastly different turnout distributions $g(T)$, does not depend on the detailed structure of $g(T)$ and is in agreement with the analytical prediction in Eq. 4.2. The RVM simulations are performed with 10^6 electoral units using $g(T)$ corresponding to power law, Gaussian, and uniform distributions (inset of Fig. 4.5(a)). The simulated distributions (open circles in Fig. 4.5(a)), for the three cases of $g(T)$, collapse on the analytical prediction $Q_{\widetilde{\mu}}\left(\widetilde{\mu}\right)$ (red line).

We further examine if prediction in Eq. 4.2 holds good for the empirical election data. Indeed, as observed in Fig. 4.5(b), the RVM prediction (black open circles) is in excellent agreement with the averaged distributions (open red circles) obtained from all the 32 countries. The averaged empirical distribution is also consistent with the analytical universal curve $Q_{\widetilde{\mu}}\left(\widetilde{\mu}\right)$ (red line). Further, the empirical distribution for each of the 32 countries (denoted by the solid-colored circles)

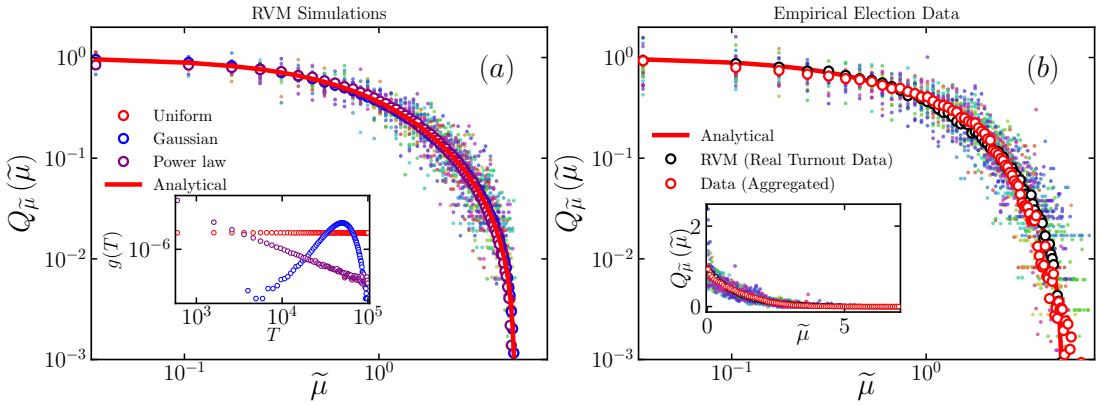

Figure 4.5: (a) $Q_{\widetilde{\mu}}(\widetilde{\mu})$ predicted by RVM for three different turnout distributions $g(T)$ (see inset). The open circles are obtained from RVM simulations with $N = 10^6$, while the solid colored circles are generated from RVM simulations with N identical to empirical election data. The red line corresponds to $Q_{\widetilde{\mu}}(\widetilde{\mu})$ in Eq. 4.2. (b) The empirical distribution of $\widetilde{\mu} = \mu/\langle\mu\rangle$ from election data of 32 countries (excluding Ethiopia and Belarus). Each color indicates a specific country for which the empirical election data is consolidated over several elections. The average of these empirical distributions (red open circles) closely follows the analytical curve (red line) and the averaged RVM predictions for each country (black open circles). The inset depicts the distributions on a linear scale.

closely follows the trend of $Q_{\widetilde{\mu}}(\widetilde{\mu})$, albeit with some fluctuations induced by the finite size of data. Similar fluctuations are evident in RVM simulations as well, seen as solid circles in Fig. 4.5(a), when the number of electoral units N is taken from the empirical election data (rather than fixed at 10^6). Empirical distributions shown in the inset of Fig. 4.5(b) demonstrate that at large x, the absolute fluctuations decrease.

Thus, the universality in Fig. 4.5 suggests that irrespective of the finer details of election processes, the mechanism underlying the core component of any competitive election – choosing one candidate from many contenders – leads to a universal distribution for the scaled specific margin $\widetilde{\mu} = \mu/\langle\mu\rangle$. This remarkable agreement between our simple Random Voting Model and empirical data from diverse democracies suggests that we have identified a fundamental statistical signature of democratic competition that transcends specific electoral systems and cultural contexts.

4.4 Discussion

In this chapter, using extensive election data from 32 countries spanning multiple decades and electorate scales, we have demonstrated a remarkable statistical universality in democratic elec-

toral competition. While raw turnout distributions vary dramatically across countries and scales, and scaled margin distributions retain country-specific features, the scaled specific margin follows a universal distribution across 32 diverse democracies.

This universality transcends the particularities of individual countries, electoral systems, and scales, revealing what appears to be a fundamental statistical signature intrinsic to competitive democratic processes. Like other universalities discovered in complex systems, this pattern emerges not despite but because of the underlying complexity, as coherent patterns can arise from the aggregation of many individual decisions. We further argue that this universality is a stylized fact of elections, and any successful election model should be able to reproduce it.

The elegance of this finding lies in its simplicity: once we properly normalize the margin by the local turnout and scale by the country-specific mean, the resulting distribution follows a consistent pattern regardless of cultural, historical, or institutional factors. It suggests that beneath the surface complexity of electoral politics lies a simpler statistical regularity, which is a signature of democratic competition, which we capture with our proposed Random Voting Model.

Building on the success of the RVM in explaining this universal pattern, the next chapter will provide a comprehensive analysis of the model from first principles. We will derive its mathematical foundations, demonstrate how it connects turnout distributions to margin distributions across different electoral contexts, and explore how this elegantly simple model can explain multiple empirical findings.

CHAPTER 5

Random Voting Model: Analytical Framework

In the previous chapter, we uncovered a remarkable universal pattern in electoral statistics: the scaled distribution of the specific margin (margin-to-turnout ratio) follows a consistent curve across diverse democracies, electoral systems, and scales. This universality emerged despite the vast differences in raw turnout and margin distributions across countries. We introduced the Random Voting Model (RVM) as a simple stochastic framework that remarkably captures this universal pattern with surprising accuracy.

Building on this discovery, this chapter provides a comprehensive analysis of the RVM from first principles. We will delve into its mathematical foundations, derive key analytical results, and demonstrate how this elegantly simple stochastic model can explain multiple empirical findings from electoral data. Through both analytical derivations and simulation results, we'll show that the RVM not only predicts the universal specific margin distribution but also connects turnout distributions to margin distributions across different electoral contexts.

5.1 Foundation of RVM

The Random Voting Model is based on the premise that electoral outcomes can be understood through a minimal statistical framework that captures the essence of competition without modeling voter psychology or strategic behavior. The model is parameter-free beyond the turnout distribution and number of candidates, relying only on simple probabilistic principles.

In this Random Voting Model, c_i number of candidates contest at i-th electoral unit with n_i electors (voters) and each elector from the i-th electoral unit casts their vote for j-th candidate with a probability p_{ij}. These probabilities are assigned as follows: for each candidate, a number between 0 and 1 is drawn uniformly at random, which is assigned as an unnormalized probability weight w_{ij} to that candidate. The weights are subsequently normalized to get the probability

$p_{ij}, j = 1, 2 \ldots c_i$ of receiving the vote of an elector. This can be mathematically stated as

$$w_{ij} \sim \mathcal{U}(0,1) \quad \text{and} \quad p_{ij} = \frac{w_{ij}}{\sum_k w_{ik}}, \text{ with } j = 1, 2 \ldots c_i, \tag{5.1}$$

where $\mathcal{U}(0,1)$ denotes a uniformly distributed random variable in $(0,1)$.

After each of the n_i electors (voters) in i-th electoral unit casts their vote for some candidate j independently with probability p_{ij}, the candidate receiving the most votes $V_{i,w}$ is declared the winner, and the candidate securing the next largest number of votes $V_{i,r}$ is the runner-up. The *margin of victory* M_i is then defined to be the vote difference between the winner and the runner-up: *i.e.* $M_i = V_{i,w} - V_{i,r}$. The empirical election data we employ shows that the top three candidates, on average, account for nearly 87% of all votes polled in an election. Hence, as part of the model specification, we fix the number of candidates in each electoral unit to be three, i.e., $c_i = 3$ for all i.

The only input to this model is the raw turnout data, i.e., the number of voters (who actually voted) in each constituency. For the model simulation, we use the turnout data of real elections as the total number of voters in different constituencies. To understand how simulations are performed, consider this notional example: if a country has $N = 100$ constituencies and data for five such elections is available. Then, the turnouts for these five elections are consolidated, resulting in 500 turnout data points. Further the model is simulated on 500 electoral units with number of electors in each electoral unit taken from the consolidated turnouts. Such a simulation of an election is performed multiple times to get the average distributions.

5.2 Universal Distribution Derivation

We now demonstrate how the RVM explains the universal distribution of scaled specific margin $Q_{\widetilde{\mu}}(\widetilde{\mu})$ observed in the previous chapter. As mentioned in the previous section (5.1), we consider the case where 3 candidates are contesting in an election. The weight assigned for the j-th candidate of the i-th electoral unit is w_{ij}. These weights are drawn independently at random from a uniform distribution between 0 and 1. The corresponding probability p_{ij} of receiving votes is calculated by normalizing these weights. Hence, we have the following,

$$w_{ij} \sim \mathcal{U}(0,1) \text{ and } p_{ij} = \frac{w_{ij}}{\sum_{k=1}^{3} w_{ik}}; \text{ with } j = 1, 2, 3. \tag{5.2}$$

For the rest of the analysis in this chapter, we focus on a single (i-th) electoral unit with voter turnout T and drop the corresponding index i for brevity. Hence,

$$w_{ij} := w_j \text{ and } p_{ij} := p_j. \tag{5.3}$$

5.2.1 Large Turnout Approximation

For a large turnout ($T \gg 1$), it is reasonable to assume the number of votes received by the j-th candidate is proportional to their probability p_j, in particular, $v_j \approx p_j T$. Hence, for $T \gg 1$, the *margin* can be approximated as

$$M \approx (p_{max} - p_{2nd\,max})T, \tag{5.4}$$

where p_{max} and $p_{2nd\,max}$ correspond to the largest and the second largest probabilities assigned to the candidates. For example, if the probabilities p_1, p_2, and p_3 assigned to the 3 candidates are $0.1, 0.6$, and 0.3, then $p_{max} = p_2 = 0.6$ and $p_{2nd\,max} = p_3 = 0.3$. The margin M can also be written in terms of w_j as the following:

$$\begin{aligned} M &\approx \left(\frac{w_{max}}{w_1 + w_2 + w_3} - \frac{w_{2nd\,max}}{w_1 + w_2 + w_3} \right) T, \\ &= \left(\frac{w_{(3)}}{w_{(1)} + w_{(2)} + w_{(3)}} - \frac{w_{(2)}}{w_{(1)} + w_{(2)} + w_{(3)}} \right) T, \\ &= \left(\frac{w_{(3)} - w_{(2)}}{w_{(1)} + w_{(2)} + w_{(3)}} \right) T, \end{aligned} \tag{5.5}$$

where $w_{(k)}$ is the k-th order statistics [88]. Hence,

$$\frac{M}{T} \approx \frac{w_{(3)} - w_{(2)}}{w_{(1)} + w_{(2)} + w_{(3)}}. \tag{5.6}$$

5.2.2 Order Statistics Framework

Consider n *iid* random variables $\{X_1, X_2 \dots X_n\}$ drawn from a distribution $\rho(x)$. When arranged in ascending order, the random variable at the k-th spot is defined as the k-th order statistic. In particular, n-th and 1-st order statistics correspond to the maximum and minimum of those n

random variables, respectively. The k-th order statistic of the random variable X is denoted by $X_{(k)}$.

The joint probability density of all the order statistics of the above-mentioned n random variables, $\mathbb{P}\left(x_{(1)}, x_{(2)}, ...x_{(n)}\right)$, defined as the probability density that the random variable $X_{(k)}$ takes the value $x_{(k)}$ for $k \in \{1, 2, \ldots, n\}$, is

$$\mathbb{P}\left(x_{(1)}, x_{(2)}, ...x_{(n)}\right) = n! \prod_{k=1}^{n} \rho\left(x_{(k)}\right). \tag{5.7}$$

5.2.3 RVM Analytical Solution

Now that we understand the joint probability density of the order statistics, for RVM, we have $n = 3$ and $\rho(x) = \mathcal{U}(0, 1)$. Hence, we have,

$$\mathbb{P}\left(w_{(1)}, w_{(2)}, w_{(3)}\right) = 3! = 6; \text{ with } 0 < w_{(1)} < w_{(2)} < w_{(3)} < 1, \tag{5.8}$$

and $\mathbb{P}\left(w_{(1)}, w_{(2)}, w_{(3)}\right) = 0$ otherwise, with the following normalization:

$$\int_0^1 dw_{(3)} \int_0^{w_{(3)}} dw_{(2)} \int_0^{w_{(2)}} 6 dw_{(1)} = 1. \tag{5.9}$$

From the joint probability distribution of all the order statistics, we calculate the approximate probability density function of specific margin $M/T = \mu$ from Eq. (5.6) as follows,

$$\begin{aligned} Q_\mu(\mu) &= 6 \int_0^1 dw_{(3)} \int_0^{w_{(3)}} dw_{(2)} \int_0^{w_{(2)}} \delta\left(\mu - \frac{w_{(3)} - w_{(2)}}{w_{(1)} + w_{(2)} + w_{(3)}}\right) dw_{(1)}, \\ &= 6 \int_0^1 dw_{(3)} \int_0^{w_{(3)}} \frac{w_{(3)} - w_{(2)}}{\mu^2} \mathbb{1}_{0 < \frac{w_{(3)} - \mu w_{(3)} - (1+\mu) w_{(2)}}{\mu} < w_{(2)}} dw_{(2)}, \\ &= 6 \int_0^1 dw_{(3)} \frac{(1-\mu)(5+7\mu) w_{(3)}^2}{2(1+\mu)^2(1+2\mu)^2}. \end{aligned} \tag{5.10}$$

$$\tag{5.11}$$

Finally, after performing this integral, we get

$$Q_\mu(\mu) = \frac{(1-\mu)(5+7\mu)}{(1+\mu)^2(1+2\mu)^2}. \tag{5.12}$$

The distribution $Q_\mu(\mu)$ does not depend on the turnout and is universal. Now, by a change of variable to scaled specific margin defined as $\widetilde{\mu} = \mu/\langle\mu\rangle$, we obtain its distribution $Q_{\widetilde{\mu}}(\widetilde{\mu})$ to be

$$Q_{\widetilde{\mu}}(\widetilde{\mu}) = \langle\mu\rangle\, Q_\mu(\widetilde{\mu}\langle\mu\rangle) = \frac{\langle\mu\rangle(1-\widetilde{\mu}\langle\mu\rangle)(5+7\widetilde{\mu}\langle\mu\rangle)}{(1+\widetilde{\mu}\langle\mu\rangle)^2(1+2\widetilde{\mu}\langle\mu\rangle)^2}, \tag{5.13}$$

where $\langle\mu\rangle = \frac{1}{2} + \ln\left(\frac{9\sqrt[4]{3}}{16}\right)$. This derived distribution $Q_{\widetilde{\mu}}(\widetilde{\mu})$ is precisely the universal curve observed in the empirical data across 32 countries in the previous chapter. The remarkable agreement between theory and data, as shown in Fig. 5.1, confirms that the RVM captures the essential statistical features underlying electoral competition. Individual predictions of $Q_{\widetilde{\mu}}(\widetilde{\mu})$ for all 32 countries are demonstrated in the Appendix A, Sec. A.3.

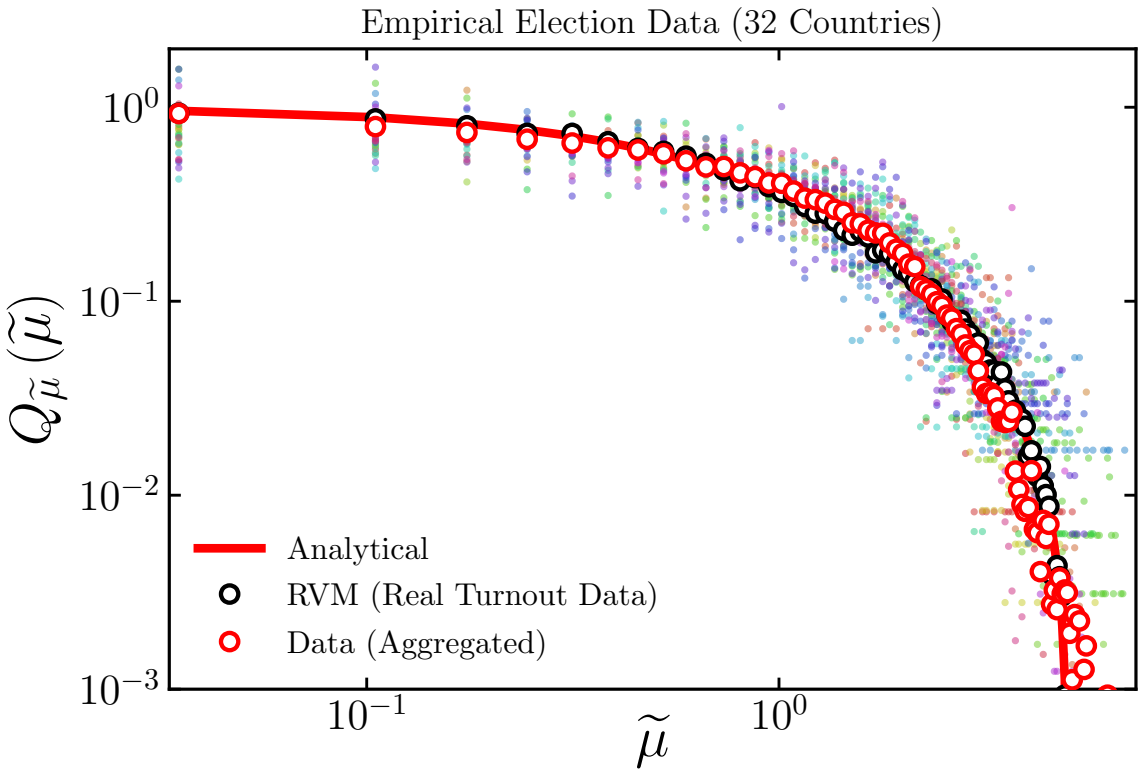

Figure 5.1: $Q_{\widetilde{\mu}}(\widetilde{\mu})$: The distribution is universal and does not depend on the turnout distribution. Each color indicates empirical $Q_{\widetilde{\mu}}(\widetilde{\mu})$ for a specific country for which the election data is consolidated over several elections. The average of these empirical distributions (red open circles) closely follows the analytical curve (red line) and the averaged RVM predictions for each country (black open circles).

5.3 Margin Distribution Prediction

Having established that the RVM predicts the universal specific margin distribution, we now explore how the model can predict the margin distribution $Q_M(M)$ from an arbitrary turnout distribution $g(T)$. From the previous section, we have the distribution of the specific margin $\mu = M/T$ to be

$$Q_\mu(\mu) = \frac{(1-\mu)(5+7\mu)}{(1+\mu)^2(1+2\mu)^2}. \tag{5.14}$$

Through a simple change of variable $(M = \mu T)$ we get,

$$\mathcal{P}(M|T) = \frac{(1-M/T)(5+7M/T)}{T(1+M/T)^2(1+2M/T)^2}. \tag{5.15}$$

For an arbitrary turnout distribution $g(T)$, we obtain the distribution of M to be,

$$Q_M(M) = \int_M^\infty g(T)\mathcal{P}(M|T)dT = \int_M^\infty g(T)\frac{(1-M/T)(5+7M/T)}{T(1+M/T)^2(1+2M/T)^2}dT. \tag{5.16}$$

Again with $u = T/M$, the above integral transforms to,

$$Q_M(M) = \int_1^\infty g(Mu)\frac{u(u-1)(5u+7)}{(1+u)^2(2+u)^2}du. \tag{5.17}$$

5.3.1 Turnout Distribution Effects

We compute $Q_M(M)$ for different turnout distributions $g(T)$. In particular, we take $g(T)$ to be (A) exponential, (B) power law, and (C) Gaussian distributions as they have vastly different tail behaviors. Finally, we also consider a uniform turnout distribution with finite support.

5.3.1.1 Exponential Turnout Distribution

In this case $g(T) = \frac{1}{\tau}e^{-T/\tau}$, with $\tau > 0$. Hence,

$$Q_M(M) = \int_1^\infty \frac{1}{\tau}e^{-Mu/\tau}\frac{u(u-1)(5u+7)}{(1+u)^2(2+u)^2}du, \tag{5.18}$$

or,

$$Q_M(M) = \frac{e^{-\frac{M}{\tau}}}{\tau^2}\left(4e^{\frac{2M}{\tau}}(\tau+M)\text{Ei}\left(-\frac{2M}{\tau}\right) - 9e^{\frac{3M}{\tau}}(\tau+2M)\text{Ei}\left(-\frac{3M}{\tau}\right) - 4\tau\right), \tag{5.19}$$

where $\text{Ei}(x) = \int_{-\infty}^{x} \frac{e^t}{t} dt$. At large margin limit ($M \to \infty$), the asymptotic behavior of the distribution is the following (up to the leading order of M):

$$Q_M(M) = \frac{\tau}{3M^2} e^{-M/\tau}. \tag{5.20}$$

This suggests that in the large margin limit, both the margin and its corresponding turnout distribution have an exponential decay with the same rate.

5.3.1.2 Power law Turnout Distribution

In this case $g(T) = \frac{\alpha-1}{T_{min}^{1-\alpha}} T^{-\alpha}$, with $\alpha > 1$ and $T > T_{min}$. Hence we have,

$$Q_M(M) = \int_1^\infty \frac{\alpha-1}{T_{min}^{1-\alpha}} (Mu)^{-\alpha} \frac{u(u-1)(5u+7)}{(1+u)^2(2+u)^2} du, \tag{5.21}$$

or,

$$Q_M(M) = C(M) \frac{\alpha-1}{T_{min}^{1-\alpha}} (M)^{-\alpha}, \tag{5.22}$$

where,

$$C(M) = \begin{cases} I_1(\infty) - I_1(T_{min}/M), \text{if } M \leq T_{min} & (5.23) \\ I_1(\infty) - I_1(1), \text{otherwise,} & (5.24) \end{cases}$$

with,

$$I_1(y) = \int \frac{y^{1-\alpha}(y-1)(5y+7)}{(1+y)^2(2+y)^2} dy, \tag{5.25}$$

and,

$$I_1(y) = \begin{cases} -\frac{4}{y+1} + \frac{9}{2(y+2)} - \frac{1}{4}7\ln(y) + 4\ln(y+1) - \frac{9}{4}\ln(y+2), \text{if } \alpha = 2 & (5.26) \\ \frac{y^{2-\alpha}\left(16\,{}_2F_1(2, 2-\alpha; 3-\alpha; -y) - 9\,{}_2F_1\left(2, 2-\alpha; 3-\alpha; -\frac{y}{2}\right)\right)}{4(\alpha-2)}, \text{otherwise,} & (5.27) \\ & (5.28) \end{cases}$$

where ${}_2F_1(a, b; c; z)$ is a hypergeometric function [89], defined as,

$${}_2F_1(a, b; c; z) = \sum_{n=0}^{\infty} \frac{(a)_n (b)_n}{(c)_n} \frac{z^n}{n!} = 1 + \frac{ab}{c}\frac{z}{1!} + \frac{a(a+1)b(b+1)}{c(c+1)}\frac{z^2}{2!} + \cdots.$$

It is evident from Eq. (5.22) that for $M > T_{min}$, the margin distribution decays with a power law exponent α, exactly the same as the turnout distribution.

5.3.1.3 Gaussian Turnout Distribution

In this case $g(T) = C_0 e^{-(T/T_0)^2}$, with $T > 0$. Hence,

$$Q_M(M) = \int_1^\infty C_0 e^{-(Mu/T_0)^2} \frac{u(u-1)(5u+7)}{(1+u)^2(2+u)^2} du. \tag{5.29}$$

At large margin limit $(M \to \infty)$, the asymptotic behavior of the distribution is the following (up to the leading order of M):

$$Q_M(M) = \frac{C_0}{12} \left(\frac{T_0}{M}\right)^4 e^{-(M/T_0)^2}, \tag{5.30}$$

and it has a Gaussian decay similar to the corresponding turnout distribution.

From the asymptotic analysis of the margin distributions for the three above-mentioned turnout distributions, we provide strong evidence that the tails of the margin distributions mimic those of the corresponding turnout distributions. For completeness, we also compute the margin distribution corresponding to a uniform turnout distribution which has a finite support (no tail behavior).

5.3.1.4 Uniform Turnout Distribution

In this case $g(T) = \frac{1}{b-a}$, when $T \in [a, b]$, otherwise $g(T) = 0$. Hence,

$$Q_M(M) = \begin{cases} \frac{1}{b-a} \int_{a/M}^{b/M} \frac{u(u-1)(5u+7)}{(1+u)^2(2+u)^2} du, \text{if } M \leq a & (5.31) \\ \frac{1}{b-a} \int_1^{b/M} \frac{u(u-1)(5u+7)}{(1+u)^2(2+u)^2} du, \text{otherwise,} & (5.32) \end{cases}$$

or,

$$Q_M(M) = \begin{cases} \frac{1}{b-a} \left(I_2(b/M) - I_2(a/M)\right), \text{if } M \leq a & (5.33) \\ \frac{1}{b-a} \left(I_2(b/M) - I_2(1)\right), \text{if } a > M \geq b & (5.34) \\ 0, \text{ otherwise,} & (5.35) \end{cases}$$

where,

$$I_2(y) = \int \frac{y(y-1)(5y+7)}{(1+y)^2(2+y)^2} dy = -\frac{4}{y+1} + \frac{18}{y+2} - 4\ln(y+1) + 9\ln(y+2). \tag{5.36}$$

5.3.2 Synthetic Turnout Simulations

We perform simulations using the following four different synthetic turnout distributions to further validate our analytical results, specifically the tail behavior of the margin distribution. We also simulate RVM with different protocols for generating p_{ij}, detailed in Section A.1 of Appendix A, to investigate its effect on predictions.

1. **Gaussian Turnout Distribution:** $g(T) = \frac{1}{\sigma\sqrt{2\pi}} \exp\left(-\frac{(T-\mu)^2}{2\sigma^2}\right)$, with $\mu = 50000$, $\sigma = 10000$ and $T > 0$.

2. **Exponential Turnout Distribution:** $g(T) = \frac{1}{\tau} \exp\left(-\frac{T}{\tau}\right)$, with $\tau = 50000$.

3. **Power law Turnout Distribution:** $g(T) = \frac{\alpha-1}{T_{min}^{1-\alpha}} T^{-\alpha}$, with $\alpha = 2$ and $T_{min} = 100$ (minimum possible turnout).

4. **Uniform Turnout Distribution:** $T \sim \mathcal{U}(a, b)$, with $a = 100$ and $b = 100000$. $\mathcal{U}(a, b)$ denotes uniform distribution between the range a and b.

Each of the RVM simulations was performed on 10^6 electoral units, with turnouts (rounded down to the nearest integer) drawn from one of these four distributions. The simulation demonstrates that the tail of the margin distribution mimics the turnout distribution's tail. This is evident in Fig. 5.2(a), (b), and (c). The tail of the margin distribution (Fig. 5.2 (c)) corresponding to power law turnouts decays with the same power law exponent. In the simulation with Gaussian turnout distribution, we find the tail of the margin distribution also has a Gaussian falloff (Fig. 5.2 (a)). Similarly, the margin distribution corresponding to exponential turnouts has an exponential tail (Fig. 5.2 (b)). As the probability density function of uniform turnout distribution and corresponding margin distribution have finite supports, their tails can not be properly defined. We find a sharp cutoff in the corresponding margin distribution. The analytical (semi-analytical for Gaussian turnout) predictions for the margin distributions (shown as black lines in Fig. 5.2) corresponding to all four aforementioned turnout distributions are in excellent agreement with the RVM simulation. In empirical county-level election data of the United States, the heavy-tailed

decay of the turnout distribution is reflected in the corresponding margin distribution (Fig. 5.2(e)). In Fig. 5.2(f), we see a similar decay trend in both margin and turnout distribution, which correspond to congressional district-level election data of the USA.

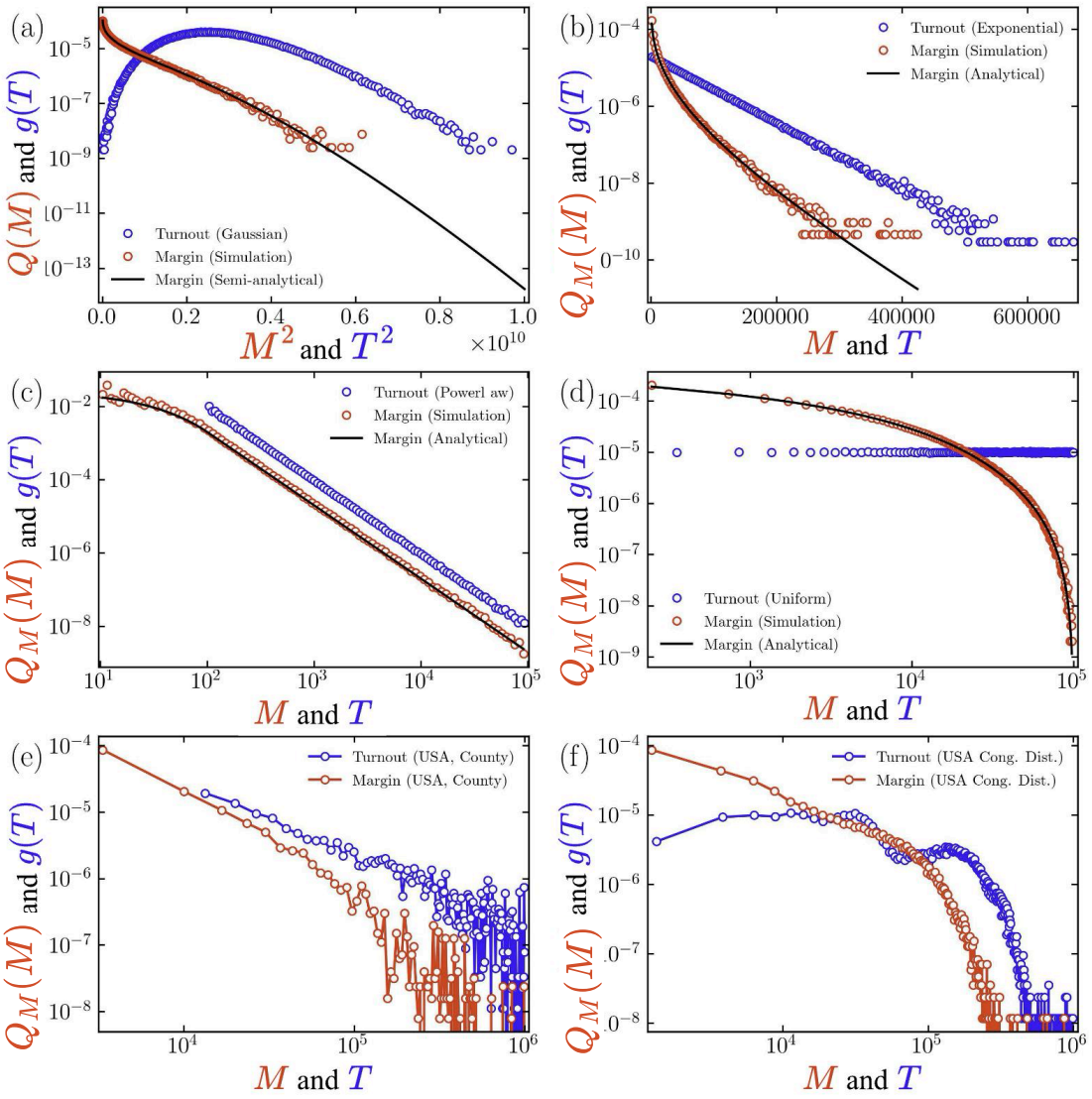

Figure 5.2: The margin distribution $Q_M(M)$ is plotted with the corresponding turnout distribution $g(T)$ to demonstrate that the tails of both these distributions are correlated. Panels (a), (b), (c), and (d) correspond to Gaussian, exponential, power law, and uniform turnout distributions, respectively. Blue open circles denote the turnout distributions. Red open circles denote the margin distribution computed through RVM simulations. Black solid lines correspond to the margin distribution computed using Eq. 5.17. For exponential, power law, and uniform turnout distributions, the integration was analytically calculated, and for the Gaussian turnout distribution, it was evaluated numerically. Panels (e) and (f) depict the margin and turnout distribution for the county-level and congressional district-level election data of the USA, respectively.

5.3.3 Scaling Requirements for Margin Analysis

While the RVM successfully explains the shape of the margin distributions $Q_M(M)$ and captures their tail behaviors remarkably well, it fails to predict the empirical mean of those distributions. The empirical study to find a scaling relation between mean margin, mean specific margin, and turnout is discussed in Section A.2 of Appendix A. To overcome this limitation, we scale the margin distribution by its mean $\langle M \rangle$, and investigate the predictive power of the RVM on the scaled margin distribution $Q_{\widetilde{M}}(\widetilde{M})$.

5.3.3.1 Predicting Scaled Margin Distributions Across Countries

As demonstrated in the previous chapter, different countries exhibit vastly different turnout distributions $g(T)$ that reflect distinct electoral systems and contexts. The key question is whether the RVM can capture the resulting variations in scaled margin distributions $Q_{\widetilde{M}}(\widetilde{M})$. Figure 5.3 (b-g) shows that the RVM predictions (solid lines) achieve excellent agreement with empirical scaled margin distributions (open circles) across diverse countries including India, USA, South Korea, Canada, Japan, and Germany. Notably, the model faithfully captures the disparate decay features observed in different countries, from the sharp cutoff characteristic of German elections to the heavier tails seen in Indian and Japanese data. This demonstrates that raw turnout data carries intrinsic information about the margin distribution, which the RVM effectively leverages without requiring any parameter tuning.

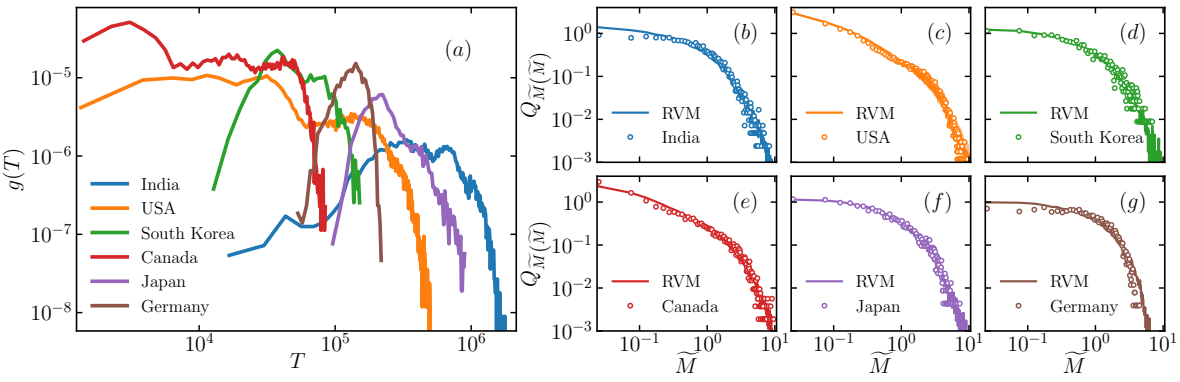

Figure 5.3: RVM predictions of scaled margin distributions across diverse electoral systems. (a) Turnout distributions $g(T)$ showing the diversity in electoral contexts. (b-g) Empirical scaled margin distributions $Q_{\widetilde{M}}(\widetilde{M})$ (open circles) compared with parameter-free RVM predictions (solid lines) for India, USA, South Korea, Canada, Japan, and Germany. The shaded regions represent prediction variability from multiple RVM realizations.

5.3.3.2 Scale-Independent Predictive Accuracy

The predictive power of the RVM extends across different electoral scales without requiring parameter adjustments. As shown in Figure 5.4 (b-g), the same model accurately predicts scaled margin distributions at both constituency-level (larger scale) and polling booth/county-level (smaller scale) for India, USA, and Canada. Despite turnout distributions that differ by orders of magnitude in scale and exhibit completely different shapes, the RVM maintains its predictive accuracy, confirming that the underlying statistical principles captured by the model are truly scale-invariant.

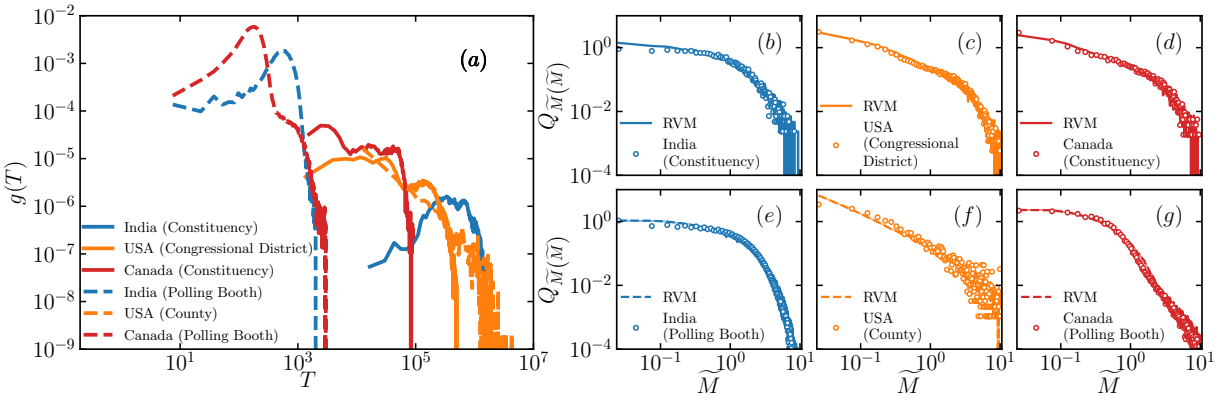

Figure 5.4: Scale-independent RVM predictions. (a) Turnout distributions $g(T)$ at two different electoral scales: dashed lines for smaller scales (polling booths/counties), solid lines for larger scales (constituencies/congressional districts). (b-g) Empirical $Q_{\widetilde{M}}(\widetilde{M})$ (open circles) and RVM predictions (lines) demonstrate excellent agreement across both scales despite vastly different turnout characteristics.

5.3.3.3 Comprehensive Validation Across All Countries

Figure 5.5 provides a comprehensive demonstration of the RVM's predictive accuracy across our complete dataset of 32 countries. The remarkable agreement between empirical distributions (colored circles) and parameter-free RVM predictions (black lines) across such diverse electoral systems – spanning different continents, political cultures, and institutional arrangements – underscores the model's robustness and the fundamental nature of the statistical principles it captures.

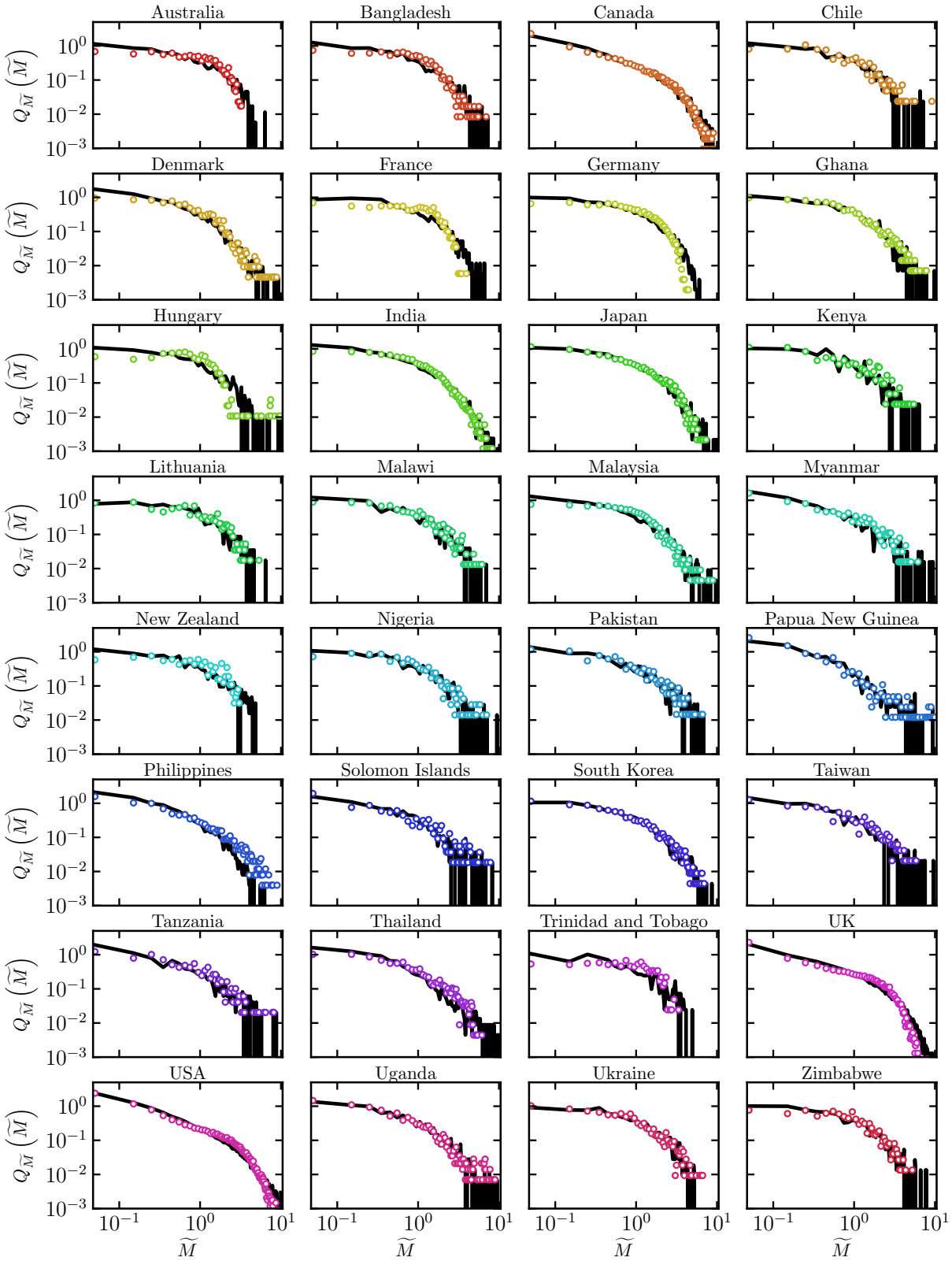

Figure 5.5: Comprehensive validation of RVM predictive accuracy. Empirical scaled margin distributions $Q_{\widetilde{M}}(\widetilde{M})$ (colored circles) compared with parameter-free RVM predictions (black solid lines) across all 32 countries in our dataset, demonstrating consistent predictive accuracy across diverse electoral systems.

5.4 Discussion

In this chapter, we have provided a comprehensive analysis of the Random Voting Model (RVM) from its first principles. We demonstrated how this elegantly simple model generates the universal distribution of scaled specific margins observed across diverse electoral systems worldwide. Through rigorous mathematical derivations, we showed that the model successfully predicts this universality without requiring any parameters beyond the turnout distribution and number of candidates.

Furthermore, we established that the RVM provides powerful insights into how turnout distributions shape margin distributions across different electoral contexts. Through both analytical solutions and simulations with various synthetic turnout distributions (Gaussian, exponential, power law, and uniform), we demonstrated that margin distributions inherit the tail behavior of their corresponding turnout distributions. This finding explains why electoral margin distributions can vary dramatically across countries while still adhering to the universal specific margin pattern.

The model's ability to predict scaled margin distributions from raw turnout data alone – without any adjustments or free parameters – is remarkable and represents a significant advance in our understanding of electoral statistics. It suggests that beneath the apparent complexity and diversity of electoral systems worldwide lies a fundamental statistical principle that governs competitive selection processes.

However, the RVM also has limitations. While it excellently predicts the shape and tail behavior of margin distributions, it struggles to reliably predict the mean margin. This necessitates scaling by empirical means when comparing model predictions to real-world data. Additionally, the model's simplified assumption of random voting does not account for strategic voting behavior, partisan affiliations, or other psychological and sociological factors that influence real elections.

Despite these limitations, the success of this minimal statistical model in capturing key universal features of electoral competition demonstrates the power of stochastic approaches in understanding complex social phenomena. In the next chapter, we will build upon this foundation to further explore the prediction of several other key electoral statistics.

CHAPTER 6

Beyond Margins: Winner and Runner-up votes

Building on our exploration of the Random Voting Model in the previous chapter, we now extend our investigation to other key electoral statistics and their relationship with voter turnout. While we established that the RVM successfully predicts the universal specific margin distribution and connects turnout distributions to margin distributions across different electoral contexts, a natural question arises: Can the distribution of other relevant electoral statistics be uncovered using voter turnout distributions?

To address this question effectively, we require large datasets covering a range of different electoral scales. India, the world's largest democracy, regularly conducts elections involving vast electorates (960 million in 2024), and its publicly available election data spans multiple decades and electoral scales. The diversity of India's linguistic and cultural landscape further adds to the complexities of its electoral outcomes, making it an excellent testing ground for assessing the robustness of the RVM framework.

In this chapter, using empirical data from Indian elections spanning several decades and vastly different electoral scales, we demonstrate a strong correlation between the distributions of votes received by winners and runner-ups and voter turnouts. Leveraging this correlation and the RVM, we analytically predict the scaled distributions of the votes secured by winners and runner-ups using the corresponding turnout distributions. This prediction remarkably holds good at all the electoral scales – from large parliamentary constituencies ($\sim 10^6$ voters) down to the smallest polling booth levels ($\sim 10^2 - 10^3$ voters). Further, we show a rather surprising scale invariance of the margin distributions, a characteristic typical of Indian elections.

6.1 The Effective Number of Candidates

While our previous analysis employed a fixed number of candidates ($n^c = 3$) for the Random Voting Model, here we refine our approach by introducing the concept of the effective number of candidates [90]. This metric, widely used in political science, captures the actual level of

competition more accurately than the raw count of candidates on a ballot.

The effective number of candidates is defined as:

$$ {}^{(E)}n_i^c = \frac{1}{\sum_{k=1}^{n_i^c}(V_{ik}/T_i)^2}. \tag{6.1} $$

In large electoral exercises such as those in India, even though many candidates join the fray, a few corner most of the votes. For instance, if all the votes are garnered by just one candidate, then $V_{i1} = T_i$, and $V_{ij} = 0$ for $j = 2, \ldots n^c$. In this case, ${}^{(E)}n_i^c = 1$. However, if all the votes are split equally among two candidates, ${}^{(E)}n_i^c = 2$, thus, Eq. 6.1 captures the idea of an effective number of candidates in i-th electoral unit.

By averaging over all the electoral units, we obtain:

$$ {}^{(E)}\tilde{n}^c = \left[\frac{1}{N} \sum_{k=1}^{N} {}^{(E)}n_k^c \right], \tag{6.2} $$

where $[\,*\,]$ denotes the operation of extracting the closest integer value. And ${}^{(E)}\tilde{n}^c$ indicates the effective number of candidates for an entire election at different electoral scales.

From empirical data of Indian elections at different scales, we find ${}^{(E)}\tilde{n}^c = 2$ at the polling booth (PB) level for the General Elections. However, for all the other three cases of Assembly Constituency in General Elections (AC-GE), Parliamentary Constituency in General Elections (PC-GE), and Assembly Constituency in State Elections (AC-SE), we obtain ${}^{(E)}\tilde{n}^c = 3$. This insight allows us to adapt our modeling approach to better match the electoral reality at each scale.

6.2 Turnout-Vote Distribution Correlation

Depending on the electoral level considered, the winner and runner-up vote distributions have vastly different scales, with the winner vote distribution having wider support than the runner-up. However, when both distributions are scaled by their respective mean values (mean taken over all elections for which data is available), the winner and runner-up vote distributions – $Q_{\widetilde{V_w}}(\widetilde{V_w})$ and $Q_{\widetilde{V_r}}(\widetilde{V_r})$ – explicitly display a strong correlation with the corresponding scaled turnout distributions $Q_{\widetilde{T}}(\widetilde{T})$. Figure 6.1 shows this correlation for four different electoral scales in India. Remarkably, at larger electoral scales (Parliamentary and Assembly constituencies), not only the

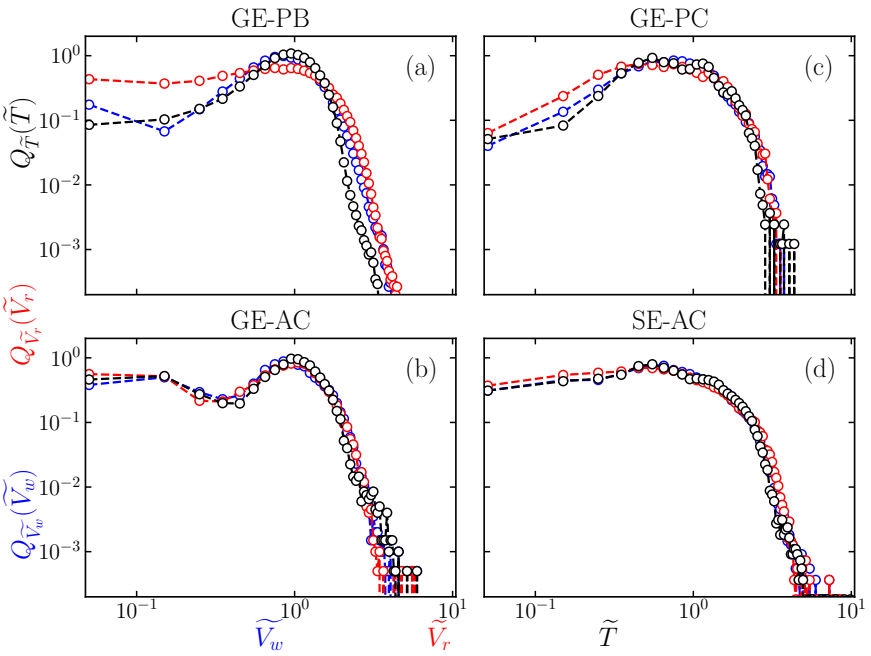

Figure 6.1: Winner, runner-up vote distributions, and turnout distributions, scaled by their respective means. Notably, at larger electoral scales (AC / PC), the winner and runner-up distributions mimic the corresponding turnout distribution.

tail but the entire scaled distributions of winner and runner-up votes mimic the corresponding scaled turnout distribution (panels (b), (c), and (d) in Fig. 6.1). This strong correlation indicates that the turnout distribution contains crucial information about different election statistics and can be leveraged to predict the scaled vote distributions of the winner and the runner-up. To explore this possibility, we apply the Random Voting Model, which has already demonstrated effectiveness at predicting the scaled distribution of margins of victory.

6.3 Vote Distribution Prediction Framework

We now extend our analytical framework to derive the distributions of votes received by winners and runner-ups in the RVM.

6.3.1 RVM Fundamentals Review

In Random Voting Model, in the i-th electoral unit, electorates vote for the j-th candidate with a probability p_{ij}. These probabilities as assigned to the candidates as follows:

$$w_{ij} \sim \mathcal{U}(0,1) \quad \text{and} \quad p_{ij} = \frac{w_{ij}}{\sum_k w_{ik}}, \text{ with } j = 1, 2 \ldots n_i^c, \tag{6.3}$$

where $\mathcal{U}(0,1)$ denotes a uniformly distributed random variable in $(0,1)$ and n_i^c is the number of candidates in the i-th electoral unit.

6.3.2 Vote Share Analysis in Large Turnout Regime

For a large turnout $(T \gg 1)$, the votes received by the j-th candidate can be approximated as $V_j \approx p_j T$ (we remove the electoral unit index i for brevity). Consequently, the vote share is defined as:

$$v_j = V_j/T \text{ with } j = 1, 2, \ldots n^c. \tag{6.4}$$

Thus, in this limit, the vote share distribution is effectively the same as the distribution of p_j. Building on the order statistics framework introduced in the previous chapter, the winner's vote share v_w and runner-up's vote share v_r can be expressed as:

$$v_w = \frac{w^{n^c}_{(n^c)}}{\sum_{k=1}^{n^c} w^{n^c}_{(k)}} \quad \text{and} \quad v_r = \frac{w^{n^c}_{(n^c-1)}}{\sum_{k=1}^{n^c} w^{n^c}_{(k)}}. \tag{6.5}$$

6.3.3 Random Voting Model with two candidates

We begin with the simpler two-candidate case before extending to the more complex three-candidate scenario. These mathematical derivations will allow us to predict the shape of vote distributions based solely on turnout data.

In the two-candidate Random Voting Model, we have $n = n^c = 2$ and $w_j \sim \mathcal{U}(0,1)$. Hence, the joint probability distribution of all the order statistics has the following form,

$$\mathbb{P}\left(w_{(1)}, w_{(2)}\right) = 2! = 2; \text{ with } 0 < w_{(1)} < w_{(2)} < 1, \tag{6.6}$$

and $\mathbb{P}\left(w_{(1)}, w_{(2)}\right) = 0$ otherwise, with the following normalization:

$$\int_0^1 dw_{(2)} \int_0^{w_{(2)}} 2dw_{(1)} = 1. \tag{6.7}$$

6.3.3.1 Winner vote share distribution

From the joint probability distribution of all the order statistics (Eq. 6.6), the approximate vote share distribution of the winner can be obtained as,

$$
\begin{aligned}
P_{v_w}(v_w) &= 2\int_0^1 dw_{(2)} \int_0^{w_{(2)}} \delta\left(v_w - \frac{w_{(2)}}{w_{(1)}+w_{(2)}}\right) dw_{(1)}, \\
&= 2\int_0^1 \frac{2w_{(2)}}{v_w^2} \mathbb{1}_{1/2\le v_w<1} dw_{(2)},
\end{aligned}
\tag{6.8}
$$

or,

$$
P_{v_w}(v_w) = \begin{cases} \dfrac{1}{v_w^2} \text{ if } \dfrac{1}{2} \le v_w < 1 & (6.9) \\ 0, \text{ otherwise.} & (6.10) \end{cases}
$$

6.3.3.2 Runner-up vote share distribution

We can similarly calculate the probability density function of the runner-up vote share as follows,

$$
\begin{aligned}
P_{v_r}(v_r) &= 2\int_0^1 dw_{(2)} \int_0^{w_{(2)}} \delta\left(v_r - \frac{w_{(1)}}{w_{(1)}+w_{(2)}}\right) dw_{(1)}, \\
&= 2\int_0^1 \frac{2w_{(2)}}{(1-v_r)^2} \mathbb{1}_{0<v_r<1/2} dw_{(2)},
\end{aligned}
\tag{6.11}
$$

or,

$$
P_{v_r}(v_r) = \begin{cases} \dfrac{1}{(1-v_r)^2} \text{ if } 0 < v_r < \dfrac{1}{2} & (6.12) \\ 0, \text{ otherwise.} & (6.13) \end{cases}
$$

6.3.4 Three-Candidate Model Analysis

In the three-candidate Random Voting Model, we have $n = n^c = 3$ and $w_j \sim \mathcal{U}(0,1)$. Then, the joint probability distribution of all the order statistics is,

$$
\mathbb{P}\left(w_{(1)}, w_{(2)}, w_{(3)}\right) = 3! = 6; \text{ with } 0 < w_{(1)} < w_{(2)} < w_{(3)} < 1, \tag{6.14}
$$

and $\mathbb{P}\left(w_{(1)}, w_{(2)}, w_{(3)}\right) = 0$ otherwise, with the following normalization:

$$\int_0^1 dw_{(3)} \int_0^{w_{(3)}} dw_{(2)} \int_0^{w_{(2)}} 6dw_{(1)} = 1. \tag{6.15}$$

6.3.4.1 Winner vote share distribution

From the joint probability distribution of all the order statistics, we calculate the approximate probability density function of the winner vote share $v_w = V_w/T$ as follows,

$$\begin{aligned} P_{v_w}(v_w) &= 6\int_0^1 dw_{(3)} \int_0^{w_{(3)}} dw_{(2)} \int_0^{w_{(2)}} \delta\left(v_w - \frac{w_{(3)}}{w_{(1)} + w_{(2)} + w_{(3)}}\right) dw_{(1)}, \\ &= 6\int_0^1 dw_{(3)} \int_0^{w_{(3)}} \frac{w_{(3)}}{v_w^2} \mathbb{1}_{0<\frac{w_{(3)} - v_w\left(w_{(2)}+w_{(3)}\right)}{v_w} < w_{(2)}} dw_{(2)}, \end{aligned} \tag{6.16}$$

or,

$$P_{v_w} = \begin{cases} 6\int_0^1 w_{(3)}^2 \frac{3v_w - 1}{2v_w^3} dw_{(3)}, \text{ if } \frac{1}{3} < v_w \leq \frac{1}{2} & (6.17) \\ 6\int_0^1 w_{(3)}^2 \frac{1 - v_w}{2v_w^3} dw_{(3)}, \text{ if } \frac{1}{2} < v_w \leq 1 & (6.18) \\ 0, \text{ otherwise.} & (6.19) \end{cases}$$

Finally, after performing the integral, we get

$$P_{v_w} = \begin{cases} \frac{3v_w - 1}{v_w^3} \text{ if } \frac{1}{3} < v_w \leq \frac{1}{2} & (6.20) \\ \frac{1 - v_w}{v_w^3}, \text{ if } \frac{1}{2} < v_w < 1 & (6.21) \\ 0, \text{ otherwise.} & (6.22) \end{cases}$$

6.3.4.2 Runner-up vote share distribution

Similarly, the probability density function of the runner-up vote share $v_r = V_r/T$ can be obtained as follows,

$$
\begin{aligned}
P_{v_r}(v_w) &= 6\int_0^1 dw_{(3)}\int_0^{w_{(3)}} dw_{(2)}\int_0^{w_{(2)}} \delta\left(v_r - \frac{w_{(2)}}{w_{(1)}+w_{(2)}+w_{(3)}}\right) dw_{(1)}, \\
&= 6\int_0^1 dw_{(3)}\int_0^{w_{(3)}} \frac{w_{(2)}}{v_r^2}\mathbb{1}_{0<(1/v_r-1)w_{(2)}-w_{(3)}<w_{(2)}} dw_{(2)},
\end{aligned}
\tag{6.23}
$$

or,

$$
P_{v_r}(v_r) = \begin{cases}
6\displaystyle\int_0^1 w_{(3)}^2 \frac{v_r(2-3v_r)}{2(1-v_r)^2(1-2v_r)^2} dw_{(3)}, \text{ if } 0 < v_r \le \frac{1}{3} & (6.24)\\
6\displaystyle\int_0^1 w_{(3)}^2 \frac{1-2v_r}{2v_r^2(1-v_r)^2} dw_{(3)}, \text{ if } \frac{1}{3} < v_r < \frac{1}{2} & (6.25)\\
0, \text{ otherwise.} & (6.26)
\end{cases}
$$

Finally, after performing the integral, we get

$$
P_{v_r}(v_r) = \begin{cases}
\dfrac{v_r(2-3v_r)}{(1-v_r)^2(1-2v_r)^2} \text{ if } 0 < v_r \le \dfrac{1}{3} & (6.27)\\
\dfrac{1-2v_r}{v_r^2(1-v_r)^2}, \text{ if } \dfrac{1}{3} < v_r < \dfrac{1}{3} & (6.28)\\
0, \text{ otherwise.} & (6.29)
\end{cases}
$$

6.3.5 Scaled Distribution Calculation Method

The winner and runner-up vote shares and specific margins are random variables scaled by the voter turnout T. However, through a simple change of variable, $Y = yT$, we can obtain the conditional distributions of the unscaled variables as,

$$
\mathcal{P}(Y|T) = \frac{1}{T} P_y(Y/T), \tag{6.30}
$$

where y can be v_w, v_r, and μ and Y represents unscaled variables V_w, V_r, and M respectively. The distribution of Y for an arbitrary turnout distribution $g(T)$ can be obtained as,

$$
Q_Y(Y) = \int g(T)\, \mathcal{P}(Y|T) dT, \tag{6.31}
$$

with $\langle Y \rangle$ defined as,

$$
\langle Y \rangle = \int Y\, Q_Y(Y) dY. \tag{6.32}
$$

Finally the distribution of *scaled* Y, defined as $\widetilde{Y} = Y/\langle Y \rangle$, can be obtained as follows,

$$Q_{\widetilde{Y}}(\widetilde{Y}) = \langle Y \rangle \, Q_Y(\widetilde{Y}\langle Y \rangle) \tag{6.33}$$

Again, the dummy random variable Y can be either, V_w or V_r.

6.4 Empirical Validation Across Scales

Having derived the analytical expressions for vote share distributions, we now turn to testing these predictions against real-world election data. This validation process will demonstrate how well our theoretical framework captures the essential features of electoral outcomes across different scales.

To validate our analytical framework, we compare the predicted distributions against empirical data from four different electoral scales in India:

1. Parliamentary Constituency level in General Elections (GE-PC): $\sim 10^6$ voters
2. Assembly Constituency level in General Elections (GE-AC): $\sim 10^5$ voters
3. Polling Booth level in General Elections (GE-PB): $\sim 10^3$ voters
4. Assembly Constituency level in State Elections (SE-AC): $\sim 10^5$ voters

Using the empirical turnout distribution $g(T)$ from election data, Eq. 6.31 is numerically integrated. The resulting distribution is then scaled using Eq. 6.33 to obtain the scaled distributions for the winner and runner-up vote shares, $Q_{\widetilde{V_w}}(\widetilde{V_w})$ and $Q_{\widetilde{V_r}}(\widetilde{V_r})$, respectively. As demonstrated in Fig. 6.2, the analytical prediction (solid lines) is remarkably consistent with the empirical vote share distributions. The predictions from RVM simulations, which use the raw turnout data and $n^c = {}^{(E)}\tilde{n}^c$ as inputs, closely follow the analytical distributions in Fig. 6.2.

The scaled distributions of winner and runner-up votes depicted across all electoral scales, in Fig. 6.2, typically exhibit a power-law behavior in the tails for $\widetilde{V}_w, \widetilde{V}_r \gg 1$. Conversely, for $\widetilde{V}_w, \widetilde{V}_r \ll 1$, the distributions display different profiles. Remarkably, these differences are well captured by RVM predictions: RVM $(T, 2)$ accurately predicts distribution at the GE-PB level, while RVM $(T, 3)$ closely matches the distributions at the GE-AC, GE-PC, and SE-AC levels. Hence, the effective number of candidates (Eq. 6.1) and the turnout distribution $g(T)$,

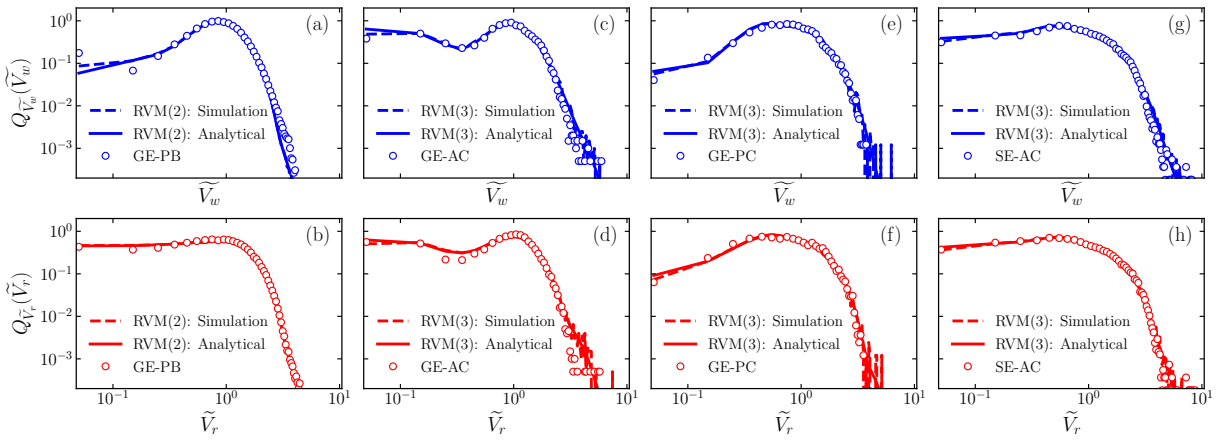

Figure 6.2: Winner and runner-up vote distributions scaled by their respective means. Panels (a, b), (c, d), and (e, f) depict, respectively, the scaled winner and runner-up vote distribution at the polling booth, assembly constituency, and parliamentary constituency level for Indian general elections. Panels (g, h) correspond to the distributions for the state elections at the assembly constituency level. The analytical predictions (solid lines) are in remarkable agreement with the empirical distributions (open circles). Predictions from RVM simulations (dashed line) closely follow the analytical curves. Note particularly the power-law behavior in the tails ($\widetilde{V} \gg 1$) across all scales, and the distinct profiles at small values ($\widetilde{V} \ll 1$) that vary with the effective number of candidates.

when used within the RVM framework, successfully predict the winner and runner-up vote share distributions across distinct electoral scales.

6.5 Scale Invariance of Margin Distributions in Indian Elections

Building on our analysis of specific margins $\mu = M/T$ from the previous chapter, we now examine the behavior of the scaled margin distributions $Q_{\widetilde{M}}(\widetilde{M})$ across different electoral scales in India.

Remarkably, as demonstrated in Fig. 6.3 (a), the scaled distributions for the margin for Indian elections at four different scales (GE-PB, GE-AC, GE-PC, and SE-AC) collapse onto a single curve. This data collapse is a direct consequence of the similarity in tail behavior in the corresponding turnout distributions. This appears to be a characteristic feature of Indian elections.

For instance, scaled margin distributions from US elections at the County and Congressional district levels do not exhibit such a collapse (Fig. 6.3 (b)). This finding highlights a unique characteristic of the Indian electoral system that deserves further investigation.

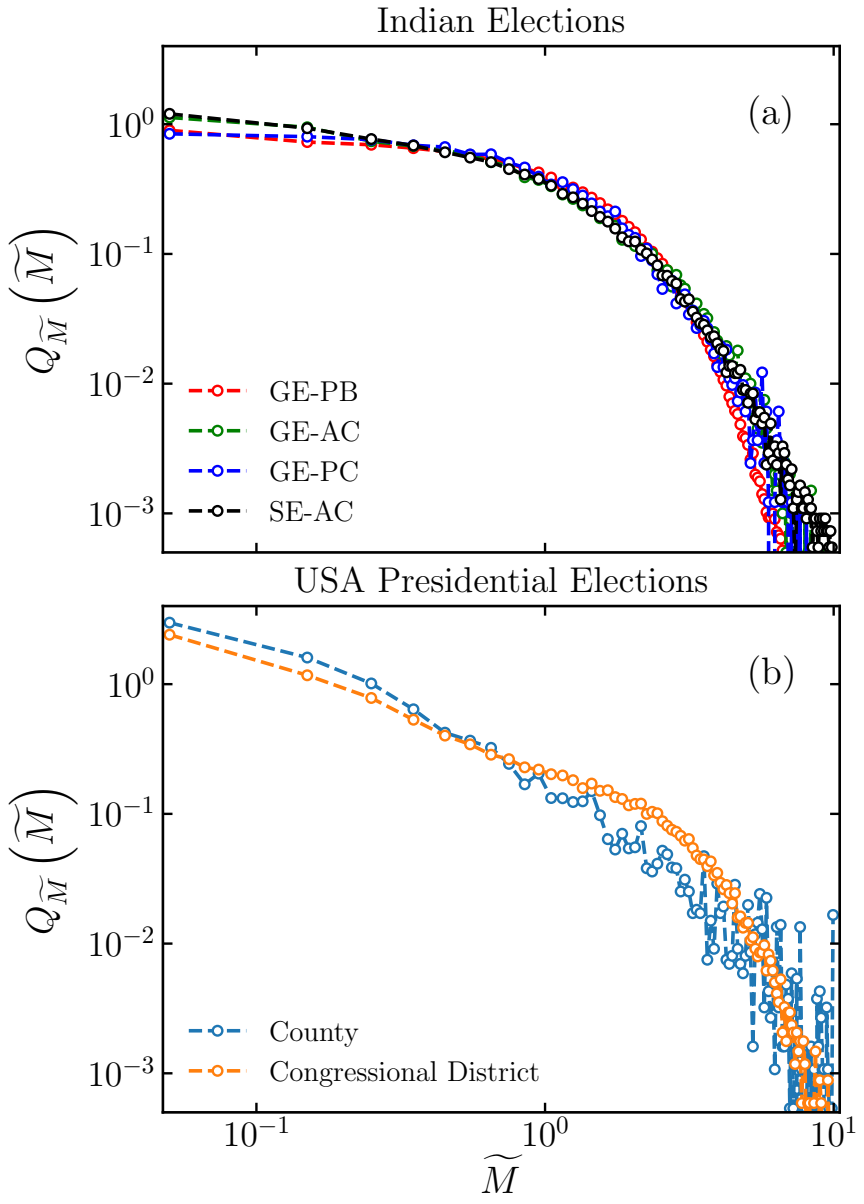

Figure 6.3: Margin distributions scaled by their respective means. (a) Data collapse in the scaled margin distributions of Indian elections at four electoral scales. Note how, despite the vastly different electoral sizes (from $\sim 10^2$ to $\sim 10^6$ voters), the distributions align remarkably well. (b) In contrast, such a collapse is absent in the election data from the USA, where county and congressional district level distributions differ significantly.

6.6 Discussion

In summary, this chapter has demonstrated that voter turnout distributions are not merely indicators of public trust and interest in the electoral process, but they also encode crucial information about several key election statistics. The Random Voting Model, enhanced with the concept of

effective number of candidates, provides a powerful framework for predicting various electoral statistics from turnout distributions alone.

Our analysis reveals that voter turnout distributions strongly correlate with winner and runner-up vote distributions, especially at larger electoral scales. This correlation is particularly evident in the remarkable agreement between the analytical predictions from our model and the empirical data. The RVM, when parameterized with the appropriate effective number of candidates ($n^c = 2$ for polling booth level, $n^c = 3$ for constituency levels), accurately predicts the scaled distributions of winner and runner-up votes across different electoral contexts.

Perhaps most striking among our findings is that Indian elections exhibit a unique scale invariance in margin distributions, with scaled margin distributions collapsing onto a single curve across vastly different electoral scales. This phenomenon, not observed in many other democratic systems, including the United States, highlights distinctive characteristics of the Indian electoral landscape. Furthermore, the universality of the scaled specific margin distribution is confirmed across multiple electoral scales within India, reinforcing the robustness of our analytical framework.

These findings deepen our understanding of electoral statistics and their relationship with voter turnout. The predictive power of the RVM framework, using only turnout data and the effective number of candidates as inputs, provides a valuable tool for electoral analysis and could potentially aid in identifying anomalies or irregularities in electoral processes.

As we move to the next chapter, we will explore the practical applications of these insights, focusing on designing interventions and developing methods to flag electoral malpractice based on deviations from the expected statistical patterns.

CHAPTER 7

From Theory to Practice: Applications and Interventions

In the previous chapter, we uncovered that the Random Voting model can predict the scaled distributions of winner and runner-up votes across vastly different electoral units, from small polling booths to large parliamentary constituencies. This finding, alongside our earlier discovery of universal patterns in specific margin distributions, demonstrates how the Random Voting Model (RVM) can effectively predict electoral statistics across diverse contexts. These insights provide not just theoretical understanding but also practical tools for addressing real-world challenges in social systems.

This chapter explores two significant applications of our research: designing interventions to mitigate polarization in social networks and developing tools for detecting electoral malpractice. Both applications demonstrate how statistical physics principles can be applied to address societal challenges. We first examine how targeted interventions can reduce polarization in online discourse, then show how statistical patterns can help identify potential electoral irregularities.

7.1 Reducing Polarization in Social Networks

Our research on opinion dynamics in Chapter 2 identified how polarized states emerge naturally in social systems, particularly in online networks where homophily – the tendency to interact with like-minded others – creates reinforcing echo chambers. The key insight from our modeling work is that these self-reinforcing patterns can be disrupted through carefully designed interventions.

7.1.1 Echo Chamber Dynamics and Challenges

Echo chambers represent a significant challenge to healthy discourse in modern digital environments. These self-reinforcing information environments arise through two primary mechanisms. First, homophily – our natural tendency to interact with like-minded others – creates initial clustering of similar opinions. Second, algorithmic recommendation systems on social platforms

amplify this tendency by optimizing for engagement, often leading to content that reinforces existing beliefs rather than challenging them.

The consequences of these echo chambers extend to both individual and societal levels. Individuals exposed to increasingly homogeneous information tend to develop more extreme opinions and decreased tolerance for opposing viewpoints. At the societal level, this fragmentation undermines the shared factual basis necessary for productive public discourse and democratic decision-making. Our research in Chapter 2 demonstrated how these dynamics can be modeled mathematically, showing that polarized states emerge naturally from homophilic interactions even without external manipulation.

The challenge lies in developing interventions that can effectively disrupt these patterns without compromising user agency or platform viability. Any practical solution must balance the need to expose users to diverse viewpoints with respect for individual preferences and platform engagement metrics.

7.1.2 Random Nudge Intervention Strategy

The "random nudge" mechanism emerged as the most promising intervention strategy from our analysis. This approach introduces a controlled probability (p) that users encounter opinions outside their usual interaction patterns. When properly calibrated, this intervention reduces polarization while avoiding radicalization. Its implementation simplicity is valuable – requiring only a measured degree of randomness in recommendation algorithms without identifying users' specific political positions.

The intervention works by modifying the interaction probability between agents as:

$$\widetilde{P}_{ij} = p \times \frac{1}{N-1} + (1-p) \times P_{ij} \tag{7.1}$$

In this formulation, $\widetilde{P}_{ij}$ represents the modified interaction probability, P_{ij} represents the original homophily-based interaction probability defined in Eq. 2.3, N is the total number of agents, and p is the nudge strength. Intuitively, this formula combines two components: a small random chance of interaction with any agent in the system, and the original preference-based interaction pattern. The parameter p controls the balance between these components. This approach preserves most natural interaction patterns while introducing just enough randomness to prevent echo chamber

formation.

In practice, this could be implemented by social media platforms as a subtle modification to their recommendation algorithms. For example, a platform might introduce a small probability that content from outside a user's typical interaction sphere appears in their feed. Importantly, this approach requires no knowledge of users' specific political positions – only the pattern of their past interactions, making it privacy-preserving and technically feasible.

7.1.3 Implementation Considerations and Constraints

Despite its promise, the random nudge intervention faces several practical limitations. The primary challenge is calibration. Too little randomness fails to disrupt echo chambers, while excessive randomness risks pushing the system toward radicalization. Our optimization analysis showed that applying stronger interventions to a smaller subset of users often outperforms weaker interventions across the entire user base.

Platform incentives present another significant challenge. Social media companies optimize for engagement metrics that often benefit from the very echo chambers this intervention aims to disrupt. Implementing such changes would require either regulatory pressure or demonstrating that moderate depolarization can coexist with robust user engagement.

User resistance must also be considered. People naturally gravitate toward content that confirms their existing beliefs, and may disengage if exposed to too much challenging content. The intervention must be calibrated not just for mathematical optimality but also for psychological acceptability.

Finally, there are legitimate questions about who should determine the appropriate level of intervention. While our research provides mathematical guidance on optimal nudge strength, the decision to implement such systems ultimately involves value judgments about the proper balance between individual choice and collective discourse health.

7.2 Electoral Integrity Assessment

The universal patterns we discovered in electoral data offer not just theoretical insights but also practical tools for assessing election integrity. Our research identified two complementary approaches for detecting potential electoral malpractice: deviations from universality patterns and

departures from Random Voting Model predictions.

7.2.1 Democratic Integrity Threats

Electoral malpractice undermines the foundational principle of democracy – that governance should reflect the genuine will of the people. When elections are manipulated, whether through ballot stuffing, voter intimidation, or administrative interference, this essential link between citizens and their government is broken. Beyond the immediate impact on specific election outcomes, persistent malpractice erodes public trust in democratic institutions and can lead to political instability, social unrest, and democratic backsliding.

The threat is particularly acute in emerging democracies where electoral systems may lack robust safeguards and independent oversight. However, even established democracies face challenges in maintaining electoral integrity, particularly as new technologies create both opportunities and vulnerabilities in electoral processes. The development of reliable methods for detecting potential malpractice is therefore crucial for protecting democratic governance worldwide.

7.2.2 Existing Detection Methods and Limitations

Electoral integrity is fundamental to democratic governance, yet traditional methods for identifying malpractice often face significant limitations. Direct observation requires extensive resources and can only monitor a fraction of polling stations. Meanwhile, post-election surveys depend on respondents' willingness to accurately report experiences, which may be compromised in environments where intimidation is present.

Statistical approaches offer a complementary tool that can identify patterns of irregularity across entire electoral systems. Previous work by Klimek et al. [91] and Jiménez et al. [92] has explored using statistical indicators to detect potential fraud. Our research extends this toolkit by providing a robust, theoretically grounded framework based on universal statistical patterns observed across diverse electoral contexts.

7.2.3 Statistical Pattern-Based Detection

Our analysis revealed pronounced deviations from the universal pattern in certain electoral contexts. Figure 7.1 shows how the distributions for Ethiopia (2010) and Belarus (2004-2019) diverge significantly from the expected pattern predicted by the Random Voting Model as well

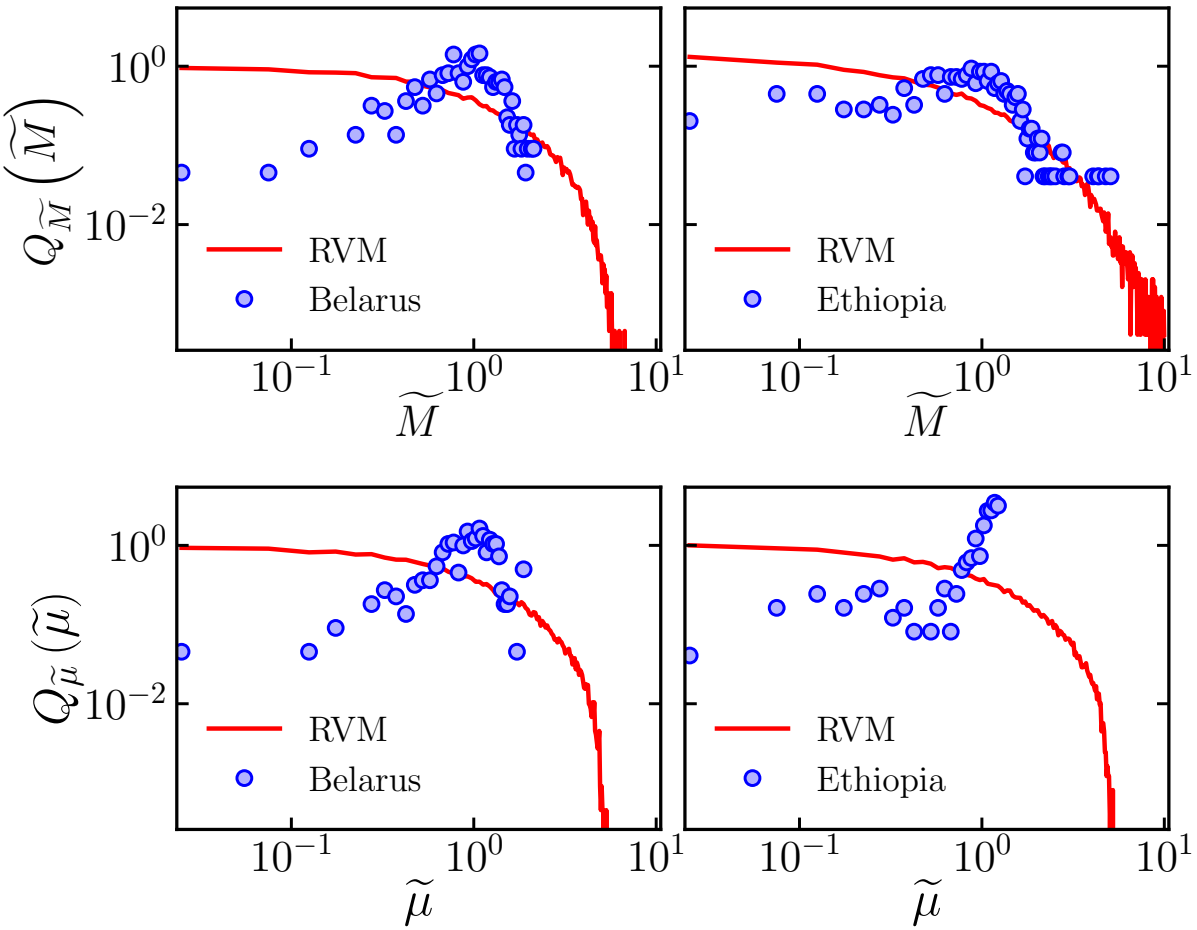

Figure 7.1: Detecting electoral malpractice through statistical signatures. The distributions (a) $Q_{\widetilde{M}}(\widetilde{M})$, and (b) $Q_{\widetilde{\mu}}(\widetilde{\mu})$ obtained from empirical data from Belarus $(2004 - 2019)$ and Ethiopia (2010) (blue circles) show significant deviation from the model predictions (red line). The light red shaded region represents the variability in RVM prediction computed from 100 realizations. These deviations from expected patterns suggest potential electoral irregularities that warrant further investigation.

as the universal distribution of scaled specific margin. In both cases, the distributions show an overrepresentation of large margins and specific margins compared to what would be expected in competitive electoral environments. This pattern is consistent with reports from independent electoral observers who documented concerns about these elections.

Our framework provides two complementary tools for flagging potential electoral malpractice. First, deviations from universality: The scaled distribution of margin-to-turnout ratio should follow a universal form across all competitive elections. Significant departures from this universal pattern can indicate manipulation. Second, departures from Random Voting Model predictions:

The RVM accurately predicts scaled margin distributions across diverse electoral contexts when using actual turnout data as input. When empirical margin distributions deviate substantially from these predictions, this suggests the possibility of non-random influences on voting patterns.

These statistical methods offer several advantages over traditional monitoring approaches. They can be applied retrospectively to historical data, allowing for the identification of patterns that might have been missed during the election. They also provide a quantitative baseline against which to compare future elections, potentially signaling deterioration or improvement in electoral integrity over time. Most importantly, they can analyze entire electoral systems rather than samples, potentially revealing systemic patterns of irregularity that might be missed by more localized approaches.

7.2.4 Method Limitations and Contextual Factors

While our statistical approach offers powerful tools for identifying potential electoral malpractice, several important caveats must be considered in practical implementation.

Statistical signatures cannot definitively prove malpractice alone – they identify patterns warranting further investigation and should complement other forms of evidence, including observer reports and historical context.

Not all deviations necessarily indicate fraud; legitimate factors like unusual demographics or natural disasters can cause statistical anomalies. These methods work best with sufficient data points, making them most reliable for elections with numerous electoral units.

Ultimately, detection is only the first step – effective remediation requires robust legal frameworks, independent electoral commissions, and political will to enforce consequences for violations.

7.3 Discussion

In this chapter, we have demonstrated how the theoretical insights developed throughout this thesis can be translated into practical applications. From designing interventions to mitigate polarization in social networks to developing statistical methods for detecting electoral malpractice, our research offers tools to address significant societal challenges.

The random nudge intervention provides a promising approach for reducing polarization with-

out compromising user privacy or engagement. By introducing controlled randomness into user interactions, this mechanism can effectively break echo chambers while avoiding the risks of radicalization.

Similarly, our statistical framework for detecting electoral malpractice offers a useful complement to traditional monitoring approaches. By identifying deviations from universal patterns and Random Voting Model predictions, this framework can help safeguard democratic processes and strengthen electoral integrity.

Both applications highlight the value of statistical physics approaches to social phenomena. By identifying underlying universal patterns and developing models that capture essential dynamics, we can gain insights that transcend specific contexts and inform effective interventions.

The final chapter will synthesize these findings, discuss limitations of our current approaches, and outline directions for future research that could further enhance our understanding of social systems and their practical applications.

CHAPTER 8

Summary and Outlook

This thesis examined collective human behavior through tools from statistical physics, dynamical systems, and network science. We focused on two domains: opinion formation in digital networks and the statistical structure of democratic elections. Across both, randomness emerged not as noise but as a key mechanism—revealing structure in electoral data and offering ways to reduce polarization.

8.1 Research Contributions and Insights

We began in Chapter 1 by framing society as a multi-scale complex system, justifying the use of statistical physics to model collective outcomes. We reviewed models in opinion dynamics and statistical regularities in elections, providing the context for the chapters that followed.

In Chapter 2, we addressed online opinion polarization using extended models of bounded confidence. We proposed the random nudge mechanism: agents occasionally interact outside their homophilic groups. Simulations showed that even a small amount of such randomness can significantly reduce polarization and dissolve echo chambers. The intervention's effectiveness showed a non-monotonic dependence on the level of randomness—too little has little effect; too much can destabilize opinions. We demonstrated the robustness of this mechanism across multiple models.

Chapter 3 shifted to data. We assembled a large-scale, curated dataset covering elections from 34 countries. This spanned polling booth to national levels and enabled us to test for statistical regularities with high resolution and cross-country consistency.

Chapter 4 identified a key empirical result: after normalizing the margin of victory by turnout and scaling by its country-level mean, we found a universal distribution of the scaled margin that holds across countries, election years, and scales. This result suggested deep statistical constraints in electoral competition.

In Chapter 5, we developed the Random Voting Model (RVM) to explain this universal distri-

bution. Using order statistics in the large-voter limit, we derived the observed universal form from first principles. Crucially, the RVM requires only the empirical turnout distribution as input—no free parameters—highlighting the central role of turnout in shaping competition.

Chapter 6 extended the RVM to India's multi-scale electoral system. By incorporating the effective number of candidates, we showed the model can predict the scaled vote shares of both winner and runner-up candidates across polling booths and parliamentary constituencies. We also found scale-invariant patterns in the scaled margin distribution.

Finally, Chapter 7 discussed applications. The random nudge can be implemented algorithmically in digital platforms to reduce polarization, while the RVM provides a quantitative benchmark for detecting anomalies in elections. We applied this to data from Ethiopia and Belarus to highlight deviations from statistical expectations.

8.2 Future Outlook and Potential Applications

The results of this thesis open several directions for both application and further research.

The random nudge intervention offers a concrete strategy for digital platforms aiming to mitigate polarization. Its algorithmic simplicity and privacy-preserving design make it suitable for deployment in recommendation systems that seek to broaden users' exposure to diverse viewpoints. Calibrated carefully, such interventions could promote healthier online discourse without being intrusive. Further empirical work—especially user-centered experiments—will be essential to evaluate practical effectiveness, user acceptance, and potential side effects.

The statistical regularities uncovered in electoral data—particularly the universality in the distribution of scaled specific margins and the predictive strength of the RVM—can inform tools for electoral monitoring. These models provide quantitative baselines against which to detect irregularities. Deviations from these signatures could serve as early indicators of anomalies, supporting election forensics and reinforcing transparency. Integrating such statistical benchmarks into existing electoral integrity frameworks could help flag outlier constituencies or polling units for further scrutiny.

Several research extensions follow naturally. In opinion dynamics, future models can incorporate multi-dimensional opinion spaces, dynamic network evolution, and the interaction between factual information, misinformation, and correction. Bridging these extensions with platform

data could improve realism and enable more effective interventions.

In the electoral context, the RVM can be enhanced by incorporating strategic voting, the role of partisanship, and campaign effects. A significant challenge—and opportunity—is to build dynamic models linking pre-election opinion evolution to final electoral outcomes. This would integrate the two central threads of this thesis into a unified framework.

Methodologically, improved statistical tools for anomaly detection are needed. This includes composite indicators using multiple tests, or models that can detect specific types of manipulation, especially when high-resolution data are available. Extending the analysis of universality and the RVM to other electoral systems, such as proportional representation or ranked-choice voting, would also test the model's generality.

More broadly, this work illustrates the value of combining statistical physics with social science. Agent-based models, grounded in empirical regularities, can serve as platforms for exploring policy interventions before real-world deployment. As such approaches are increasingly considered in policy and platform design, continuous attention to the ethical implications—regarding surveillance, algorithmic control, and user autonomy—is essential. Acknowledging model limitations, especially oversimplified assumptions about human behavior, should motivate the development of richer, data-informed frameworks.

8.3 Concluding Perspective

This work explored how randomness and statistical structure govern collective outcomes in society. The random nudge mechanism showed how minimal interventions can reduce polarization. The Random Voting Model revealed universal patterns in elections, pointing to deeper organizing principles beneath democratic competition.

Together, these results show that complex social dynamics can be modeled, understood, and even influenced using principled tools from physics. While simplified, such models can illuminate regularities that are otherwise hard to see. We hope this thesis serves as a step towards building a rigorous, empirically grounded, and ethically aware science of collective behavior.

Bibliography

[1] S. Galam. *Sociophysics: A Physicist's Modeling of Psycho-political Phenomena*. Understanding Complex Systems. Springer New York, 2012.

[2] Shannon C McGregor. Social media as public opinion: How journalists use social media to represent public opinion. *Journalism*, 20(8):1070–1086, 2019.

[3] Serge Galam, Yuval Gefen, and Yonathan Shapir. Sociophysics: A new approach of sociological collective behaviour. i. mean-behaviour description of a strike. *Journal of Mathematical Sociology*, 9(1):1–13, 1982.

[4] Serge Galam and Serge Moscovici. Towards a theory of collective phenomena: Consensus and attitude changes in groups. *European Journal of Social Psychology*, 21(1):49–74, 1991.

[5] Morris H DeGroot. Reaching a consensus. *Journal of the American Statistical association*, 69(345):118–121, 1974.

[6] Richard A Holley and Thomas M Liggett. Ergodic theorems for weakly interacting infinite systems and the voter model. *The annals of probability*, pages 643–663, 1975.

[7] Sidney Redner. Reality-inspired voter models: A mini-review. *Comptes Rendus Physique*, 20(4):275–292, 2019.

[8] Katarzyna Sznajd-Weron and Jozef Sznajd. Opinion evolution in closed community. *International Journal of Modern Physics C*, 11(06):1157–1165, 2000.

[9] Katarzyna Sznajd-Weron, Józef Sznajd, and Tomasz Weron. A review on the sznajd model—20 years after. *Physica A: Statistical Mechanics and its Applications*, 565:125537, 2021.

[10] Charles G Lord, Lee Ross, and Mark R Lepper. Biased assimilation and attitude polarization: The effects of prior theories on subsequently considered evidence. *Journal of personality and social psychology*, 37(11):2098, 1979.

[11] Paul DiMaggio, John Evans, and Bethany Bryson. Have american's social attitudes become more polarized? *American journal of Sociology*, 102(3):690–755, 1996.

[12] Delia Baldassarri and Andrew Gelman. Partisans without constraint: Political polarization and trends in american public opinion. *American Journal of Sociology*, 114(2):408–446, 2008.

[13] Robert Axelrod. The dissemination of culture: A model with local convergence and global polarization. *Journal of conflict resolution*, 41(2):203–226, 1997.

[14] Serge Galam. Minority opinion spreading in random geometry. *The European Physical Journal B-Condensed Matter and Complex Systems*, 25:403–406, 2002.

[15] Serge Galam and Frans Jacobs. The role of inflexible minorities in the breaking of democratic opinion dynamics. *Physica A: Statistical Mechanics and its Applications*, 381:366–376, 2007.

[16] Serge Galam. Stubbornness as an unfortunate key to win a public debate: an illustration from sociophysics. *Mind & Society*, 15:117–130, 2016.

[17] Serge Galam. Collective beliefs versus individual inflexibility: The unavoidable biases of a public debate. *Physica A: Statistical Mechanics and its Applications*, 390(17):3036–3054, 2011.

[18] Guillaume Deffuant, David Neau, Frederic Amblard, and Gérard Weisbuch. Mixing beliefs among interacting agents. *Advances in Complex Systems*, 3(01n04):87–98, 2000.

[19] Hegselmann Rainer and Ulrich Krause. Opinion dynamics and bounded confidence: models, analysis and simulation. 2002.

[20] Fabian Baumann, Philipp Lorenz-Spreen, Igor M Sokolov, and Michele Starnini. Modeling echo chambers and polarization dynamics in social networks. *Physical Review Letters*, 124(4):048301, 2020.

[21] Michela Del Vicario, Gianna Vivaldo, Alessandro Bessi, Fabiana Zollo, Antonio Scala, Guido Caldarelli, and Walter Quattrociocchi. Echo chambers: Emotional contagion and group polarization on facebook. *Scientific reports*, 6(1):37825, 2016.

[22] Wesley Cota, Silvio C Ferreira, Romualdo Pastor-Satorras, and Michele Starnini. Quantifying echo chamber effects in information spreading over political communication networks. *EPJ Data Science*, 8(1):35, 2019.

[23] Kiran Garimella, Gianmarco De Francisci Morales, Aristides Gionis, and Michael Mathioudakis. Political discourse on social media: Echo chambers, gatekeepers, and the price of bipartisanship. In *Proceedings of the 2018 world wide web conference*, pages 913–922, 2018.

[24] Matteo Cinelli, Gianmarco De Francisci Morales, Alessandro Galeazzi, Walter Quattrociocchi, and Michele Starnini. The echo chamber effect on social media. *Proceedings of the National Academy of Sciences*, 118(9):e2023301118, 2021.

[25] Fabian Baumann, Philipp Lorenz-Spreen, Igor M Sokolov, and Michele Starnini. Emergence of polarized ideological opinions in multidimensional topic spaces. *Physical Review X*, 11(1):011012, 2021.

[26] Fernando P Santos, Yphtach Lelkes, and Simon A Levin. Link recommendation algorithms and dynamics of polarization in online social networks. *Proceedings of the National Academy of Sciences*, 118(50):e2102141118, 2021.

[27] Kazutoshi Sasahara, Wen Chen, Hao Peng, Giovanni Luca Ciampaglia, Alessandro Flammini, and Filippo Menczer. Social influence and unfollowing accelerate the emergence of echo chambers. *Journal of Computational Social Science*, 4(1):381–402, 2021.

[28] Vítor V Vasconcelos, Sara M Constantino, Astrid Dannenberg, Marcel Lumkowsky, Elke Weber, and Simon Levin. Segregation and clustering of preferences erode socially beneficial coordination. *Proceedings of the National Academy of Sciences*, 118(50):e2102153118, 2021.

[29] Petter Törnberg. Echo chambers and viral misinformation: Modeling fake news as complex contagion. *PLoS one*, 13(9):e0203958, 2018.

[30] Michela Del Vicario, Alessandro Bessi, Fabiana Zollo, Fabio Petroni, Antonio Scala, Guido

Caldarelli, H Eugene Stanley, and Walter Quattrociocchi. The spreading of misinformation online. *Proceedings of the national academy of Sciences*, 113(3):554–559, 2016.

[31] Philip W Anderson. More is different: Broken symmetry and the nature of the hierarchical structure of science. *Science*, 177(4047):393–396, 1972.

[32] Steven Strogatz, Sara Walker, Julia M Yeomans, Corina Tarnita, Elsa Arcaute, Manlio De Domenico, Oriol Artime, and Kwang-Il Goh. Fifty years of 'more is different'. *Nature Reviews Physics*, 4(8):508–510, 2022.

[33] Claudio Castellano, Santo Fortunato, and Vittorio Loreto. Statistical physics of social dynamics. *Rev. Mod. Phys.*, 81:591–646, May 2009.

[34] Arkadiusz Jedrzejewski and Katarzyna Sznajd Weron. Statistical physics of opinion formation: Is it a spoof? *Comptes Rendus Physique*, 20(4):244–261, 2019.

[35] Maxi San Miguel and Raul Toral. Introduction to the chaos focus issue on the dynamics of social systems. *Chaos: An Interdisciplinary Journal of Nonlinear Science*, 30(12), 2020. See all the papers that are part of this special issue.

[36] Serge Galam. *Sociophysics: A Physicist's Modeling of Psycho-political Phenomena*. Springer New York, NY, 2012.

[37] Steven J. Brams. *Mathematics and Democracy : Designing better voting and fair-division procedures*. Princeton University Press, Princeton, 2008.

[38] S Fortunato. Santo fortunato· michael macy· sidney redner. *J Stat Phys*, 151:1–8, 2013.

[39] Jean-Philippe Bouchaud. From statistical physics to social sciences: the pitfalls of multidisciplinarity. *Journal of Physics: Complexity*, 4(4):041001, dec 2023.

[40] Parongama Sen and Bikas K Chakrabarti. *Sociophysics: an introduction*. OUP, Oxford, 2014.

[41] Matjaž Perc, Jillian J. Jordan, David G. Rand, Zhen Wang, Stefano Boccaletti, and Attila Szolnoki. Statistical physics of human cooperation. *Physics Reports*, 687:1–51, 2017.

[42] Marko Jusup, Petter Holme, Kiyoshi Kanazawa, Misako Takayasu, Ivan Romić, Zhen Wang, Sunčana Geček, Tomislav Lipić, Boris Podobnik, Lin Wang, Wei Luo, Tin Klanjšček, Jingfang Fan, Stefano Boccaletti, and Matjaž Perc. Social physics. *Physics Reports*, 948:1–148, 2022.

[43] Sidney Redner. Reality-inspired voter models: A mini-review. *Comptes Rendus Physique*, 20(4):275–292, 2019.

[44] F. Reif. *Fundamentals of Statistical and Thermal Physics*. McGraw Hill, Tokyo, 1965.

[45] Álvaro Corral. Long-term clustering, scaling, and universality in the temporal occurrence of earthquakes. *Phys. Rev. Lett.*, 92:108501, Mar 2004.

[46] Álvaro Corral. Universal earthquake-occurrence jumps, correlations with time, and anomalous diffusion. *Phys. Rev. Lett.*, 97:178501, Oct 2006.

[47] Vasiliki Plerou, Parameswaran Gopikrishnan, Bernd Rosenow, Luís A. Nunes Amaral, and H. Eugene Stanley. Universal and nonuniversal properties of cross correlations in financial time series. *Phys. Rev. Lett.*, 83:1471–1474, Aug 1999.

[48] R. N. Costa Filho, M. P. Almeida, J. S. Andrade, and J. E. Moreira. Scaling behavior in a proportional voting process. *Phys. Rev. E*, 60:1067–1068, Jul 1999.

[49] Santo Fortunato and Claudio Castellano. Scaling and universality in proportional elections. *Phys. Rev. Lett.*, 99:138701, Sep 2007.

[50] C. Borghesi and J.-P. Bouchaud. Spatial correlations in vote statistics: a diffusive field model for decision-making. *Eur. Phys. J. B*, 75(3):395–404, June 2010.

[51] MC Mantovani, HV Ribeiro, MV Moro, S Picoli, and RS Mendes. Scaling laws and universality in the choice of election candidates. *Europhysics Letters*, 96(4):48001, 2011.

[52] Eszter Bokányi, Zoltán Szállási, and Gábor Vattay. Universal scaling laws in metro area election results. *PLOS ONE*, 13(2):1–11, 02 2018.

[53] Arnab Chatterjee, Marija Mitrović, and Santo Fortunato. Universality in voting behavior: an empirical analysis. *Scientific reports*, 3(1):1049, 2013.

[54] Volker Hösel, Johannes Müller, and Aurelien Tellier. Universality of neutral models: Decision process in politics. *Palgrave Communications*, 5(1):1–8, 2019.

[55] Aleksejus Kononovicius. Modeling of the parties' vote share distributions. *Acta Physica Polonica A*, 133(6):1450, 2018.

[56] Aleksejus Kononovicius. Compartmental voter model. *Journal of Statistical Mechanics: Theory and Experiment*, 2019(10):103402, oct 2019.

[57] Angelo Mondaini Calvão, Nuno Crokidakis, and Celia Anteneodo. Stylized facts in brazilian vote distributions. *PLOS ONE*, 10(9):1–20, 09 2015.

[58] Christian Borghesi, Jean-Claude Raynal, and Jean-Philippe Bouchaud. Election turnout statistics in many countries: Similarities, differences, and a diffusive field model for decision-making. *PLOS ONE*, 7(5):1–12, 05 2012.

[59] Juan Fernández-Gracia, Krzysztof Suchecki, José J. Ramasco, Maxi San Miguel, and Víctor M. Eguíluz. Is the voter model a model for voters? *Phys. Rev. Lett.*, 112:158701, Apr 2014.

[60] Dan Braha and Marcus A. M. de Aguiar. Voting contagion: Modeling and analysis of a century of u.s. presidential elections. *PLOS ONE*, 12(5):1–30, 05 2017.

[61] Jérôme Michaud, Ilkka H Mäkinen, Attila Szilva, and Emil Frisk. A spatial analysis of parliamentary elections in sweden 1985–2018. *Applied Network Science*, 6(1):1–28, 2021.

[62] Shintaro Mori, Masato Hisakado, and Kazuaki Nakayama. Voter model on networks and the multivariate beta distribution. *Phys. Rev. E*, 99:052307, May 2019.

[63] Gary C Jacobson. The marginals never vanished: Incumbency and competition in elections to the us house of representatives, 1952-82. *American Journal of Political Science*, pages 126–141, 1987.

[64] Stewart JH McCann. Threatening times," strong" presidential popular vote winners, and the victory margin, 1824–1964. *Journal of personality and social psychology*, 73(1):160, 1997.

[65] Casey B Mulligan and Charles G Hunter. The empirical frequency of a pivotal vote. *Public Choice*, 116(1):31–54, 2003.

[66] Thomas R Magrino, Ronald L Rivest, and Emily Shen. Computing the margin of victory in {IRV} elections. In *2011 Electronic Voting Technology Workshop/Workshop on Trustworthy Elections (EVT/WOTE 11)*, 2011.

[67] Lirong Xia. Computing the margin of victory for various voting rules. In *Proceedings of the 13th ACM conference on electronic commerce*, pages 982–999, 2012.

[68] Arnab Bhattacharyya and Palash Dey. Predicting winner and estimating margin of victory in elections using sampling. *Artificial Intelligence*, 296:103476, 2021.

[69] Election data of india. https://www.eci.gov.in.

[70] Constituency-level elections archive [data file and codebook]. http://www.electiondataarchive.org.

[71] Election data of canada. https://www.elections.ca.

[72] MIT Election Data and Science Lab. County Presidential Election Returns 2000-2020, 2018.

[73] David G Myers and Helmut Lamm. The group polarization phenomenon. *Psychological bulletin*, 83(4):602, 1976.

[74] Daniel J Isenberg. Group polarization: A critical review and meta-analysis. *Journal of personality and social psychology*, 50(6):1141, 1986.

[75] Nicola Perra, Bruno Gonçalves, Romualdo Pastor-Satorras, and Alessandro Vespignani. Activity driven modeling of time varying networks. *Scientific reports*, 2(1):469, 2012.

[76] Michele Starnini and Romualdo Pastor-Satorras. Topological properties of a time-integrated activity-driven network. *Physical Review E*, 87(6):062807, 2013.

[77] Antoine Moinet, Michele Starnini, and Romualdo Pastor-Satorras. Burstiness and aging in social temporal networks. *Physical review letters*, 114(10):108701, 2015.

[78] Suyu Liu, Nicola Perra, Márton Karsai, and Alessandro Vespignani. Controlling contagion processes in activity driven networks. *Physical review letters*, 112(11):118702, 2014.

[79] Christopher Brian Currin, Sebastián Vallejo Vera, and Ali Khaledi-Nasab. Depolarization of echo chambers by random dynamical nudge. *Scientific Reports*, 12(1):9234, 2022.

[80] Elizabeth Dubois and Grant Blank. The echo chamber is overstated: the moderating effect of political interest and diverse media. *Information, communication & society*, 21(5):729–745, 2018.

[81] Jaume Ojer, Michele Starnini, and Romualdo Pastor-Satorras. Modeling explosive opinion depolarization in interdependent topics. *arXiv preprint arXiv:2212.07879*, 2022.

[82] Silvia Milano, Mariarosaria Taddeo, and Luciano Floridi. Recommender systems and their ethical challenges. *Ai & Society*, 35:957–967, 2020.

[83] Emil Noordeh, Roman Levin, Ruochen Jiang, and Harris Shadmany. Echo chambers in collaborative filtering based recommendation systems. *arXiv preprint arXiv:2011.03890*, 2020.

[84] Joe Whittaker, Seán Looney, Alastair Reed, and Fabio Votta. Recommender systems and the amplification of extremist content. *Internet Policy Review*, 10(2):1–29, 2021.

[85] Charles Evans and Atoosa Kasirzadeh. User tampering in reinforcement learning recommender systems. *arXiv preprint arXiv:2109.04083*, 2021.

[86] Muhammad Haroon, Anshuman Chhabra, Xin Liu, Prasant Mohapatra, Zubair Shafiq, and Magdalena Wojcieszak. Youtube, the great radicalizer? auditing and mitigating ideological biases in youtube recommendations. *arXiv preprint arXiv:2203.10666*, 2022.

[87] Marilena Hohmann, Karel Devriendt, and Michele Coscia. Quantifying ideological polarization on a network using generalized euclidean distance. *Science Advances*, 9(9):eabq2044, 2023.

[88] Barry C. Arnold, N. Balakrishnan, and H. N. Nagaraja. *A First Course in Order Statistics*. Society for Industrial and Applied Mathematics, 2008.

[89] Milton Abramowitz and Irene A. Stegun. *Handbook of Mathematical Functions with Formulas, Graphs, and Mathematical Tables*. Dover, New York, ninth dover printing, tenth gpo printing edition, 1964.

[90] Markku Laakso and Rein Taagepera. "effective" number of parties: a measure with application to west europe. *Comparative political studies*, 12(1):3–27, 1979.

[91] Peter Klimek, Yuri Yegorov, Rudolf Hanel, and Stefan Thurner. Statistical detection of systematic election irregularities. *Proceedings of the National Academy of Sciences*, 109(41):16469–16473, 2012.

[92] Raúl Jimenez, Manuel Hidalgo, and Peter Klimek. Testing for voter rigging in small polling stations. *Science advances*, 3(6):e1602363, 2017.

APPENDIX A

Appendix A

A.1 Scaled Margin Distributions for Different p_{ij} Distributions

To investigate the effect of the distribution of p_{ij} on the prediction of scaled margin distribution, we simulated RVM using the following three protocols for choosing p_{ij}.

1. **Protocol 1:** $w_{ij} \sim \mathcal{U}(0,1)$ and $p_{ij} = \frac{w_{ij}}{\sum_{k=1}^{3} w_{ik}}$; with $j = 1, 2, 3$.
2. **Protocol 2:** $w_{i1} \sim \mathcal{U}(0,1), w_{i2} \sim \mathcal{U}(0, 1 - w_{i1}), w_{i3} = 1 - w_{i1} - w_{i2}$ and $p_{ij} = \frac{w_{ij}}{\sum_{k=1}^{3} w_{ik}} = w_{ij}$; with $j = 1, 2, 3$.
3. **Protocol 3:** $w_{ij} = p_{ij} = \frac{1}{3}$, with $j = 1, 2, 3$.

In Fig. A.1, we demonstrate the differences in the prediction of scaled margin distributions for synthetically generated turnout distributions when the three aforementioned protocols are used. Panel (a) shows that, for turnouts drawn from a uniform distribution, the predictions using protocols 1 and 3 are similar, while protocol 2 produces a scaled margin distribution that decays faster. In panel (b), we see similar results for turnout drawn from a Gaussian distribution. However, panel (c) depicts that, for turnouts drawn from a power law distribution, the predictions using protocols 1 and 2 are almost identical, while protocol 3 produces a vastly different scaled margin distribution.

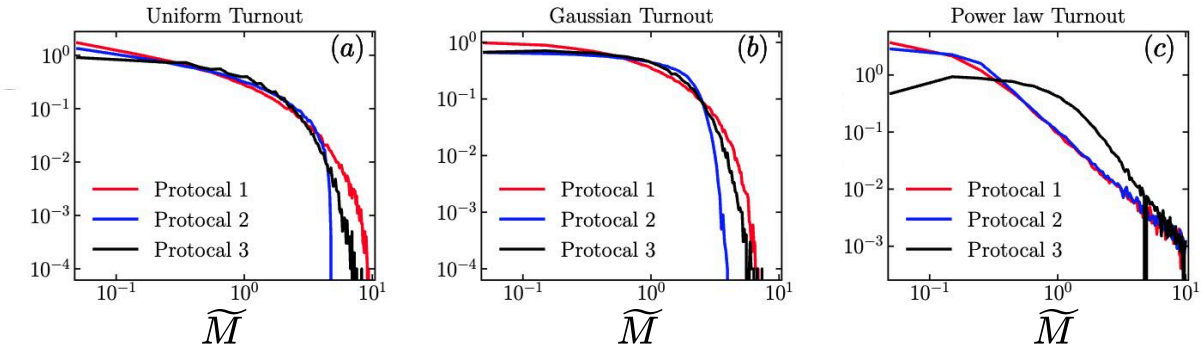

Figure A.1: Prediction of scaled margin distribution for three different protocols of choosing p_i, the probability of receiving votes. Panels (a), (b), and (c) are for uniform, Gaussian, and Power law turnout distributions, respectively.

A.2 Scaling of $\langle M \rangle$ and $\langle \mu \rangle$ vs T

At a large turnout limit ($T \gg 1$), the distributions of μ and M produced by RVM are the following,

$$Q_\mu(\mu) = \frac{(1-\mu)(5+7\mu)}{(1+\mu)^2(1+2\mu)^2},$$
$$\mathcal{P}(M|T) = \frac{(1-M/T)(5+7M/T)}{T(1+M/T)^2(1+2M/T)^2}.$$

From this, we find $\langle \mu \rangle = \frac{1}{2} + \ln\left(\frac{9\sqrt[4]{3}}{16}\right)$ and $\langle M \rangle = T\left(\frac{1}{2} + \ln\left(\frac{9\sqrt[4]{3}}{16}\right)\right)$. We investigate if such linear scaling of $\langle M \rangle$ with T exists in empirical data. As shown in Fig. A.2, for some countries (India, Canada, the United States, and the UK), there is a region of linearity in the $\langle M \rangle$ vs T plots. Correspondingly, $\langle \mu \rangle$ is constant in those regions. Japan and Germany pose as counterexamples to this linearity hypothesis, and developing a better understanding of this scaling provides a rich avenue for further research.

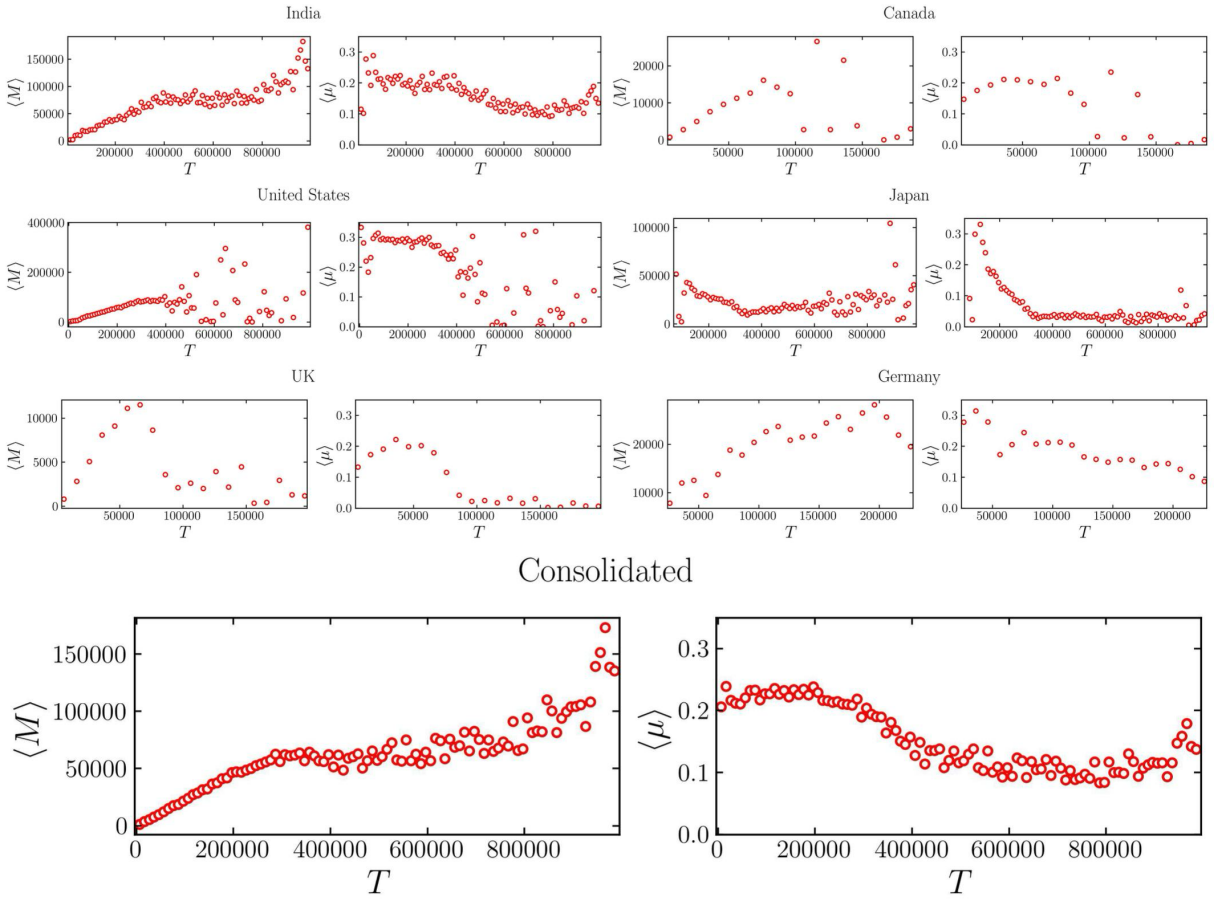

Figure A.2: $\langle M \rangle$ vs T and $\langle \mu \rangle$ vs T for India, Canada, the United States, Japan, the UK, and Germany. The bottom-most panels display plots of the consolidated election data, combining data from 32 countries.

A.3 Figures Containing $Q_{\widetilde{\mu}}(\widetilde{\mu})$ for 32 Countries

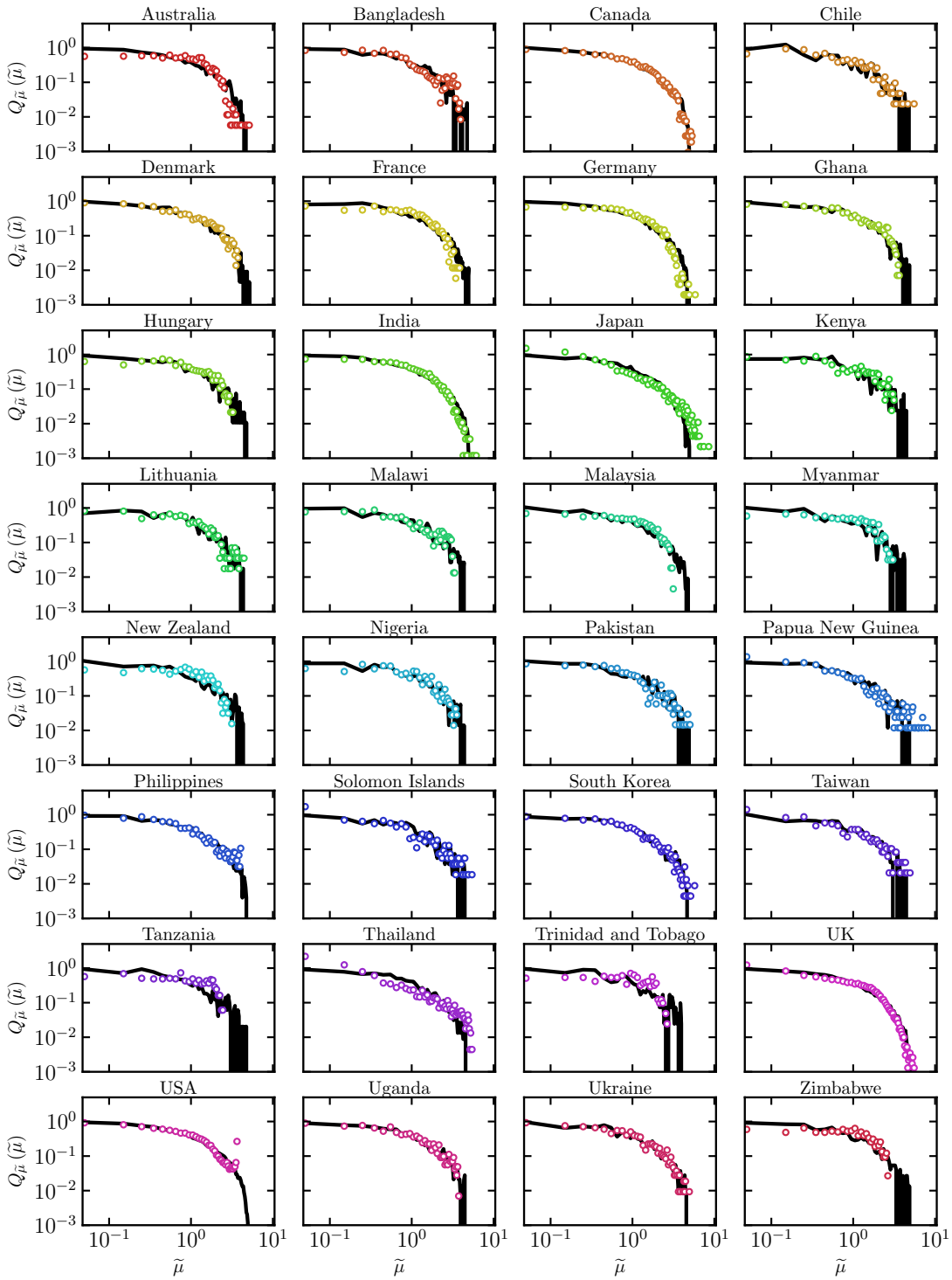

Figure A.3: The empirical distribution of the scaled specific margin (colored open circle), along with RVM model prediction (black solid line) for 32 countries.